“Growth folds above propagating normal faults”

Coleman, A.J., Duffy, O.B. and Jackson, C. A.-L.

All data presented in this preprint can be found here:

https://figshare.com/s/c6663901f6ca8c6f6fe4

Growth folds above propagating normal faults

Alexander J. Coleman[1]*, Oliver B. Duffy[2] and Christopher A.-L. Jackson[1]

[1]Basins Research Group (BRG), Department of Earth Science and Engineering, Imperial College, Prince Consort Road, London SW7 2BP, UK

[2]Bureau of Economic Geology, The University of Texas at Austin, University Station, Box X, Austin, Texas 78713-7508, USA

*Corresponding author's e-mail: a.coleman14@imperial.ac.uk

Keywords

Fault-propagation fold, forced fold, normal fault, fault-related fold, rift, extension, salt-influenced rift, growth fold

Abstract

Growth folds above the upper tips of normal faults are ubiquitous in extensional settings, especially during the early phases of extension and in salt-rich basins. As slip accumulates on the underlying normal fault, the geometry and size of the fold changes. These changes reflect the dip, throw, displacement and propagation rate of the underlying normal fault, as well as the thickness and rheology of the overlying cover. These changes also have a marked impact on the architecture and distribution of synkinematic sediments, as well as the styles of secondary deformation accommodating strain within the growing fold. Here, we analyse a large dataset of natural, and physically- and numerically-modelled growth folds to: (i) characterise their diagnostic features; (ii) investigate the controls on their geometry, size and differences; and (iii) describe how they grow with increasing extensional strain. We demonstrate that larger fault throws and a thicker and weaker cover are associated with larger growth folds. In contrast, small

fault throws as well as thin and strong brittle cover are associated with smaller growth folds. We show that the geometry and size of growth folds vary through time; the width (and thus, the wavelength) of the fold is established relatively early during fold growth, whereas fold amplitude increases gradually with increasing fault throw. Fold width and amplitude become increasingly similar during fold evolution, until the fold is breached by the underlying normal fault. We also derive a number of preliminary empirical relationships between readily observable structural and stratigraphic parameters in our dataset that may help estimate the geometry and size of poorly exposed (i.e. in the field) or imaged (i.e. in the subsurface) growth folds. In addition, we discuss how fault growth models (i.e. constant-length vs. propagating) may impact the three-dimensional evolution of growth folds. Finally, our work shows that growth folds are likely more common than previously thought. For example, although they are well-documented in areas characterised by weak, ductile cover strata and low strain rates, our dataset illustrates that growth folds may also occur in brittle, relatively strong rocks and in regions with high strain rates. However, the underlying controls on fold occurrence remain elusive.

1. Introduction

Fault-related folds are ubiquitous in extensional settings (Fig. 1; Appendix A) and strongly control the evolution of basin physiography through time. One of the most common fault-related folds, particularly during the early phases of extension are 'growth folds' (Fig. 2) (e.g. Gawthorpe and Leeder, 2000; Jackson and Lewis, 2016). Growth folds developed above the upper tips of normal faults are classified as either: 'fault-propagation folds' or 'forced folds'. Where deformation is predominantly localised along a fault or faults at depth but *gradually* transitions upwards into a distributed zone of folding, we use the term 'fault-propagation folding' (Fig. 3A; after Withjack et al., 2002; cf. Withjack et al., 1990; Gawthorpe et al., 1997).

Where the deformation at depth is fault-related but *abruptly* transitions to folding at shallow levels, we use the term 'forced folding' (Fig. 3B; sensu Stearns, 1978; cf. Withjack and Callaway, 2000; Withjack et al., 2002). Forced folds are particularly common where rigid crystalline basement rocks are directly overlain by relatively ductile sedimentary rocks (Stearns, 1978)

Fault-propagation and forced folds grow as slip accumulates on the underlying fault at depth, with concomitant changes in the geometry and size of the folds. This has a marked impact on the architecture and distribution of synkinematic sediments (e.g. Gawthorpe et al., 1997; Lewis et al., 2015), as well as the styles of secondary deformation accommodating strain within the growing fold (e.g. Ameen, 1988; Ameen, 1990; Cosgrove and Ameen, 1999; Sharp et al., 2000a; Jackson et al., 2006; Tavani et al., 2018). Furthermore, the geometry and evolution of growth folds have implications for how and where hydrocarbons are trapped (e.g. Mitra, 1990) and for fluid flow in normal fault zones (e.g. Wibberley et al., 2008; Tavani et al., 2018), determining strain in sedimentary and volcanic basins (e.g. Morley, 1996; Coleman et al., 2017), and for interpreting fault length for earthquake hazard evaluation (e.g. Allmendinger and Shaw, 2000; Blakeslee and Kattenhorn, 2013).

Despite the importance of growth folds, the relationship between the geometry and size of a fold as it evolves remains poorly-understood. Whilst physical and numerical models have shed light on these relationships (e.g. Withjack et al., 1990; Hardy and McClay, 1999; Finch et al., 2004), documenting a parametric relationship between structural factors related to the causal fault (e.g. fault throw, fault dip, etc.) and stratigraphic factors related to the folded strata (e.g. cover thickness, rheology, etc.), they are rarely quantitatively compared to natural examples. Furthermore, several questions remain unanswered regarding the geometry and evolution of growth folds: how does the geometry and size of growth folds change with ongoing fault slip? Do fault-propagation and forced folds grow differently, and if so, why? Do physical and

numerical models accurately describe growth folds in nature? And what controls the occurrence of growth folds?

To answer these questions, this study firstly reviews the wealth of recent literature that has advanced our understanding of growth folds. We focus on two key aspects: (i) how growth folds influence the geometry and distribution of synkinematic strata; and (ii) how strain is accommodated within growth folds. We then quantitatively analyse a large dataset of c. 420 natural examples from > 150 sedimentary and volcanic basins, and c. 250 physical and c. 180 numerical models to investigate: (i) how growth folds evolve with increasing fault throw in two- and three-dimensions, (ii) the differences between fault-propagation folds and forced folds, (iii) what controls the occurrence of growth folds in extensional settings, and (iv) which factors exert the greatest control on growth fold geometry and size. To the best of our knowledge, this is the largest known global compilation of parameters related growth folds. In addition, we construct a data-driven interpretation method to aid the identification of growth folds, so that they are not confused with other fault-related folds (e.g. frictional drag, inversion and drape folds; Fig. 1). We also derive a number of empirical relationships that use readily observable and thus, quantifiable structural and stratigraphic parameters to estimate the geometry and size of poorly exposed (i.e. in the field) or imaged (i.e. in the subsurface) growth folds.

2. Growth folding: key stratigraphic and structural concepts

2.1. Stratigraphic record of growth folds

Growth folds developed above the upper tips of normal faults have a marked impact on the evolving geomorphology of extensional basins, and thus, the architecture and distribution of synkinematic strata (e.g. Jackson and Leeder, 1994; Maurin and Niviere, 1999; Corfield and

Sharp, 2000; Sharp et al., 2000b; Corfield et al., 2001; Ford et al., 2007; Lewis et al., 2015). Synkinematic strata thus record the geometry and growth of growth folds (cf. Gawthorpe et al., 1997; Corfield et al., 2001; Patton, 2004; Lewis et al., 2015).

As growth folds grow above the tips of blind normal faults, synkinematic strata typically thin towards the fold crest and thicken basinwards (Gawthorpe et al., 1997; Gawthorpe and Hardy, 2002; Patton, 2004; Lewis et al., 2015; Fig. 4A). Unconformities develop towards and atop the fold; basinward of the fold these same unconformities pass into correlative conformities (Sharp et al., 2000b; Patton, 2004). The geometry and occurrence of these unconformities are principally controlled by the interplay of base-level and the structural relief related to growth folding (Burbank et al., 1996; Gupta et al., 1999; Corfield et al., 2001; Lewis et al., 2015; cf. Fig. 5).

During base-level rise, if the rate of fold amplification is less than the rate of rising base level, the synkinematic growth wedge will extend across the fold crest. When the rate of fold amplification is greater than the rate of base-level rise, the fold crest may be sub-aerially exposed and eroded, with strata within the synkinematic growth wedge onlapping onto the dipping fold limb and not extending across the fold crest (Gawthorpe et al., 1997; Gupta et al., 1999; Lewis et al., 2015). If synkinematic strata do not cover the entirety of the fold and/or erosion takes place, information about the fold geometry (and its growth) are not preserved in the rock record. This partially explains why the growth folds and the structural style of early rifts, particularly in continental settings, is poorly constrained (cf. Gawthorpe and Leeder, 2000).

Synkinematic base-level changes control not only control the architecture of synkinematic strata, but also their composition. For example, Lewis et al. (2015) suggest two end-member scenarios: (i) growth folding during base-level rise (Fig. 5A), and (ii) growth folding during

base-level fall (Fig. 5B). In the first scenario (Fig. 5A), fold growth occurs during periods of base-level rise and basin deepening. A wedge-shaped package of mudstone-dominated strata that onlaps and thins onto the fold is deposited at this time. Sandstone-dominated strata are deposited immediately after fold amplification, are tabular, and have a sharp contact with the underlying mudstone-dominated unit (Lewis et al., 2015). In the second scenario (Fig. 5B), fold growth occurs during periods of base-level fall and basin shallowing. During this time a wedge-shaped package of sandstone-dominated synkinematic strata that onlaps and thins onto the fold are deposited at this time. Mudstone-dominated strata are deposited immediately following fold growth, are isopachous, and have a sharp contact with underlying sandstone-dominated units (Lewis et al., 2015). In reality, the architecture of growth-fold related stratigraphy is not only dependent on changes in base-level and growth of the underlying causal fault, but also their interaction with rheological heterogeneities and neighbouring faults.

Growth folds in basins with rheological heterogeneities, such as thick salt, may show geometries and evolutionary modes that differ significantly from those formed in basins with largely homogeneous and brittle strata. During early extension, salt may inhibit the propagation of sub-salt faults mechanically decoupling them from, but being kinematically responsible for, forced folds in the supra-salt strata (e.g. Withjack and Callaway, 2000; Ford et al., 2007; Lewis et al., 2013; Ge et al., 2016; Jackson and Lewis, 2016; Coleman et al., 2017). The size and geometry of these supra-salt forced folds at this time depends, in part, on how throw varies along-strike on the causal sub-salt fault. Fold size (i.e. amplitude and width) is largest towards the fault centre where sub-salt throw is greatest, decreasing towards the fault tips (Fig. 1A in Corfield and Sharp, 2000; cf. Fig. 11 in Sharp et al., 2000b; Conneally et al., 2017).

As the sub-salt fault throw increases, the fold grows and salt typically flows along-strike below the supra-salt strata towards the location of maximum throw (Richardson et al., 2005). Supra-salt synkinematic depocentres are created in the hangingwall of the sub-salt faults, but because

148 of a combination of forced folding and inflating salt, they are offset some distance into the
149 hangingwall the fault and thin over the fold crest (Fig. 6A; Richardson et al., 2005). As the sub-
150 salt faults grow and their tips propagate laterally, not only does the forced fold lengthen, but the
151 sub-salt faults may interact with neighbouring sub-salt faults (Fig. 6B). Linkage of the sub-salt
152 faults may drive changes in the position of throw maximum on the longer fault system; this
153 may stimulate further along-strike flow of salt towards the newly formed high-displacement
154 fault centre (Richardson et al., 2005). Synkinematic depocentres associated with each of the
155 forced folds and their associated fault segments will subsequently merge to create a single,
156 larger depocentre (Fig. 6C). Synkinematic sediments within the newly formed, amalgamated
157 depocentre will then thin over the crest of the forced fold and salt swell (Richardson et al., 2005;
158 cf. Fig. 4A). Additional across-strike salt flow may further complicate stacking patterns within
159 synkinematic strata (cf. Duffy et al., 2013; Warsitzka et al., 2017), and may even mask changes
160 in base-level and accommodation, independent of regional extension (Duffy et al., 2013).

161 During the latter stages of fold evolution, in either salt-rich or salt-free settings, growth folds
162 may be breached as the upward propagating fault tip breaks-surface. At this point, a
163 hangingwall depocentre may form next to the fault and associated growth strata may thicken
164 towards the fault (e.g. Gawthorpe et al., 1997; Corfield and Sharp, 2000; Sharp et al., 2000a;
165 Kane et al., 2010; Duffy et al., 2013; Fig. 4B). Fold breaching may not by synchronous along
166 the full length of the fault, and instead, unbreached folds may pass along-strike into breached
167 folds (Fig. 4) (e.g. Gawthorpe et al., 1997; Gupta et al., 1999; Corfield and Sharp, 2000; Sharp
168 et al., 2000b; Corfield et al., 2001; Khalil and McClay, 2002; Willsey et al., 2002; White and
169 Crider, 2006; Lewis et al., 2013; Lewis et al., 2015; Khalil and McClay, 2016). Consequently,
170 the architecture and distribution of synkinematic strata may vary significantly along-strike
171 within the same extensional basin (Gawthorpe et al., 1997; Corfield and Sharp, 2000;
172 Richardson et al., 2005; Kane et al., 2010; Lewis et al., 2015).

173

174 **2.2. Secondary structures in growth folds**

175 Growth folds can accommodate a significant proportion of extensional strain. As these folds
176 grow, the style and distribution of associated fracture and fault populations will change (Fig. 7)
177 (e.g. Sharp et al., 2000a; Bonini et al., 2015; Tavani et al., 2018).

178 As a growth fold initially starts to form above a propagating normal fault (herein termed 'master
179 fault'), secondary normal and reverse faults deform the cover (e.g. Fig. 7 in Koopman et al.,
180 1987; Fig. 13 in Harvey and Stewart, 1998; Fig. 7 in Withjack and Callaway, 2000; Fig. 13 in
181 Jackson et al., 2006; Fig. 11A in Tavani et al., 2018). These secondary faults may nucleate at
182 the uppermost tip of the master fault and propagate upwards (e.g. Withjack et al., 1990; Mitra,
183 1993; Paul and Mitra, 2015), or nucleate in the folded cover and propagate downwards (Parfitt
184 and Peacock, 2001; Peacock and Parfitt, 2002; Martel and Langley, 2006; White and Crider,
185 2006), forming sigmoidal geometries with normal offsets at their base and reverse offsets at
186 their top (Sharp et al., 2000a; Sharp et al., 2000b; Jackson et al., 2006; Paul and Mitra, 2015;
187 Fig. 7D). Although reverse faults are common in physical models (e.g. Horsfield, 1977;
188 Withjack and Callaway, 2000; Paul and Mitra, 2015), bed-parallel stretching associated with
189 layer-parallel slip may annihilate these features locally and far-field stresses may sum to the
190 local stress.

191 As the fold amplifies, secondary faults are rotated, translated and become inactive as the dipping
192 fold limb steepens. To accommodate further strain within the fold, new secondary faults form
193 (e.g. Horsfield, 1977; Mitra and Islam, 1994; Patton et al., 1998; Berg and Skar, 2005; Jackson
194 et al., 2006; Tavani and Granado, 2015; Paul and Mitra, 2015; Tavani et al., 2018). These faults
195 often offset earlier-formed faults until they too deactivate and are offset, either by newly formed
196 faults or by the propagating master fault (e.g. Matthews and Work, 1978; Palmquist, 1978;

197 Patton et al., 1998; Sharp et al., 2000a; Berg and Skar, 2005; Fodor et al., 2005; Egholm et al.,
198 2007). These earlier faults, depending on their orientation and geometry, may even inhibit or
199 promote the propagation of the underlying normal fault to the surface (Bonini et al., 2015).

200 The location of and density of the secondary longitudinal normal and reverse faults through
201 time is directly related to the along-strike curvature of the growth fold, and the geometry and
202 displacement of the underlying master fault. The greater the along-strike curvature, the denser
203 the population of secondary longitudinal faults in the immediate hangingwall (Sharp et al.,
204 2000a; Jackson et al., 2006). The width of this secondary fault zone, normal to the fold hinge,
205 depends on the geometry of the growth fold and thus, the slip and dip of the underlying master
206 fault. Concerning the secondary faults striking parallel to the master fault, gently-dipping faults
207 produce broader folds and wider zones of fracturing compared to steeply-dipping faults
208 (Horsfield, 1977; Withjack et al., 1990; Willsey et al., 2002; Paul and Mitra, 2015). Cross faults
209 (cf. Destro, 1995) are also expected along the strike of the master fault to accommodate
210 variations in displacement. Dependent on the type of cover strata and their rheology boudinage,
211 sigmoidal veins and foliation textures may also develop to accommodate flexural slip along
212 bedding planes (Fig. 11 in Gross et al., 1997; Fig. 10 in Lynch et al., 1998; Sharp et al., 2000b;
213 Fig. 7A). Where flexural slip cannot take place, fracturing and faulting increases (cf. Couples
214 and Lewis, 1999; Fig. 7B - C).

215 In host rocks containing relatively thick layer–parallel detachments of salt or mudstone, gravity-
216 induced thin-skinned faults may develop during the latter stages of fold growth, when the
217 dipping fold limb become very steep (e.g. Fig. 3 in Withjack et al., 1989; Morley and Guerin,
218 1996; Sharp et al., 2000b; Withjack and Callaway, 2000; Fig. 9B in Jackson et al., 2006; see
219 also Stewart et al., 1997; Stewart, 1999; Stewart and Argent, 2000). As larger amounts of strain
220 are localised onto the detachment surfaces, the ductile units may become stretched and thin (cf.
221 'tectonic thinning' after Brown, 1988). If the detachment on the footwall thins sufficiently,

222 supra-detachment secondary normal faults may link at depth with the master fault (cf. Figs.
223 7D).

224 **2.3. Controls on the geometry and size of growth folds**

225 The geometry, size and occurrence of growth folds above propagating normal faults is widely
226 understood to be controlled by the interplay of structural factors (principally related to fault
227 geometry and size) and stratigraphic factors (principally related to the rheology and thickness
228 of the cover) (see below). Critically however, the relative importance of each of these structural
229 and stratigraphic factors upon the geometry and size of a growth fold is not well-constrained
230 and has been largely investigated through physical and numerical models (Fig. 8 and references
231 there-in). This is because: (i) we only observe the *final* geometry of natural growth folds ; (ii)
232 few examples of growth folds in nature are covered by high-resolution growth strata that permit
233 detailed analysis of the folds geometric evolution; (iii) a large number of inter-related factors
234 control the evolution of fold shape; and (iv) it is difficult to quantify some of these factors
235 because, for example, growth strata may not be preserved or the parameters themselves may
236 change through time (e.g. detachment thickness, the proportion of rheologically strong vs. weak
237 strata).

238 Structural factors relate to the kinematic and geometric evolution of the underlying fault, and
239 include the dip, throw, and shape of the fault, as well as the strain rate (controlling the fault tip
240 propagation and displacement rate). Stratigraphic factors relate to the mechanical behaviour,
241 thickness and rheology of the strata, and includes the confining pressure (depth of burial),
242 differential compaction, and rheological heterogeneity. The effect of each controlling factor on
243 the fold size and fold-shape-factor (the ratio of fold amplitude-to-width; FSF) is summarised in
244 Fig. 8. When the fold-shape-factor is greater than 1 (FSF > 1), the fold width is larger than its
245 amplitude. Where the fold-shape-factor is equal to 1 (FSF ~ 1), the fold width and amplitude

246 are the same. Where the fold-shape-factor is less than 1 (FSF < 1), the fold width is smaller
247 than the fold amplitude. We refer to FSF values significantly greater than 1 as 'large' or 'high',
248 whereas values close to 1 are referred to as as 'small' or 'low'. In the following section, we
249 review how each structural and stratigraphic factor influences the two-dimensional (2D)
250 geometry and size of the growth fold as the throw on the underlying fault increases.

251

252 **2.3.1. Influence of structural factors on the geometry and size of growth folds**

253 Prior studies show that structural factors strongly control the 2D geometry and size of growing
254 folds. Here, we summarise how the dip, throw and displacement rate of the fault, affects fold
255 geometry and size (Figs. 8A – C).

256 As a fault propagates towards the surface, fault dip plays an increasingly important role in fold
257 geometry (e.g. Horsfield, 1977; Tsuneishi, 1978; Vendeville, 1987; Richard, 1989; Withjack et
258 al., 1990; Koyi et al., 1993; Howard and John, 1997). Gently-dipping faults form wide folds
259 (high FSFs) with gently-dipping fold limbs, whereas steeply-dipping faults form narrow folds
260 (low FSFs) with steeply-dipping fold limbs (Fig. 8A). As there is a larger amount of rock
261 material in front of the propagating fault tip for gently-dipping faults compared to steeply-
262 dipping faults, all else being equal, a steeply-dipping fault will be break-surface earlier than a
263 gently-dipping fault (Fig. 9). Where the fault dip changes with depth, complex growth fold
264 geometries may develop. For example, if a fault propagates through a mechanically layered
265 sequence, 'flats' and 'ramps' may form in weak and strong layers, respectively, and forced folds
266 may form at multiple stratigraphic levels (Stewart et al., 1997; Lewis et al., 2013; Rotevatn and
267 Jackson, 2014; Gabrielsen et al., 2016; Vasquez et al., 2018; Deng and McClay, 2019; Serck
268 and Braathen, 2019).

Fault throw, in contrast to fault dip, controls not only the fold geometry but also size. As throw increases, so does the fold amplitude and width; as a result, FSF changes through time (e.g. Fig. 4 in Horsfield, 1977; Fig. 5 in Ameen, 1988; Fig. 4 in Withjack et al., 1990). Small throws are associated with small folds with high FSFs, whereas large throws are associated with large folds with low FSFs (e.g. Horsfield, 1977; Patton et al., 1998; Fig. 8B). If the throw becomes too large, eventually the fold will be unable to accommodate any further strain and will be breached (e.g. Fig. 7 in Withjack and Callaway, 2000; cf. Fig. 4B). Once breached, folding ceases.

Similar to fault throw, the displacement rate of the fault (which may be linked to the propagation rate of the upper fault tip) can control not only the shape and size of a growth fold, but also whether a such structures form at all (e.g. Allmendinger, 1998; Withjack and Callaway, 2000; Cardozo et al., 2003; Finch et al., 2004; Jin and Groshong, 2006; Ford et al., 2007; Hardy and Allmendinger, 2011; Carola et al., 2013; Tavani and Granado, 2015; Deckers, 2015; Wilson et al., 2015). Slowly-propagating faults form wide folds with high FSFs as they take longer to breach the cover, hence more folding occurs (e.g. Fig. 11A in Withjack and Callaway, 2000). For example, low propagation rates are required in the Rhine Graben to form forced folds (Ford et al., 2007). In contrast, rapidly-propagating faults form narrow folds with low FSFs and in some cases, may propagate so quickly through their cover that growth folds do not develop at all (Fig. 8C) (e.g. Fig. 10 vs. 11 in Withjack and Callaway, 2000).

Growth folds should thus be common in basins where the upper tip propagation rate of individual faults is slow, and rare in basins with rapidly-propagating faults. Growth folds may therefore be more common in rifts forming in response to low strain rates. We may hypothesise that rapidly-extending basins (cf. Nicol et al., 1997; Meyer et al., 2002; Mueller, 2017) will be associated with rapidly slipping and propagating fault, and few growth folds. In contrast, slowly-extending basins may be prone to slower slipping and propagating faults, and thus more growth folds. Importantly, the presence of mechanically weak barriers to fault propagation, such

294 as shale or salt (e.g. Morley and Guerin, 1996; Maurin and Niviere, 1999; Duffy et al., 2013;
295 Jackson and Lewis, 2016; Coleman et al., 2017), may result in slowly-propagating faults, and
296 thus favour the development of growth folds, even within rapidly extending basins. This is due
297 to deformation energy being dissipated over larger rock volumes via ductile processes (e.g.
298 layer parallel slip). The rheological behaviour of these mechanical barriers is dependent on the
299 strain rate (cf. Withjack and Callaway, 2000).

300 We may also expect the prevalence of growth folds will vary temporally and spatially within
301 an extensional fault array. For example, during rift initiation, where regional strain is distributed
302 over a large number of isolated faults, each with relatively low fault-propagation rates, growth
303 folds may be common across the rift. On the other hand, during rift climax, where regional
304 strain is not only localised onto a few, well-connected large faults, but also towards the rift axis
305 (Cowie, 1998; Gupta et al., 1998; Cowie et al., 2000; Gawthorpe and Leeder, 2000; Cowie et
306 al., 2005), growth folds may be expected to develop in the strain shadows of larger faults or
307 abandoned faults away from the strain locus, perhaps towards the rift margins.

308

309 **2.3.2. Influence of stratigraphic factors on the geometry and size of growth folds**

310 Stratigraphic factors also control the geometry and size of growth folds. Here, we summarise
311 the influence of the rheology and thickness of the cover, the detachment thickness, and the
312 confining pressure (depth of burial) on fold growth (Figs. 8D – G).

313 As a fault tip propagates upwards, it may encounter ductile as well as brittle lithologies within
314 the folded cover sequence. These rheological variations have a profound impact on the style
315 and magnitude of growth folding. For example, cover comprising weak, ductile rocks, such as
316 salt or overpressured shale, typically produce wider folds (high FSFs) than those in brittle
317 sequences (low FSFs) (Withjack et al., 1990; Withjack and Callaway, 2000; Finch et al., 2004;

318 Fig. 8D). As rheologically-weak strata tend to inhibit the upward propagation of a fault (e.g.
319 Nicol et al., 1996; Couples and Lewis, 1999; Corfield and Sharp, 2000; Wilkins and Gross,
320 2002; Benedicto et al., 2003; Soliva and Benedicto, 2005; Soliva et al., 2005; Lăpădat et al.,
321 2016), folding lasts longer (with all else being equal) and the fold is breached later (compared
322 to a brittle-cover only scenario). Thus, growth folds in rheologically-weak cover may be large
323 and well-developed, whereas growth folds developed in homogeneous, rheologically-strong
324 cover sequences (e.g. in volcanic basins) are likely to be small and relatively rare. Given that
325 rheological variations in the cover can control the geometry and size of growth folds, it follows
326 that cover with rheological heterogeneities such as multiple salt or shale layers, may be
327 expected to produce broader folds (high FSFs) as the fault tip becomes temporarily arrested by
328 each of the mechanical barriers. However, these hypotheses remain untested.

329 In addition to its rheology, the thickness of the cover also controls fold geometry and shape
330 (Fig. 8E). Where the cover is thin, less folding is expected as there is a smaller rock volume
331 ahead of the propagating fault tip. In this case the propagating fault also takes a shorter time to
332 breach the fold compared to when the cover is thick (e.g. Allmendinger, 1998). Furthermore,
333 physical (Withjack and Callaway, 2000) and numerical models show thin cover typically
334 produces narrow, poorly-developed folds (i.e. low FSFs) whereas thick cover is associated with
335 wide, well-developed folds (i.e. high FSFs). Although these findings are commonly shown in
336 models, it is unknown if these concepts apply to natural systems.

337 Cover with very thin detachments (i.e. rheologically weak strata) do not significantly inhibit
338 fault tip propagation, thus growth folds developed in such systems tend to be narrow, poorly-
339 developed and have low FSFs (Fig. 8F). On the other hand, thick detachments generate wide,
340 well-developed folds with high FSFs, as detachments buffer displacement and tip propagation
341 on the underlying fault (Richard, 1991; Vendeville et al., 1995; Withjack and Callaway, 2000;

342 Stewart, 2007; Lăpădat et al., 2016; Hardy, 2018). This prediction, largely derived from
343 physical models (see Hardy, 2018, for an exception), has never been tested in nature.

344 The final stratigraphic factor that influences fold geometry is confining pressure (Fig. 8G) (e.g.
345 Friedman et al., 1976; Weinberg, 1979; Bartlett et al., 1981; Koyi et al., 1993; Patton et al.,
346 1998; Schöpfer et al., 2007). As a growth fold is buried and the confining pressure increases,
347 the rocks within the cover progressively compact and the rheology changes. Patton et al. (1998)
348 (their Fig. 7) show that the same cover lithology, under different confining pressures, can lead
349 to significant changes in the fold width. Shallowly-buried folds at low confining pressures are
350 typically narrower (low FSFs) than deeply buried folds at higher confining pressures (high
351 FSFs). This occurs as the bulk ductility of the cover and zone of microfracturing increases with
352 higher confining pressures (Patton et al., 1998). Given that the hangingwall and footwall fault
353 blocks lie at different depths with different confining pressures, the rheology of the cover may
354 be different across the fault. For example, across-fault differential compaction may alter the dip
355 of beds defining the middle limb of the growth fold. In the shallowly-buried footwall where
356 compaction is less, the dips are gentler, whereas in the deeply-buried hangingwall, compaction
357 is greatest and the dips are steeper (Jin et al., 2009). Furthermore, burial-related differential
358 compaction, along after faulting and folding has ceased, will also influence fold shape, typically
359 resulting in a decrease in fold amplitude (e.g. Skuce, 1996; Færseth and Lien, 2002).

360

361 **3. Quantitative Comparative Analysis to Identify Relationships Between Growth Fold**
362 **Parameters**

363 To investigate whether structural and stratigraphic parameters inferred to control fold geometry
364 in nature and models are common to growth folds independent of scale, we have measured and
365 quantitatively compared several geometrical parameters (as defined in Fig. 3) from published

examples of growth folds. In cross-section, the *amplitude* and *width* are determined by the vertical and horizontal distances between the 'toe' and 'head' of the fold, respectively. The toe is defined as the point at which a marker bed meets the regional datum on the hangingwall of a normal fault. The head is defined as the point where a marker bed drops below the regional datum on the footwall of a normal fault. As previously mentioned, the *fold-shape-factor* (*FSF*) is the ratio of the amplitude-to-width; this parameter is used to quantitatively compare fault-propagation *and* forced folds, irrespective of their scale. High *FSF* values (e.g. FSF = 5) indicate the fold width is significantly larger than its amplitude, whereas low values (e.g. FSF = 1.1) indicate the fold width is only marginally greater than its amplitude (e.g. Figure 3). The *prekinematic thickness* is the supra-basement stratigraphic thickness of the largely tabular, isopachous strata deposited prior to extension. For forced folds, the detachment thickness is the stratigraphic thickness of the detachment layer that separates folded strata above and faulted strata below. Where applicable, the *cover-detachment* (*C:D*) ratio (prekinematic thickness/detachment thickness) is used to quantitatively compare forced folds, irrespective of their scale. *C:D* ratios greater than 1 indicate the prekinematic cover is thicker than the detachment thickness, whereas *C:D* ratios less than 1 indicate that the detachment thickness is thicker than the prekinematic cover thickness. *Fault dip* is measured from the underlying master fault. *Fault throw* is the vertical change in elevation of a prekinematic marker bed across a fault; for forced folds, throw is measured immediately below the detachment.

3.1. Structural and stratigraphic controls on growth fold geometry from nature and models

We conducted quantitative comparative analysis of parameters measured from published cross-sections oriented perpendicular to the underlying master fault for c. 600 fault-propagation folds (Fig. 10; Appendix B) and c. 300 forced folds (Fig. 11; Appendix C). The resulting global

dataset characterises fault-propagation and forced folds from extensional settings (see Appendices D – E for all measured data). Without growth strata, the kinematic evolution of these growth folds is difficult to constrain. However, by compiling this database of fault-propagation and forced folds of different sizes and shapes, and at different stages of their development (Table 1), we can assess the dynamics of these structures. We can also predict the parameters and geometry for folds that are poorly-imaged in seismic reflection data or only partly preserved or exposed in the field.

For each fold, numerous geometrical parameters were recorded (Fig. 3). Measurements of geometrical parameters from models and natural examples all have uncertainties; however, only high confidence examples have been used for the statistical analysis, and the associated uncertainties have been noted and are presented (see Appendix F for the full details).

3.1.1. Regression analysis: first-order controls on growth fold geometry and relationships between straigraphic and structural factors

The extensive dataset features >150 different localities and >800 examples, each with its own unique tectonic parameters (e.g. strain rate, lithology, overall tectonic setting) allowing us to compare geometrical characteristics of growth folds in volcanic and sedimentary extensional systems. By doing this we can try to isolate the primary controls on the geometric and kinematic evolution of growth folds in two-dimensions.

Relationships between these parameters are investigated in a series of cross plots (Figs. 12 – 13), which show best-fit lines generated by least-square regression methods for moderate-strong correlations (moderate coefficient of determination, $R^2 = 0.5 – 0.8$; strong coefficient of determination, $R^2 = 0.8 – 1.0$). Equations describing best-fit lines between parameter pairs showing a moderate-strong correlation are shown in Table 2. Best-fit lines have been plotted

using linear, and power-law functions. The function that shows the best-fit to the data, characterised by the highest R^2 value, has been selected for each parameter pair.

We observe two types of relationships between parameters. The first type comprises positive and negative correlations between parameters from related domains (e.g. fold amplitude vs. fold-shape-factor). The second type comprises positive and negative correlations between parameters from unrelated dimensional domains (e.g. amplitude vs. prekinematic thickness). The second type of relationship is more meaningful, given it highlights potential links between parameters that are not genetically related. The presence of several moderate – strong correlations between these parameters in our database is remarkable in its own right, as it indicates that growth folds at different scales, in different extensional settings and with varying lithological heterogeneity, can be described quantitatively by our regression equations. These equations are potentially powerful tools that enable estimation of unknown parameters by utilising other known parameters extracted from folds. Although these equations are constrained by an extensive database of studied growth folds, these equations must be further tested as future studies come to light, especially at outcrop scale ($<10^2$ m), where fewer examples exist.

3.1.1.1. Fault-propagation folds

Natural fault-propagation folds show moderate-to-strong correlations between: (1) fault throw and fold amplitude, (2) fault throw and fold width, (3) prekinematic thickness and fold amplitude, (4) prekinematic thickness and fold width, (5) fold amplitude and width (Table 1; Figs. 12A - E). These correlations suggest that the fault throw and thickness of the prekinematic strata cover control the size of the fold, and thus, large throws generate large fault-propagation fold amplitudes and widths.

439 Physical models show that fault throw and fold amplitude are moderately correlated for fault-
440 propagation folds (Table 1; Fig. 12F), similar to natural examples. This suggests that fault throw
441 is the principal control on fold amplitude.

442 Numerical models show strong correlations between: (1) fault throw and fold amplitude, (2)
443 fault throw and fold width, (3) prekinematic thickness and fold amplitude, (4) prekinematic
444 thickness and fold width, and (5) fold amplitude and fold width. In other words, these
445 correlations suggest that large fault throws and thick prekinematic cover generate large, wide
446 folds with large amplitudes (Table 1; Fig. 12H – L), similar to the natural examples, but
447 somewhat different to that observed in physical models.

448

449 **3.1.1.2. Forced folds**

450 Natural examples of forced folds show moderate-to-strong correlations for: (1) fault throw and
451 fold amplitude, (2) fault throw and fold width, (3) prekinematic thickness and fold amplitude,
452 (4) prekinematic thickness and fold width and (5) fold amplitude and fold width, similar to
453 fault-propagation folds (Table 1; Figs. 13A – B, E - G). In addition, forced folds also shown
454 moderate-to-strong correlations for (6) detachment thickness and fold amplitude, and (7)
455 detachment thickness and fold width (Figs. 13C - D). These correlations suggest that large fault
456 throws, a thick prekinematic cover, and a thicker detachment produce larger folds.

457 Physical models of forced folds lack moderate-to-strong correlations between fault, fold and
458 stratigraphic geometrical parameters. This suggests that no single measured fault- or
459 stratigraphic-related parameter controls the amplitude and width of the forced fold, at least for
460 the physical model examples. To the best of our knowledge, only Hardy (2018) has modelled
461 forced folds numerically; a quantitative analysis of such a small sample size would not thus be

appropriate. Fault-propagation fold numerical models based on the concept of trishear (Ford et al., 2007) have also not been included in our analysis.

3.1.2. Principal Component Analysis (PCA): identifying relationships between stratigraphic and structural factors

We used principal component analysis (PCA) to investigate whether the quantitative relationships identified in the regression analyses are reasonable, not only for models but also for naturally occurring systems. Application of PCA also allowed us to assess whether data scatter is obscuring trends between structural and stratigraphic factors. PCA simplifies the complexity of high-dimensional multi-variate data, such as our growth fold dataset (Appendices D – E), while retaining trends and patterns (e.g. Jolliffe, 1993; Jolliffe, 2002; Ringnér, 2008; Abdi and Williams, 2010; Josse and Husson, 2016; Lever et al., 2017). PCA thus allows us to identify possible relationships between growth fold parameters that are non-linear, or at least, very complex.

Here, we briefly describe PCA but for further details, see Appendix G – H. All data are plotted in multi-dimensional space as a "cloud" **(**cf. Fig. 14A**)**. The direction of the most significant data variation is then calculated (the red lines on Fig. 14A), and the growth fold parameters associated with the data variation (i.e. variables that broadly correlate with one-another) are then grouped as a "principal component" (PC). A PC may consist of any number, or some part of a variable. Variables that do not correlate may be then grouped into individual PCs until all of the data variation is accounted for **(**cf. Fig. 14B**)**. Furthermore, the number of principal components may be less or equal to, the number of variables in the dataset and typically reduces the number of dimensions. Using the first and second PC (PC1 and PC2, respectively) as axes, which account for the majority of data variation, the data may be projected (cf. Fig. 14C**).** Where

data variations correlate with PC1, the arrow is parallel to the axis. Where data correlate with PC2 opposed to PC1, the arrow is parallel to the PC2 axis and perpendicular to the PC1 axis. Where the arrow is not parallel to either axis, the growth fold variable may be either partially associated with both PCs (and the comprised variables) or neither, and instead, is due to the projection. The length of the arrows represents the projection of the data relative to PC1 and PC2 axis. If the arrow for a particular variable is short, the data is out-of-plane relative to PC1 and PC2. If the arrow is long, the data is in-plane **(**Fig. 14C**)**. With this information, we can then determine which parameters are correlated and speculate a geological reasoning for the relationship. Where missing values for particular parameters are missing (i.e. data gaps), then a best-fit, iterative value is used to fill in the record (as discussed in Appendix H) and the uncertainty in the PCs is shown **(**cf. Fig. 14D**)**. Where the shaded area on Fig. 14D is relatively small, the uncertainty is also small. Where the shaded area is relatively large, the uncertainty is also large and the position of PC1 and PC2 through the data "cloud" (for example, on Fig. 14A) is uncertain. A full description of the PCA method is described in Josse and Husson (2016).

3.1.2.1. Fault-propagation folds

In natural examples of fault-propagation folds, the first three PCs account for 85% of total data variation (Fig. 15A). The first PC comprises the amplitude and width of the fold, the thickness of the strata and the underlying fault throw, whereas the second and third PCs describe the dip of the fault and the fold-shape-factor. The percentage of total variation accounted for by each of the first PCs are 52%, 21% and 12%, respectively. In other words, our analysis indicates that the thickness of the prekinematic cover and fault throw likely control the fold amplitude and width, whereas fault dip controls the *relationship between* fold amplitude and width.

509 In physical models, principal components 1 – 3 account for 78% of the data variance (Fig. 15B).
510 PC1 comprises the prekinematic thickness and fold size parameters, PC2 comprises of fold
511 shape and fault dip and throw, and PC3 comprises prekinematic thickness, fold shape and fault
512 throw. The percentage of total variation accounted for by each of the first PCs are 38%, 24%
513 and 16%, respectively. These results indicate that the thickness of the prekinematic cover
514 controls fold amplitude and width, whereas the dip and throw of the fault controls the width
515 and thus, the *relationship between* fold amplitude and width.

516 In numerical models, the first three principal components account for 93% of the data variance
517 (Fig. 15C). The percentage of total variation accounted for by each of the first PCs are 63%,
518 19% and 11%, respectively. PC1 describes fault throw and dip, prekinematic thickness, and fold
519 size. PC2 describes fold shape, width and fault dip. PC3 is associated with fault dip only.
520 Furthermore, the dip and throw of the underlying fault and thickness of the prekinematic cover
521 control the fold size, whereas the fault dip controls the fold width and thus, the *relationship*
522 *between* the fold width and amplitude.

523

524 **3.1.2.2. Forced folds**

525 In natural examples, the first three principal components account for 74% of total data variation
526 (Fig. 16A). The first PC comprises the fold amplitude, width, the thickness of the cover and the
527 fault throw, whereas the second PC describes the fold shape and fold width, and the dip of the
528 fault. The third PC comprises of the fold amplitude and width, and the cover thickness. The
529 percentage of total variation accounted for by each of the first PCs are 36%, 23% and 15%,
530 respectively. Our analysis indicates that the fault throw and the cover thickness controls the fold
531 size, whereas the dip of the fault controls the width of the fold and thus, the relationship between
532 fold width and amplitude.

In physical models, principal components 1 – 3 account for 71% of the total data variance (Fig. 16B). The percentage of total variation accounted for by each of the first PCs are 30%, 23% and 18%, respectively. The first PC comprises of the cover thickness, fold shape and fold width, whereas the second PC comprises of the fold amplitude and width, and fault throw. The third PC consists of the dip of the fault, the thickness of the cover and the proportion of ductile lithologies in the cover. In other words, the thickness of the cover and the fault throw control the shape and the size of the forced fold. The dip of the fault, in contrast to the natural examples, is not a major factor on fold shape or size.

4. Physical and numerical models as analogs for growth folds in nature

By comparing the correlations between structural and stratigraphic parameters from our regression (Figs. 12 – 13) and principal component analysis (Figs. 15 – 16), we can now investigate whether physical and numerical models accurately describe growth folds in nature.

In physical models, the degree to which and the structural and stratigraphic factors control fold geometry, and the relative importance of these factors, varies substantially (i.e. there is a high amount of scatter and weak correlations between fault-fold parameters; Table 2). For example, only fault throw and fold amplitude are moderately correlated for physical models of fault-propagation folds (Fig. 12F), whereas there are no moderate-to-strong correlations for physical models of forced folds. This could be due to the extensive range of material types (and their relative rheologies) used to simulate cover rocks (e.g. sand, wet clay, gypsum powder, limestone) and intra-stratal detachment (e.g. silicon, asphalt, wax, oil, clay), and the temporal and spatial scaling used in the models (see Koyi, 1997; Panien et al., 2006; Schreurs et al., 2006; Schellart and Strak, 2016, for a discussion on the variability associated with physical modelling approaches).

When any one individual model of a growth fold is taken in isolation, the correlations between structural and stratigraphic factors and fold geometry is similar to that observed in nature. For example, fold amplitude increases with throw for fault-propagation (Fig. 17A) and forced folds (Fig. 17B). However, when all models are analysed together, the correlations are weaker or apparently, non-existent due to the large data variance (Fig. 17). Thus, for a physical model to be an appropriate analogue to a natural example, the rheologic, stratigraphic and structural parameters must be broadly equivalent; not all physical models will be appropriate for comparing the geometry and size of natural examples, especially their evolution through time.

Purely kinematic models, where rock properties are not incorporated in the model (e.g. Erslev, 1991; Hardy and Ford, 1997; Cardozo et al., 2011), and mechanical models, where rock properties are incorporated (e.g. Finch et al., 2004; Hardy and Finch, 2006; Egholm et al., 2007; Hardy and Finch, 2007; Figs. 12F – L), produce very similar geometrical relationships to fault-propagation folds in nature (Figs. 12A – E). The similar correlations identified for both kinematic and mechanical models, and natural examples of fault-propagation folds, suggest that cover rheology is not as important as fault throw and cover thickness in determining fold shape and size. In addition, the correlations between structural and stratigraphic factors in numerical models and nature (e.g. fault throw vs. fold amplitude, prekinematic thickness vs fold amplitude, etc.) suggest that the final geometry of a growth fold may be accurately predicted by a model (cf. Cardozo et al., 2011). However, the two-dimensional geometric and kinematic evolution of growth folds in nature remains poorly-constrained, especially in areas lacking high-resolution growth strata.

5. Geometrical evolution of growth folds in response to increasing extensional strain

579 Having established the two-dimensional geometrical relationships between the geometry of the
580 growth fold, the underlying propagating normal fault and the thickness of the cover, we now
581 investigate how fault-propagation and forced folds grow with increasing displacement on the
582 underlying fault. Given that we can only measure the final, present-day geometry of natural
583 folds, we cannot know how these folds grew with increasing extensional strain. Physical and
584 numerical models therefore provide snapshots of the growth fold geometry at different fault
585 displacements (cf. Hardy and McClay, 1999; Ford et al., 2007; Cardozo et al., 2011). In this
586 section, we use published models of growth folds above upward propagating normal faults to
587 investigate how each of the controlling factors (cf. Fig. 8) affect two-dimensional fold geometry
588 and size through time (Figs. 18 – 21). In all cases, only a single controlling factor is changed
589 (i.e. throw is plotted against amplitude and the fold-shape-factor for each variable). Essentially,
590 these plots show how the two-dimensional shape of the fold (fold amplitude and width) varies
591 as throw is accrued on the causal fault. For example, we can see that the two-dimensional shape
592 of fault-propagation folds developed in relatively weak or rheologically heterogeneous cover
593 (Fig. 18A; cf. Withjack et al., 1990) in physical models is different to that of fault-propagation
594 folds in relatively strong cover. Fault-propagation folds are typically wider in weak cover
595 compared to strong cover. The same is also true for numerical models of fault-propagation folds
596 (Fig. 19A), and for physical models forced folds (Fig. 20A; 20E).

597 In summary, these plots show that weak or rheologically heterogeneous cover (Figs. 18A; 19A;
598 20A; 20E), higher confining pressures (i.e. greater burial depths; Fig. 18C), increased
599 proportions of ductile material in the cover (Fig. 20E; 21A) and thick cover thicknesses (Figs.
600 19D; 20D), together with gently-dipping faults (Figs. 18B; 19C; 20C; 21B), low fault
601 propagation tip rates (Fig. 19B) and low regional strain rates and displacement rates (Fig. 20B)
602 produce wide folds in physical (Ameen, 1988; Richard, 1989; Withjack et al., 1990; Withjack

603 and Callaway, 2000; Miller and Mitra, 2011) and numerical models (Allmendinger, 1998;
604 Hardy and McClay, 1999; Finch et al., 2004; Hardy, 2018).

605 In all cases, folds initially have relatively high FSF values as final fold widths are established
606 very early during fold growth and remain largely constant throughout. In contrast, fold
607 amplitude increases gradually as throw accrues on the underlying normal fault – as exemplified
608 in Fig. 22. Therefore, the initial (and largest) FSF that develops is controlled by the structural
609 and stratigraphic factors that control fold width. As the fold grows and amplitude slowly
610 increases as throw accrues on the underlying fault, the FSF gradually decreases (Figs. 18 – 21).
611 But is the same also true for natural examples of growth folds? To assess this, we draw upon
612 several natural examples from the Halten Terrace and Egersund Basin, offshore Norway, and
613 Gulf of Suez, Egypt, where high-resolution strata provide a snapshot of the geometry and size
614 of these growth folds through time.

615 On the Halten Terrace, a relatively long-lived (<60 Myr), <10 km wide and <2 km amplitude
616 growth fold is preserved above a basement-involved normal fault (Corfield and Sharp, 2000;
617 Corfield et al., 2001). Here, synkinematic strata of the Jurassic, the Garn and Melke formations,
618 progressively onlap onto the growth fold, recording changes in its syn-depositional geometry.
619 Observations from Corfield et al. (2001), shown in Fig. 23, indicate the earliest synkinematic
620 unit (unit 1 of the Garn Fm) is thickest in Well 6505/12-10 (Smørbukk Nord) and pinches out
621 towards wells 6506/12-5 (Smørbukk Sør) and 6506/11-2 (Smørbukk Sør-Vest). This indicates
622 that growth folding likely started during the deposition of the Garn Formation (c. 170 Ma). By
623 assuming that the depocentre position is indicated by the thickest part of the Garn Formation,
624 the axis of the hangingwall syncline was c. 6 – 8 km west of the Smørbukk-Trestakk Fault. The
625 overlying Melke Formation (c. 164 Ma) is also thickest in the same location i.e. Well 6506/12-
626 10 (Fig. 23A), suggesting the depocentre did not migrate as the fold grew and the near-final
627 fold width was established very early during fold growth (i.e. within the first c. 6 Myr of

628 folding). This suggests that growth folds in models (e.g. Fig. 18 – 21) show a similar geometric
629 evolution to those in nature (Fig. 23) (i.e. they widen relatively early during fold growth; Path
630 2 on Fig. 24).

631 The near-final fold width is also established during early fold growth in other locations. For
632 example, Jurassic-to-Cretaceous growth strata next to the Stavanger Fault System, Egersund
633 Basin, offshore Norway are thickest in a synclinal, syndepositional depocentre located c. 5 km
634 basinward of the controlling normal fault (Fig. 5C and Fig. 8B-C in Lewis et al., 2013). This
635 depocentre remained in the same position throughout a protracted period (c. 65 Myr from Fig.
636 8D in Lewis et al., 2013) of fold growth. Early widening is also observed in the Gulf of Suez,
637 Egypt where the earliest synkinematic strata (the Abu Zenima and Nukhul formations; c. 21
638 Ma) are thickest in the centre of the El Qaa syncline and thin towards the Baba-Sidri Fault (see
639 Fig. 2 in Gawthorpe et al., 1997; Fig. 4). This suggests that the depocentre was located c. 2 km
640 outboard of the Baba-Sidri Fault during the first c. 2 Myr of folding until rift climax in the
641 Rudeis Formation (Lewis et al., 2015; c. 15 Ma), being fixed in this position until the fault
642 breached the surface. Given this understanding of how folds widen early, this raises the question
643 of how fold amplitude then changes with increasing strain?

644 In contrast to fold width, fold amplitude is more difficult to discern based on synkinematic
645 strata alone. This is largely because, depending on the interplay of base-level (eustasy) and
646 structural relief, and whether the footwall is prone to erosion, synkinematic strata may not cover
647 the fold crest (cf. Patton, 2004; Lewis et al., 2015; Fig. 5). In the Halten Terrace example (from
648 Corfield and Sharp, 2000; Corfield et al., 2001), the fold amplitude through time is poorly
649 constrained. However, physical (e.g. Horsfield, 1977; Tsuneishi, 1978; Withjack et al., 1990;
650 Withjack and Callaway, 2000) and numerical models (e.g. Finch et al., 2004; Hardy, 2011;
651 Smart and Ferrill, 2018), as well as studies of natural structures (e.g. Lăpădat et al., 2016;
652 Conneally et al., 2017), suggest that fold amplitude is similar to fault throw, and that both

653 increase in concert. Moreover, the rate at which a fold amplifies is likely dependent on the fault
654 displacement rate. For the Halten Terrace example (cf. Corfield and Sharp, 2000; Corfield et
655 al., 2001) this means that the rate of increase in the fold amplitude likely reflected the
656 displacement rate on the underlying Smørbukk-Trestakk Fault. Temporal changes in fault
657 displacement rate are reported from a number of faults from basins worldwide (e.g. Nicol et al.,
658 1997; Nicol et al., 2005; Jackson, 2018), so it is possible that the rate at which the fold amplifies
659 may correspondingly vary through time. For salt-rich settings or basins with rheological
660 heterogeneities, if the detachment flow rate in the cover rocks is different to the fault
661 displacement rate, the fold amplification rate may not increase in concert with fault throw.

662 **6. Discussion**

663 **6.1. How do fault-propagation and forced folds grow?**

664 We define a *growth fold pathway* as the track that an evolving fault-propagation or forced fold
665 takes as it amplifies and widens on Fig. 24. Growth fold pathways provide important insights
666 into fold growth and allows us to predict the 2D geometry and size of growth folds through
667 time. When plotted together, we observe a relationship between fold amplitude and width,
668 suggesting these increase together as the underling fault accumulates displacement (Path 1 on
669 Fig. 24A. However, it is striking that in the physical, mechanical and kinematic models (cf.
670 Ameen, 1988; Richard, 1989; Withjack et al., 1990; Patton et al., 1998; Hardy and McClay,
671 1999; Withjack and Callaway, 2000; Finch et al., 2004; Miller and Mitra, 2011; Figs. 18 - 21;
672 22A - B), this is not the case. In these models we instead see how the final fold width is
673 established relatively early during fold growth, when the fold amplitude (and underlying fault
674 throw) is small (see the dashed lines on Figs. 9, 18 – 21). As fault displacement increases so
675 does the the fold amplitude, whereas the fold width remains largely constant (Path 2 on Fig.
676 24A). These growth fold pathways help explain how natural examples of fault-propagation and

677 forced folds may evolve in extensional settings (e.g. the Halten Terrace, offshore Norway, in
678 Fig. 23). Furthermore, when seismic imaging or exposure is poor (cf. Botter et al., 2014), high-
679 resolution growth strata are not available (such as during sub-aerial continental rifting -
680 Gawthorpe and Leeder, 2000; Patton, 2004), or there is not an appropriate physical or numerical
681 model, these pathways may be used to make quantitative estimates for fold geometry and size
682 through time in 2D.

683 So far, we have discussed the geometry and evolution of fault-propagation and forced folds in
684 2D. However, growth folds change shape and size along- and across-strike. Changes in the 3D
685 geometry of growth folds is thus dependent on the 3D geometry and growth of the underlying
686 master fault (Fig. 25). If the fault lengthens whilst it accumulates displacement (Fig. 25A; i.e.
687 the 'isolated fault model' – e.g. Walsh and Watterson, 1988; Dawers and Anders, 1995; Fig. 4A
688 in Jackson et al., 2017), the overlying growth fold will also lengthen with time. Alternatively,
689 if the fault rapidly lengthens before accumulating displacement (i.e. the 'constant-length fault
690 model' - e.g. Childs et al., 1995; Meyer et al., 2002; Walsh et al., 2003; Jackson and Rotevatn,
691 2013; Tvedt et al., 2016; Fig. 4B in Jackson et al., 2017), the length of the overlying growth
692 fold may be very large for a relatively small amount of displacement on the underlying fault
693 (Fig. 25B). Regardless of the preferred fault growth model (i.e. isolated vs constant-length), the
694 fold will eventually be breached. This increase in displacement rate and ultimate fold breaching
695 reflect an increase in the regional extension rate (cf. Nicol et al., 1997; Hardy and McClay,
696 1999; Meyer et al., 2002; Mueller, 2017), or simply a local increase in displacement rate as
697 strain becomes focused onto larger, well-connected faults during the latter stages of extension
698 (e.g. Gawthorpe and Leeder, 2000; Cowie et al., 2005; Finch and Gawthorpe, 2017).

699

700 **6.2. What are the differences between how fault-propagation and forced folds grow?**

Given that fault-propagation and forced folds have different shapes and sizes for a given throw on the underlying fault, their growth pathways may be different. For example, forced folds appear to have larger amplitudes (Fig. 26A) and widths (Fig. 26B) for a given fault throw than fault-propagation folds. Although in part, scatter in the database could explain the differences between fault-propagation and forced folds, we do observe several examples where along- and across- flow of salt or shale has clearly altered the two-dimensional geometry of a fold (cf. Fig. 2A; B). For example, as a forced fold grows, salt may move from the hangingwall into the footwall during extension (Koyi et al., 1993; Burliga et al., 2012). The rate of salt flow may be enhanced by sediment loading (e.g. the Cormorant structure, Jeanne d'Arc Basin - Withjack and Callaway, 2000; cf. Warsitzka and Kukowski, 2015; Warsitzka et al., 2017), causing the fold amplitude to increase (Fig. 24F) more rapidly than a fault-propagation fold. In addition, the fold amplitude may increase very rapidly compared to fold width, and more rapidly than a fault-propagation fold. Alternatively, salt may flow laterally away from a pre-existing sub-salt step in the basement (Fig. 24G), creating a 'withdrawal drape fold' (Fig. 16 in Withjack and Callaway, 2000; cf. Fig. 1), and *not* a growth fold. As salt is evacuated from beneath the supra-salt strata in the hangingwall, the rate at which the withdrawal drape fold amplifies may vary relative to growth folds (cf. Fig. 24F-G); withdrawal drape folds are geometrically similar and may grow in very similar way to true forced folds (cf. Path 2 on Fig. 24A).

Forced folds tend to have larger fold amplitudes and widths compared to fault-propagation folds (Figs. 26C - D) for the same total cover thickness (i.e. the thickness of the detachment and the prekinematic cover). Richard (1989) and Hardy (2018) show that as the thickness of the detachment is increased relative to the prekinematic thickness (i.e. the detachment content of the cover increases, and the C:D ratio decreases), growth folds are wider for a given fold amplitude and fault throw (Figs. 20E; 21A). This behaviour might be because, as the overall

cover is weakened (by the introduction of ductile material), extensional strain may be distributed over a wider area (cf. Fig. 8D).

6.3. What controls the occurrence of growth folds?

Why do growth folds occur in some basins but not others? Prior studies (e.g. Corfield and Sharp, 2000; Ford et al., 2007) highlight two key factors that may induce growth folding: (i) the presence of weak lithologies or mechanical heterogeneities in the cover, and (ii) low displacement (and low upper tip fault propagation) rates. Here, we discuss these factors in turn, drawing upon key examples from our growth fold dataset to critically assess whether these factors may control growth fold occurrence.

Folding is expected to be more common in relatively rheologically-weak cover, as the strain is not only distributed over a wide area but also these rheological heterogeneities inhibit upward fault propagation (cf. Couples and Lewis, 1998; Withjack and Callaway, 2000; Finch et al., 2004; Ford et al., 2007; Roche et al., 2012; Jackson and Lewis, 2016; Hardy, 2018). In contrast, folding is less likely in relatively rheologically-strong cover as strain is focused in the vicinity of the fault, permitting rapid propagation and leaving little time for folding (cf. Withjack and Callaway, 2000; Finch et al., 2004; Hardy and Finch, 2007; Hardy, 2011). Rheologically strong and brittle volcanic sequences may therefore be expected to lack growth folds (e.g. Fig. 2 in Hardy, 2013). Our database suggests this is not always the case, however. For example, growth folds are documented on the flanks of Kilauea, Hawaii (Kattenhorn et al., 2000; Parfitt and Peacock, 2001; Peacock and Parfitt, 2002; Holland et al., 2006; Martel and Langley, 2006; Kaven and Martel, 2007; Podolsky and Roberts, 2008), the Modoc Plateau, USA (White and Crider, 2006; Blakeslee and Kattenhorn, 2013; Crider, 2015; Kattenhorn et al., 2016), and the Reykjanes Peninsula, Iceland (Bull et al., 2003; Grant and Kattenhorn, 2004; Bull et al., 2005;

749 Trippanera et al., 2015) suggesting that cover rheology is *not* the principal control on growth
750 fold occurrence. Cover lithology and rheology may affect the geometry and size of growth folds
751 (Fig. 8D). It is possible intra-basaltic heterogeneity (e.g. paleosols, volcaniclastics, rubble
752 horizons, mineralisation, pre-existing fractures) may weaken the cover rheology (cf. Finch et
753 al., 2004; e.g. Walker et al., 2012; Walker et al., 2013; Bubeck et al., 2018; Smart and Ferrill,
754 2018) and thus, permit folding. In general, however, growth folds are seemingly more
755 widespread in basins with rheological heterogeneity, such as salt or thick mudstone (cf. Jackson
756 et al., 2006; Jackson and Lewis, 2016; Coleman et al., 2017), although they clearly also occur
757 in predominantly brittle successions (cf. Gawthorpe et al., 1997; Willsey et al., 2002) in largely
758 homogeneous crust (cf. Gawthorpe and Leeder, 2000).

759 Growth fold occurrence has also been linked to the interplay of the propagation rate and
760 displacement rates of the upper tips of normal faults, which may in part be related to the
761 rheology of the cover (Hardy and McClay, 1999; Finch et al., 2004; Jackson et al., 2006). We
762 can therefore speculate that relatively high propagation rates are less likely to cause growth
763 folding as rapidly-propagating fault tips breach the surface early during fold growth. Rapidly-
764 propagating faults may be expected in regions with high strain rates (cf. Nicol et al., 1997;
765 Meyer et al., 2002; Mueller, 2017), during the latter stages of rifting (rift climax; cf. Cowie,
766 1998; Cowie et al., 2000; Gawthorpe and Leeder, 2000; Cowie et al., 2005), towards the rift
767 axis (Cowie et al., 2005), or within fault arrays comprising relatively few, fast slipping faults
768 (Walsh et al., 2003; Wilson et al., 2013; Nixon et al., 2014). However, do growth folds develop
769 in these areas? Are they more widespread than perhaps they are given credit for?

770 On the flanks of Kilauea, Hawaii (e.g. Macdonald, 1957; Duffield, 1975; Kattenhorn et al.,
771 2000; Parfitt and Peacock, 2001; Martel and Langley, 2006; Kaven and Martel, 2007; Podolsky
772 and Roberts, 2008; Bubeck et al., 2018) and in the eastern Gulf of Corinth (e.g. Vita-Finzi and
773 King, 1985), fault-propagation folds are currently forming despite very high regional extension

774 rates (Kilauea Volcano - 9 – 12 cm/yr from Owen et al., 1995; Gulf of Corinth - 5 – 15 mm/yr
775 from Bell et al., 2011). Similarly, ancient growth folds have formed under different extension
776 rates. In the Halten Terrace, km-scale growth folds formed over <60 Myr time period (Corfield
777 and Sharp, 2000; Corfield et al., 2001; Marsh et al., 2010; Coleman et al., 2017; Fig. 23), while
778 in the Gulf of Suez, similarly-sized growth folds formed over 4 Myr (Sharp et al., 2000a; Sharp
779 et al., 2000b; cf. Fig. 4). Even though salt is present in the Halten Terrace, which may have
780 inhibited the upward propagation of fault tips to the surface, this variability highlights that
781 regional extension rate does not seem to be the dominant control the occurrence of growth folds.
782 Instead, the formation of growth folds is likely dependent on the propagation and displacement
783 rates on *individual faults*. These rates likely vary spatially and temporally within extensional
784 fault arrays, as suggested by Withjack and Callaway (2000; in the Jeanne d'Arc Basin), Willsey
785 et al. (2002), Ford et al. (2007) and Bubeck et al. (2018).

786 During rift initiation, strain is distributed over many small, isolated faults with low slip and
787 propagation rates (Cowie, 1998; Gupta et al., 1998; Cowie et al., 2000; Cowie et al., 2005).
788 These conditions favour the development of growth folds (cf. Gawthorpe and Leeder, 2000).
789 However, as these small faults interact and link during rift climax, slip is transferred onto
790 increasingly large, well-connected faults (Cowie, 1998; Cowie et al., 2000; Gawthorpe and
791 Leeder, 2000) that may rapidly propagate through the cover. Where strain may vary along strike,
792 growth folds may not develop at all (cf. Bubeck et al., 2018). Furthermore, growth folds may
793 develop in some locations with similar cover rheology and similar throws, but not in others (e.g.
794 Faroe Islands - Walker et al., 2012; Walker et al., 2013; e.g. presence of growth folds in the
795 western, but not eastern Koa'e Fault System, Kilauea, Hawaii - Bubeck et al., 2018). In contrast,
796 growth folds above isolated small faults in the stress shadows of these larger faults may be
797 preserved. Examples include isolated faults in the vicinity of the Strathspey-Brent-Statfjord
798 fault system of the Northern North Sea, offshore UK (McLeod et al., 2000), the Nopolo

Structure of the Gulf of California, USA (Willsey et al., 2002), or intra-rift faults found in the El Qaa fault block, Gulf of Suez, Egypt (Lewis et al., 2015). In addition, as strain becomes focused onto larger faults, particularly towards the rift axis (Cowie et al., 2005), growth folds may preferentially develop at the rift margins in association with relatively slow-slipping faults (e.g. Laubscher, 1982).

Finally, faults forming part of a large network (i.e. distributed deformation) may propagate at a slower rate compared to faults within a small fault network, where the strain is localised onto fewer faults (Walsh et al., 2003; Putz-Perrier and Sanderson, 2009; Wilson et al., 2013; Nixon et al., 2014). Although this is likely the case, as shown in physical models with one basement fault and high strain rates (e.g. Withjack and Callaway, 2000; Miller and Mitra, 2011; Paul and Mitra, 2015), few attempts have been made to measure the displacement rates of individual faults (see Ford et al., 2007 for an exception). In addition, the displacement rates (and possibly, the propagation rates) may be greatest towards the centre of fault networks but lower towards the tips (Cowie and Roberts, 2001; Papanikolaou and Roberts, 2007). Furthermore, growth folds may be expected to be rarer or at least breached (cf. Parfitt and Peacock, 2001; Grant and Kattenhorn, 2004; Martel and Langley, 2006; White and Crider, 2006; Tavani et al., 2013; Tavani and Granado, 2015) towards the centre of a fault network.

We do not claim here to know why growth folds occur in particular locations more readily than others, but this data compilation suggests that growth folds are far more prevalent than they have been credited for. Perhaps, growth folds occur in every basin worldwide, but instead, their small size (especially where folds are poorly-developed under high fault tip propagation rates; cf. Bubeck et al., 2018) and the lack of high-resolution synkinematic strata, particularly during early extension, make it difficult to identify them.

6.4. What controls the geometry and size of growth folds?

Natural examples of fault-propagation and forced folds show similar relationships between fold size and geometry, and the properties of the underlying fault and cover. This suggests that the structural and stratigraphic factors controlling fault-propagation and forced folds are largely similar. The only exception is the presence and thickness of the detachment in forced folds, which by definition, drives an abrupt transition from faulting to folding (cf. Withjack et al., 2002). We find that fault throw, and the thickness of the cover are the major controls on fault-propagation and forced fold geometry and size (Figs. 12 – 13). Although cover rheology and fault dip undoubtedly control fold geometry and size, as shown in physical (Figs. 8; 18; 20) and numerical models (Figs. 19; 21), their role is masked by the dataset scatter (as in Fig. 17). Here, we discuss in mechanical terms why the identified correlations may exist between growth fold parameters, and which parameters exert the greatest influence of fold size and shape.

Our analysis suggests that large fault throws and thicker prekinematic cover for fault-propagation and forced folds generates large fold amplitudes and widths, as suggested by Horsfield (1977), Withjack et al. (1990), Withjack and Callaway (2000), and Miller and Mitra (2011). As fault throw increases, intuitively the amplitude of the folded cover also increases as the hangingwall block is progressively displaced downwards relative to the footwall (Fig. 26A). Furthermore, fault throw is the principal control on fold amplitude and explains why the values are very similar for the majority of growth folds. These results are corroborated by Lăpădat et al. (2016), in their Fig. 13C and D. Once the fold is breached, fold amplitude is independent of the fault throw (Appendix D – E) (cf. Lăpădat et al., 2016).

As fault throw (and fold amplitude) increases, fold width also increases (Fig. 26B; cf. also Figs 6C, 16C and 16 in Conneally et al., 2017). However, as discussed earlier, we suspect that fold width is largely set during the initial stages of growth folding (cf. Path 2 on Fig. 24) and that, although it may increase slightly as throw is accrued on the underlying fault, width may be

847 instead dependent on the rheology (or flexural rigidity) of the cover and/or or the dip of the
848 underlying fault (Figs. 8A; 8C).

849 The thickness of the prekinematic cover strongly affects fold growth. Thicker cover generates
850 larger amplitude and width folds (Figs. 8E; 19D; 20D; 26C - D). We interpret that as the cover
851 thickness increases, there is a larger amount of rock in front of the propagating fault tip. By
852 increasing the thickness of the cover, the duration of folding will increase (all else being equal),
853 permitting the growth of large folds with large throws.

854 We showed that for weaker cover rheologies, folds become much wider for a given throw (Figs.
855 18A; 19A). This likely reflects that strain is accommodated in a relatively narrow zone near the
856 fault tip in strong cover, but this same strain is far more horizontally distributed in weak cover.
857 Similarly, gently-dipping faults distribute strain over a wider area compared to steeply-dipping
858 faults, and thus, the dip of the fault will also control the fold width (Figs. 8A; 9). Given that
859 both the rheology of the cover and dip of the fault strongly control fold width, they also strongly
860 control the fold shape (cf. Patton, 2004). This is especially the case during the initial stages of
861 folding, since the fold amplitude will be initially low (as fault throw is small), but the final
862 width is established very early (cf. Path 2 on Fig. 24).

863 In addition to the aforementioned structural and stratigraphic factors, forced fold geometry and
864 size is also affected by the thickness of the detachment (Figs. 8F; 13C - D). We suggest that
865 detachments significantly weaken the overall strength of the cover and therefore, thicker
866 detachments may distribute extensional strain over a broader area and increase the fold width.
867 Given that the fold width is larger for a forced fold compared to a fault-propagation fold (Fig.
868 26B), thicker detachments also increase the fold-shape-factor for a given amount of fault throw.
869 This is similar to increasing the ductile portion of the cover, where folds have similar amplitudes

for a given fault throw, but the width of the fold increases as the detachment content increases (Figs. 20E; 21A; Richard, 1989; Hardy, 2018).

As the detachment thickness also increases the total cover thickness, and thus, the amount of rock in front of the propagating fault tip, the duration of folding also increases, all else being equal. The detachment may also inhibit the vertical propagation of the fault tip, and dissipate energy over a wider area. A forced fold therefore has longer to grow before becoming breached by the underlying fault. This allows forced folds to reach larger amplitudes and widths compared to fault-propagation folds, and to not be breached despite relatively large fault throws. Ductile flow of the detachment, for example in response to salt expulsion (cf. Fig. 5 in Koyi et al., 1993; Figs. 5 - 6 in Burliga et al., 2012; Figs. 5 - 6 in Warsitzka and Kukowski, 2015; Fig. 10 in Warsitzka et al., 2017), may also increase the amplitude of the forced fold. In some cases, the amplitude of the forced fold may be larger than the throw on the underlying fault (Fig. 26A).

Temporal and spatial changes in the structural and stratigraphic parameters discussed above are commonplace in extensional settings (cf. Withjack and Callaway, 2000; Duffy et al., 2013; Jackson and Lewis, 2016) and thus, growth fold evolution may differ significantly between fault segments in different intra-rift settings (e.g. the rift margin vs. rift axis, transfer zones vs fault segment centres etc.). Fold growth evolution may also vary between salt-free and salt-rich basins. We present conceptual models for how growth folds may vary between salt-free and salt-rich basins (Fig. 27), with particular emphasis on their 3D geometry and size in relation to the dip, throw and displacement rate of master faults, the rheology, thickness, and rheological heterogeneity of the cover. These concepts are testable using natural examples, physical and numerical models, which may fill in gaps in our understanding in how growth folds develop through time and their occurrence.

7. Conclusions

- Growth folds are very common in sedimentary and volcanic basins, and perhaps more prevalent than they have been historically given credit for. Not only do they form as transient features during the early stages of salt-free rifting and persist throughout most of salt-rich rifting, but they also occur in a wide range of settings, including those with high regional strain rates that were previously interpreted to be unlikely to host these folds. They also occur in relatively brittle (e.g. volcanic sequences in Iceland and Hawaii) and ductile cover sequences (e.g. salt or shale-rich sequences). Furthermore, rheology alone is unlikely to be the principal control on growth fold occurrence. Instead, we speculate that the propagation rate of individual faults may vary within an area and may control the distribution of growth folds.
- Fault-propagation and forced folds rapidly attain their near-final width relatively early during fold growth before they amplify. The rate of fold amplification is likely a function of the throw on the underlying normal fault. Their shape therefore changes throughout fold growth, evolving from a relatively broad, low amplitude fold to a fold where the amplitude and width are largely similar.
- By comparing correlations of measured fold parameters between fault-propagation and forced folds, we show that:
    - For a given throw, the amplitude and width of a forced fold is larger than that of a fault-propagation fold.
    - For a given fold width, the amplitude of a forced fold is generally larger than that of a fault-propagation fold.
    - For a given prekinematic thickness, the width of a forced fold is greater than that of a fault-propagation fold.

- We also derive a number of parametric equations that are potentially powerful tools in estimating unknown fold geometry and size in profile by utilising other known structural and stratigraphic parameters. However, their robustness will need to be tested with further examples.
- Growth folds are also dependent on the character of the underlying normal fault. As the fault grows in three-dimensions, so does the overlying growth fold. If the fault length and throw accumulate gradually and synchronously, growth folds may be expected to lengthen gradually along-strike. If faults rapidly establish their along-strike length before accumulating displacement, the along-strike length of the fold may be very large for a small amount of throw.
- During extension or sediment loading, salt expulsion in the hangingwall and/or the development of salt pillows in the footwall for example, typically leads to increased fold amplitudes and widths for forced folds. Forced folds can therefore grow differently to and may be geometrically distinct from fault-propagation folds.
- Physical models effectively capture the geometrical features of natural examples of fault-propagation and forced folds, although their structural and stratigraphic parameters are not well correlated, in contrast to natural examples where moderate to strong correlations are present. However, an individual physical model, when analysed independently of other models shows similar parameter correlations to natural examples (e.g. fault throw vs. fold amplitude). Overall, comparisons between physical models and natural examples should be used with care, especially if used to infer the geometrical evolution of growth folds.
- Numerical models show similar correlations between stratigraphic and structural parameters to natural examples. However, numerical models, especially those where mechanical properties of rock units are not incorporated (i.e. kinematic models), cannot

accurately describe the small-scale deformation observed in nature or physical models. Kinematic models however, do match the final geometry of growth folds in physical models and in nature, allowing the evolving fold geometry to be inferred. This is particularly useful in areas lacking synkinematic sediments.

Acknowledgements

We thank Stephen Watkins for his valuable suggestions, observations and advice on fault-related folding in extensional settings, and Thilo Wrona for his help regarding multi-variate data analysis. We also extend our thanks to the Basins Research Group (BRG), particularly Thomas Phillips, for additional discussions and their guidance throughout. John Cosgrove and Atle Rotevatn are thanked for their comments and feedback on an earlier version of the manuscript. We thank the Editor, Carlo Doglioni, as well as Stefano Tavani, Marco Herwegh and an anonymous reviewer for their constructive reviews that greatly improved this manuscript.

8. References

Abdi, H., and Williams, L. J., 2010, Principal component analysis: Wiley interdisciplinary reviews: computational statistics, v. 2, no. 4, p. 433-459.

Allmendinger, R. W., 1998, Inverse and forward numerical modeling of trishear fault-propagation folds: Tectonics, v. 17, no. 4, p. 640-656.

Allmendinger, R. W., and Shaw, J. H., 2000, Estimation of fault propagation distance from fold shape: Implications for earthquake hazard assessment: Geology, v. 28, no. 12, p. 1099-1102.

966 Ameen, M., 1990, Macrofaulting in the Purbeck-Isle of Wight monocline: Proceedings of the
967 Geologists' Association, v. 101, no. 1, p. 31-46.
968 Ameen, M. S., 1988, Folding of layered cover due to dip-slip basement faulting: Imperial
969 College London (University of London).
970 Badley, M. E., Price, J. D. and Backshall, L. C., 1989, Inversion, reactivated faults and related
971 structures: seismic examples from the southern North Sea: Geological Society, London,
972 Special Publications, v. 44, p. 201-219.
973 Bartlett, W., Friedman, M., and Logan, J., 1981, Experimental folding and faulting of rocks
974 under confining pressure Part IX. Wrench faults in limestone layers: Tectonophysics, v.
975 79, no. 3-4, p. 255-277.
976 Bell, R. E., McNeill, L. C., Henstock, T. J., and Bull, J. M., 2011, Comparing extension on
977 multiple time and depth scales in the Corinth Rift, Central Greece: Geophysical Journal
978 International, v. 186, no. 2, p. 463-470.
979 Benedicto, A., Schultz, R., and Soliva, R., 2003, Layer thickness and the shape of faults:
980 Geophysical Research Letters, v. 30, no. 20.
981 Berg, S. S., and Skar, T., 2005, Controls on damage zone asymmetry of a normal fault zone:
982 outcrop analyses of a segment of the Moab fault, SE Utah: Journal of Structural
983 Geology, v. 27, no. 10, p. 1803-1822.
984 Bernal, A., Hardy, S., and Gawthorpe, R., 2018, Three-Dimensional Growth of Flexural Slip
985 Fault-Bend and Fault-Propagation Folds and Their Geomorphic Expression:
986 Geosciences, v. 8, no. 4, p. 110.
987 Billings, M. P. 1972. Structural geology, Prentice-Hall Englewood Cliffs, NJ.
988 Blakeslee, M. W., and Kattenhorn, S. A., 2013, Revised earthquake hazard of the Hat Creek
989 fault, northern California: A case example of a normal fault dissecting variable-age
990 basaltic lavas: Geosphere, v. 9, no. 5, p. 1397-1409.

991 Bonini, L., Basili, R., Toscani, G., Burrato, P., Seno, S. and Valensise, G., 2015. The role of pre-
992 existing discontinuities in the development of extensional faults: an analog modeling
993 perspective: Journal of structural geology, v. 74, p.145-158.
994 Botter, C., Cardozo, N., Hardy, S., Lecomte, I., and Escalona, A., 2014, From mechanical
995 modeling to seismic imaging of faults: A synthetic workflow to study the impact of
996 faults on seismic: Marine and Petroleum Geology, v. 57, p. 187-207.
997 Brown, W. G., 1988, Deformational style of Laramide uplifts in the Wyoming foreland:
998 Interaction of the Rocky Mountain foreland and the Cordilleran thrust belt: Geological
999 Society of America Memoir, v. 171, p. 1-25.
1000 Bubeck, A., Walker, R. J., Imber, J., and MacLeod, C. J., 2018, Normal fault growth in layered
1001 basaltic rocks: The role of strain rate in fault evolution: Journal of Structural Geology,
1002 v. 115, p. 103-120.
1003 Bull, J. M., Minshull, T. A., Mitchell, N. C., Thors, K., Dix, J. K., and Best, A. I., 2003, Fault
1004 and magmatic interaction within Iceland's western rift over the last 9 kyr: Geophysical
1005 Journal International, v. 154, no. 1, p. F1-F8.
1006 Bull, J. M., Minshull, T. A., Mitchell, N. C., Dix, J. K., and Hardardottir, J., 2005, Magmatic
1007 and tectonic history of Iceland's western rift zone at Lake Thingvallavatn: Geological
1008 Society of America Bulletin, v. 117, no. 11, p. 1451.
1009 Burbank, D., Meigs, A., and Brozović, N., 1996, Interactions of growing folds and coeval
1010 depositional systems: Basin Research, v. 8, no. 3, p. 199-223.
1011 Burliga, S., Koyi, H. A., and Chemia, Z., 2012, Analogue and numerical modelling of salt
1012 supply to a diapiric structure rising above an active basement fault: Geological Society,
1013 London, Special Publications, v. 363, no. 1, p. 395-408.

1014 Cardozo, N., Bhalla, K., Zehnder, A. T., and Allmendinger, R. W., 2003, Mechanical models of
1015 fault propagation folds and comparison to the trishear kinematic model: Journal of
1016 Structural Geology, v. 25, no. 1, p. 1-18.
1017 Cardozo, N., Jackson, C. A.-L., and Whipp, P. S., 2011, Determining the uniqueness of best-fit
1018 trishear models: Journal of Structural Geology, v. 33, no. 6, p. 1063-1078.
1019 Carola, E., Tavani, S., Ferrer, O., Granado, P., Quintà, A., Butillé, M., and Muñoz, J. A., 2013,
1020 Along-strike extrusion at the transition between thin- and thick-skinned domains in the
1021 Pyrenean Orogen (northern Spain): Geological Society, London, Special Publications,
1022 v. 377, no. 1, p. 119-140.
1023 Childs, C., Watterson, J., and Walsh, J. J., 1995, Fault overlap zones within developing normal
1024 fault systems: Journal of the Geological Society, v. 152, no. 3, p. 535-549.
1025 Coleman, A. J., Jackson, C. A.-L., and Duffy, O. B., 2017, Balancing sub- and supra-salt strain
1026 in salt-influenced rifts: Implications for extension estimates: Journal of Structural
1027 Geology, v. 102, p. 208-225.
1028 Conneally, J., Childs, C., and Nicol, A., 2017, Monocline formation during growth of
1029 segmented faults in the Taranaki Basin, offshore New Zealand: Tectonophysics, v. 721,
1030 p. 310-321.
1031 Corfield, S., and Sharp, I., 2000, Structural style and stratigraphic architecture of fault
1032 propagation folding in extensional settings: a seismic example from the Smørbukk area,
1033 Halten Terrace, Mid-Norway: Basin Research, v. 12, no. 3-4, p. 329-341.
1034 Corfield, S., Sharp, I., Häger, K.-O., Dreyer, T., and Underhill, J., 2001, An integrated study of
1035 the garn and melke formations (middle to upper jurassic) of the smorbukk area, halten
1036 terrace, mid-norway, *in* Ole, J. M., and Tom, D., eds., Norwegian Petroleum Society
1037 Special Publications, Volume Volume 10, Elsevier, p. 199-210.

1038 Cosgrove, J. W., and Ameen, M. S., 1999, A comparison of the geometry, spatial organization
1039 and fracture patterns associated with forced folds and buckle folds: Geological Society,
1040 London, Special Publications, v. 169, no. 1, p. 7-21.
1041 Couples, G. D., and Lewis, H., 1998, Lateral variations of strain in experimental forced folds:
1042 Tectonophysics, v. 295, no. 1, p. 79-91.
1043 Couples, G. D., Lewis, H., and Tanner, P. G., 1998, Strain partitioning during flexural-slip
1044 folding: Geological Society, London, Special Publications, v. 127, no. 1, p. 149-165.
1045 Couples, G. D., and Lewis, H., 1999, Effects of interlayer slip in model forced folds: Geological
1046 Society, London, Special Publications, v. 169, no. 1, p. 129-144.
1047 Cowie, P., Gupta, S., and Dawers, N., 2000, Implications of fault array evolution for synrift
1048 depocentre development: insights from a numerical fault growth model: Basin
1049 Research, v. 12, no. 3-4, p. 241-261.
1050 Cowie, P. A., 1998, A healing–reloading feedback control on the growth rate of seismogenic
1051 faults: Journal of Structural Geology, v. 20, no. 8, p. 1075-1087.
1052 Cowie, P. A., and Roberts, G. P., 2001, Constraining slip rates and spacings for active normal
1053 faults: Journal of Structural Geology, v. 23, no. 12, p. 1901-1915.
1054 Cowie, P. A., Underhill, J. R., Behn, M. D., Lin, J., and Gill, C. E., 2005, Spatio-temporal
1055 evolution of strain accumulation derived from multi-scale observations of Late Jurassic
1056 rifting in the northern North Sea: A critical test of models for lithospheric extension:
1057 Earth and Planetary Science Letters, v. 234, no. 3–4, p. 401-419.
1058 Crider, J. G., 2015, The initiation of brittle faults in crystalline rock: Journal of Structural
1059 Geology, v. 77, p. 159-174.
1060 Davis, G.H., Reynolds, S.J., Kluth, C.F. and Kluth, C., 2011, Structural geology of rocks and
1061 regions, John Wiley & Sons.

1062 Dawers, N. H., and Anders, M. H., 1995, Displacement-length scaling and fault linkage: Journal
1063 of Structural Geology, v. 17, no. 5, p. 607-614.
1064 Deckers, J., 2015, Decoupled extensional faulting and forced folding in the southern part of the
1065 Roer Valley Graben, Belgium: Journal of Structural Geology, v. 81, p. 125-134.
1066 Deng, H., & McClay, K., 2019, Development of extensional fault and fold system: Insights
1067 from 3D seismic interpretation of the Enderby Terrace, NW Shelf of Australia: Marine
1068 and Petroleum Geology, v. 104, p. 11 - 28.
1069 Destro, N., 1995, Release fault: A variety of cross fault in linked extensional fault systems in
1070 the Sergipe-Alagoas Basin, NE Brazil: Journal of Structural Geology, v. 17, p. 615-619.
1071 Dooley, T., McClay, K., and Pascoe, R., 2003, 3D analogue models of variable displacement
1072 extensional faults: applications to the Revfallet Fault system, offshore mid-Norway:
1073 Geological Society, London, Special Publications, v. 212, no. 1, p. 151-167.
1074 Duffield, W. A., 1975, Structure and origin of the Koae fault system, Kilauea volcano, Hawaii,
1075 US Government Printing Office.
1076 Duffy, O. B., Gawthorpe, R. L., Docherty, M., and Brocklehurst, S. H., 2013, Mobile evaporite
1077 controls on the structural style and evolution of rift basins: Danish Central Graben,
1078 North Sea: Basin Research, v. 25, no. 3, p. 310-330.
1079 Egholm, D. L., Sandiford, M., Clausen, O. R., and Nielsen, S. B., 2007, A new strategy for
1080 discrete element numerical models: 2. Sandbox applications: Journal of Geophysical
1081 Research: Solid Earth, v. 112, no. 1-12.
1082 Ehrlich, R. and Gabrielsen, R. H., 2004, The complexity of a ramp–flat–ramp fault and its effect
1083 on hanging-wall structuring: an example from the Njord oil field, offshore mid-Norway:
1084 Petroleum Geoscience, v. 10, p. 305-317.
1085 Erslev, E. A., 1991, Trishear fault-propagation folding: Geology, v. 19, no. 6, p. 617.

1086 Færseth, R. B., and Lien, T., 2002, Cretaceous evolution in the Norwegian Sea—a period
1087 characterized by tectonic quiescence: Marine and Petroleum Geology, v. 19, no. 8, p.
1088 1005-1027.
1089 Ferrill, D. A., Morris, A. P., and Smart, K. J., 2007, Stratigraphic control on extensional fault
1090 propagation folding: Big Brushy Canyon monocline, Sierra del Carmen,
1091 Texas: Geological Society, London, Special Publications, v. 292, p. 203-217.
1092 Finch, E., Hardy, S., and Gawthorpe, R., 2004, Discrete-element modelling of extensional fault-
1093 propagation folding above rigid basement fault blocks: Basin Research, v. 16, no. 4, p.
1094 467-488.
1095 Finch, E., and Gawthorpe, R., 2017, Growth and interaction of normal faults and fault network
1096 evolution in rifts: insights from three-dimensional discrete element modelling:
1097 Geological Society, London, Special Publications, v. 439, p. SP439. 423.
1098 Fodor, L., Turki, S., Dalub, H., and Al Gerbi, A., 2005, Fault-related folds and along-dip
1099 segmentation of breaching faults: syn-diagenetic deformation in the south-western Sirt
1100 basin, Libya: Terra Nova, v. 17, no. 2, p. 121-128.
1101 Ford, M., Le Carlier de Veslud, C., and Bourgeois, O., 2007, Kinematic and geometric analysis
1102 of fault-related folds in a rift setting: The Dannemarie basin, Upper Rhine Graben,
1103 France: Journal of Structural Geology, v. 29, no. 11, p. 1811-1830.
1104 Friedman, M., Handin, J., Logan, J., Min, K., and Stearns, D., 1976, Experimental folding of
1105 rocks under confining pressure: Part III. Faulted drape folds in multilithologic layered
1106 specimens: Geological Society of America Bulletin, v. 87, no. 7, p. 1049-1066.
1107 Gabrielsen, R. H., Sokoutis, D., Willingshofer, E., and Faleide, J. I., 2016, Fault linkage across
1108 weak layers during extension: an experimental approach with reference to the Hoop
1109 Fault Complex of the SW Barents Sea: Petroleum Geoscience.

1110 Gawthorpe, R. L., Sharp, I., Underhill, J. R., and Gupta, S., 1997, Linked sequence stratigraphic
1111 and structural evolution of propagating normal faults: Geology, v. 25, no. 9, p. 795.
1112 Gawthorpe, R. L., and Leeder, M. R., 2000, Tectono-sedimentary evolution of active
1113 extensional basins: Basin Research, v. 12, no. 3-4, p. 195-218.
1114 Gawthorpe, R. L., and Hardy, S., 2002, Extensional fault-propagation folding and base-level
1115 change as controls on growth-strata geometries: Sedimentary Geology, v. 146, no. 1, p.
1116 47-56.
1117 Ge, Z., Gawthorpe, R. L., Rotevatn, A., and Thomas, M. B., 2016, Impact of normal faulting
1118 and pre-rift salt tectonics on the structural style of salt-influenced rifts: The Late Jurassic
1119 Norwegian Central Graben, North Sea: Basin Research, p. n/a-n/a.
1120 Grant, J. V., and Kattenhorn, S. A., 2004, Evolution of vertical faults at an extensional plate
1121 boundary, southwest Iceland: Journal of Structural Geology, v. 26, no. 3, p. 537-557.
1122 Grecula, M., Flint, S., Potts, G., Wickens, D., and Johnson, S., 2003, Partial ponding of turbidite
1123 systems in a basin with subtle growth-fold topography: Laingsburg-Karoo, South
1124 Africa: Journal of Sedimentary Research, v. 73, no. 4, p. 603-620.
1125 Gross, M. R., Becker, A., and Gutiérrez-Alonso, G., 1997, Transfer of displacement from
1126 multiple slip zones to a major detachment in an extensional regime: Example from the
1127 Dead Sea rift, Israel: Geological Society of America Bulletin, v. 109, no. 8, p. 1021-
1128 1035.
1129 Gupta, S., Cowie, P. A., Dawers, N. H., and Underhill, J. R., 1998, A mechanism to explain rift-
1130 basin subsidence and stratigraphic patterns through fault-array evolution: Geology, v.
1131 26, no. 7, p. 595-598.
1132 Gupta, S., Underhill, J., Sharp, I., and Gawthorpe, R., 1999, Role of fault interactions in
1133 controlling synrift sediment dispersal patterns: Miocene, Abu Alaqa Group, Suez Rift,
1134 Sinai, Egypt: Basin Research, v. 11, no. 2, p. 167-189.

1135 Hardy, S., and Ford, M., 1997, Numerical modeling of trishear fault propagation folding:
1136 Tectonics, v. 16, no. 5, p. 841-854.
1137 Hardy, S., and McClay, K., 1999, Kinematic modelling of extensional fault-propagation
1138 folding: Journal of Structural Geology, v. 21, no. 7, p. 695-702.
1139 Hardy, S., and Finch, E., 2006, Discrete element modelling of the influence of cover strength
1140 on basement-involved fault-propagation folding: Tectonophysics, v. 415, no. 1-4, p.
1141 225-238.
1142 Hardy, S., and Finch, E., 2007, Mechanical stratigraphy and the transition from trishear to kink-
1143 band fault-propagation fold forms above blind basement thrust faults: A discrete-
1144 element study: Marine and Petroleum Geology, v. 24, no. 2, p. 75-90.
1145 Hardy, S., 2011, Cover deformation above steep, basement normal faults: Insights from 2D
1146 discrete element modeling: Marine and Petroleum Geology, v. 28, no. 5, p. 966-972.
1147 Hardy, S., and Allmendinger, R. W., 2011, Trishear: A review of kinematics, mechanics, and
1148 applications, *in* McClay, K., ed., Thrust fault-related folding, AAPG Memoir 94, AAPG,
1149 p. 95-119.
1150 Hardy, S., 2018, Coupling a frictional-cohesive cover and a viscous substrate in a discrete
1151 element model: First results of application to thick- and thin-skinned extensional
1152 tectonics: Marine and Petroleum Geology, v. 97, p. 32-44.
1153 Harvey, M. J., and Stewart, S. A., 1998, Influence of salt on the structural evolution of the
1154 Channel Basin: Geological Society, London, Special Publications, v. 133, no. 1, p. 241-
1155 266.
1156 Heggland, R., 1998, Gas seepage as an indicator of deeper prospective reservoirs. A study based
1157 on exploration 3D seismic data: Marine and Petroleum Geology, v. 15, no. 1, p. 1-9.
1158 Holland, M., Urai, J. L., and Martel, S., 2006, The internal structure of fault zones in basaltic
1159 sequences: Earth and Planetary Science Letters, v. 248, no. 1, p. 301-315.

1160 Horsfield, W., 1977, An experimental approach to basement-controlled faulting: Geologie en
1161 Mijnbouw, v. 56, no. 4, p. 363-370.
1162 Howard, K. A., and John, B. E., 1997, Fault-related folding during extension: Plunging
1163 basement-cored folds in the Basin and Range: Geology, v. 25, no. 3, p. 223-226.
1164 Jackson, C. A.-L., Gawthorpe, R. L., and Sharp, I. R., 2006, Style and sequence of deformation
1165 during extensional fault-propagation folding: examples from the Hammam Faraun and
1166 El-Qaa fault blocks, Suez Rift, Egypt: Journal of Structural Geology, v. 28, no. 3, p.
1167 519-535.
1168 Jackson, C. A.-L., and Rotevatn, A., 2013, 3D seismic analysis of the structure and evolution
1169 of a salt-influenced normal fault zone: A test of competing fault growth models: Journal
1170 of Structural Geology, v. 54, p. 215-234.
1171 Jackson, C. A.-L., Bell, R. E., Rotevatn, A., and Tvedt, A. B. M., 2017, Techniques to determine
1172 the kinematics of synsedimentary normal faults and implications for fault growth
1173 models: Geological Society, London, Special Publications, v. 439.
1174 Jackson, C. A. L., and Lewis, M. M., 2016, Structural style and evolution of a salt-influenced
1175 rift basin margin; the impact of variations in salt composition and the role of polyphase
1176 extension: Basin Research, v. 28, no. 1, p. 81-102.
1177 Jackson, J., and Leeder, M., 1994, Drainage systems and the development of normal faults: an
1178 example from Pleasant Valley, Nevada: Journal of Structural Geology, v. 16, no. 8, p.
1179 1041-1059.
1180 Jin, G., and Groshong, R. H., 2006, Trishear kinematic modeling of extensional fault-
1181 propagation folding: Journal of Structural Geology, v. 28, no. 1, p. 170-183.
1182 Jin, G., Groshong, R. H., and Pashin, J. C., 2009, Growth trishear model and its application to
1183 the Gilbertown graben system, southwest Alabama: Journal of Structural Geology, v.
1184 31, no. 9, p. 926-940.

1185 Johnson, K. M., and Johnson, A. M., 2002, Mechanical models of trishear-like folds: Journal of
1186 Structural Geology, v. 24, no. 2, p. 277-287.
1187 Jolliffe, I. T., 1993, Principal component analysis: A beginner's guide — II. Pitfalls, myths and
1188 extensions: Weather, v. 48, no. 8, p. 246-253.
1189 Jolliffe, I. T., 2002, Principal component analysis, New York, Springer.
1190 Josse, J., and Husson, F., 2016, missMDA: a package for handling missing values in
1191 multivariate data analysis: Journal of Statistical Software, v. 70, no. 1, p. 1-31.
1192 Kane, K. E., Jackson, C. A.-L., and Larsen, E., 2010, Normal fault growth and fault-related
1193 folding in a salt-influenced rift basin: South Viking Graben, offshore Norway: Journal
1194 of Structural Geology, v. 32, no. 4, p. 490-506.
1195 Kattenhorn, S. A., Aydin, A., and Pollard, D. D., 2000, Joints at high angles to normal fault
1196 strike: an explanation using 3-D numerical models of fault-perturbed stress fields:
1197 Journal of structural Geology, v. 22, no. 1, p. 1-23.
1198 Kattenhorn, S. A., Krantz, B., Walker, E. L., and Blakeslee, M. W., 2016, Evolution of the Hat
1199 Creek fault system, northern California.
1200 Kaven, J. O., and Martel, S. J., 2007, Growth of surface-breaching normal faults as a three-
1201 dimensional fracturing process: Journal of Structural Geology, v. 29, no. 9, p. 1463-
1202 1476.
1203 Keller, J. V. A., and Lynch, G., 1999, Displacement transfer and forced folding in the Maritimes
1204 basin of Nova Scotia, eastern Canada: Geological Society, London, Special
1205 Publications, v. 169, no. 1, p. 87-101.
1206 Khalil, S., and McClay, K., 2002, Extensional fault-related folding, northwestern Red Sea,
1207 Egypt: Journal of Structural Geology, v. 24, no. 4, p. 743-762.

1208 Khalil, S. M., and McClay, K. R., 2016, 3D geometry and kinematic evolution of extensional
1209 fault-related folds, NW Red Sea, Egypt: Geological Society, London, Special
1210 Publications, v. 439, p. 1-11.
1211 Koch, J.-O., and Heum, O., 1995, Exploration trends of the Halten Terrace: Norwegian
1212 Petroleum Society Special Publications, v. 4, p. 235-251.
1213 Koopman, A., Speksnijder, A., and Horsfield, W., 1987, Sandbox model studies of inversion
1214 tectonics: Tectonophysics, v. 137, no. 1-4, p. 379-388.
1215 Koyi, H., Talbot, C. J., and Tørudbakken, B. O., 1993, Salt diapirs of the southwest Nordkapp
1216 Basin: analogue modelling: Tectonophysics, v. 228, no. 3, p. 167-187.
1217 Koyi, H., Talbot, C. J., and Torudbakken, B., 1995, Analogue models of salt diapirs and seismic
1218 interpretation in the Nordkapp Basin, Norway: Petroleum geoscience, v. 1, no. 2, p. 185-
1219 192.
1220 Koyi, H., 1997, Analogue modelling: from a qualitative to quantitative technique - a historical
1221 outline: Journal of Petroleum Geology, v. 20, no. 2, p. 223-238.
1222 Lăpădat, A., Imber, J., Yielding, G., Iacopini, D., McCaffrey, K. J. W., Long, J. J., and Jones,
1223 R. R., 2016, Occurrence and development of folding related to normal faulting within a
1224 mechanically heterogeneous sedimentary sequence: a case study from Inner Moray
1225 Firth, UK: Geological Society, London, Special Publications, v. 439.
1226 Laubscher, H., 1982, Die Sudostecke des Rheingrabens-ein kinematisches und dynamisches
1227 problem: Eclogae Geologicae Helvetiae, v. 75, no. 1, p. 101-116.
1228 Lever, J., Krzywinski, M., and Altman, N., 2017, Points of significance: Principal component
1229 analysis: Nature Methods, v. 14, p. 641-642.
1230 Lewis, M. M., Jackson, C. A.-L., and Gawthorpe, R. L., 2013, Salt-influenced normal fault
1231 growth and forced folding: The Stavanger Fault System, North Sea: Journal of
1232 Structural Geology, v. 54, p. 156-173.

1233 Lewis, M. M., Jackson, C. A.-L., Gawthorpe, R. L., and Whipp, P. S., 2015, Early synrift
1234 reservoir development on the flanks of extensional forced folds: A seismic-scale outcrop
1235 analog from the Hadahid Fault System, Suez Rift, Egypt: AAPG Bulletin, no.
1236 20,150,119.
1237 Lingrey, S., and Vidal-Royo, O., 2015, Evaluating the quality of bed length and area balance in
1238 2D structural restorations: Interpretation, v. 3, no. 4, p. SAA133-SAA160.
1239 Lynch, G., Keller, J. V., and Giles, P. S., 1998, Influence of the Ainslie Detachment on the
1240 stratigraphy of the Maritimes Basin and mineralization in the Windsor Group of
1241 northern Nova Scotia, Canada: Economic Geology, v. 93, no. 6, p. 703-718.
1242 Macdonald, G. A., 1957, Faults and monoclines on Kilauea Volcano, Hawaii: Geological
1243 Society of America Bulletin, v. 68, no. 2, p. 269-271.
1244 Machette, M. N., S. F. Personius, A. R. Nelson, D. P. Schwartz, and W. R. Lund, 1991, The
1245 Wasatch fault zone, Utah—segmentation and history of Holocene earthquakes: Journal
1246 of Structural Geology, v. 13, p. 137–149.
1247 Marsh, N., Imber, J., Holdsworth, R., Brockbank, P., and Ringrose, P., 2010, The structural
1248 evolution of the Halten Terrace, offshore Mid-Norway: extensional fault growth and
1249 strain localisation in a multi-layer brittle–ductile system: Basin Research, v. 22, no. 2,
1250 p. 195-214.
1251 Martel, S. J., and Langley, J. S., 2006, Propagation of normal faults to the surface in basalt,
1252 Koae fault system, Hawaii: Journal of Structural Geology, v. 28, no. 12, p. 2123-2143.
1253 Matthews III, V., and Work, D. F., 1978, Laramide folding associated with basement block
1254 faulting along the northeastern flank of the Front Range, Colorado: Laramide folding
1255 associated with basement block faulting in the western United States: Geological
1256 Society of America Memoir, v. 151, p. 101-124.

1257 Maurin, J. C., and Niviere, B., 1999, Extensional forced folding and decollement of the pre-rift
1258 series along the Rhine graben and their influence on the geometry of the syn-rift
1259 sequences: Geological Society, London, Special Publications, v. 169, no. 1, p. 73-86.
1260 McLeod, A. E., Dawers, N. H., and Underhill, J. R., 2000, The propagation and linkage of
1261 normal faults: insights from the Strathspey–Brent–Statfjord fault array, northern North
1262 Sea: Basin Research, v. 12, no. 3-4, p. 263-284.
1263 Meyer, V., Nicol, A., Childs, C., Walsh, J., and Watterson, J., 2002, Progressive localisation of
1264 strain during the evolution of a normal fault population: Journal of Structural Geology,
1265 v. 24, no. 8, p. 1215-1231.
1266 Miller, J. F., and Mitra, S., 2011, Deformation and secondary faulting associated with basement-
1267 involved compressional and extensional structures: AAPG bulletin, v. 95, no. 4, p. 675-
1268 689.
1269 Mitra, S., 1990, Fault-propagation folds: geometry, kinematic evolution, and hydrocarbon
1270 Traps: AAPG Bulletin, v. 74, no. 6, p. 921-945.
1271 Mitra, S., 1993, Geometry and kinematic evolution of inversion structures: AAPG Bulletin, v.
1272 77, no. 7, p. 1159-1191.
1273 Mitra, S., and Islam, Q. T., 1994, Experimental (clay) models of inversion structures:
1274 Tectonophysics, v. 230, no. 3, p. 211-222.
1275 Mohammedyasin, S. M., Lippard, S. J., Omosanya, K. O., Johansen, S. E., and Harishidayat,
1276 D., 2016, Deep-seated faults and hydrocarbon leakage in the Snøhvit Gas Field,
1277 Hammerfest Basin, Southwestern Barents Sea: Marine and Petroleum Geology, v. 77,
1278 p. 160-178.
1279 Morley, C., 1996, Discussion of potential errors in fault heave methods for extension estimates
1280 in rifts, with particular reference to fractal fault populations and inherited fabrics:
1281 Geological Society, London, Special Publications, v. 99, no. 1, p. 117-134.

1282 Morley, C., and Guerin, G., 1996, Comparison of gravity-driven deformation styles and
1283 behavior associated with mobile shales and salt: Tectonics, v. 15, no. 6, p. 1154-1170.
1284 Mueller, K., 2017, Variation in slip rates on active faults: Natural growth or stress transients?:
1285 Geology, v. 45, no. 3, p. 287-288.
1286 Nicol, A., Watterson, J., Walsh, J., and Childs, C., 1996, The shapes, major axis orientations
1287 and displacement patterns of fault surfaces: Journal of Structural Geology, v. 18, no. 2-
1288 3, p. 235-248.
1289 Nicol, A., Walsh, J., Watterson, J., and Underhill, J., 1997, Displacement rates of normal faults:
1290 Nature, v. 390, no. 6656, p. 157.
1291 Nixon, C. W., Bull, J. M., and Sanderson, D. J., 2014, Localized vs distributed deformation
1292 associated with the linkage history of an active normal fault, Whakatane Graben, New
1293 Zealand: Journal of Structural Geology, v. 69, p. 266-280.
1294 Ostanin, I., Anka, Z., di Primio, R., and Bernal, A., 2013, Hydrocarbon plumbing systems above
1295 the Snøhvit gas field: structural control and implications for thermogenic methane
1296 leakage in the Hammerfest Basin, SW Barents Sea: Marine and Petroleum Geology, v.
1297 43, p. 127-146.
1298 Owen, S., Segall, P., Freymueller, J., Mikijus, A., Denlinger, R., Árnadóttir, T., Sako, M., and
1299 Bürgmann, R., 1995, Rapid Deformation of the South Flank of Kilauea Volcano,
1300 Hawaii: Science, v. 267, no. 5202, p. 1328-1332.
1301 Palmquist, J. C., 1978, Laramide structures and basement block faulting: Two examples from
1302 the Big Horn Mountains, Wyoming, *in* Matthews, I. I. I. V., ed., Laramide Folding
1303 Associated with Basement Block Faulting in the Western United States, Geological
1304 Society of America.

1305 Panien, M., Schreurs, G., and Pfiffner, A., 2006, Mechanical behaviour of granular materials
1306 used in analogue modelling: insights from grain characterisation, ring-shear tests and
1307 analogue experiments: Journal of Structural Geology, v. 28, no. 9, p. 1710-1724.
1308 Papanikolaou, I. D., and Roberts, G. P., 2007, Geometry, kinematics and deformation rates
1309 along the active normal fault system in the southern Apennines: Implications for fault
1310 growth: Journal of Structural Geology, v. 29, no. 1, p. 166-188.
1311 Parfitt, E. A., and Peacock, D. C. P., 2001, Faulting in the South Flank of Kilauea Volcano,
1312 Hawai'i: Journal of Volcanology and Geothermal Research, v. 106, no. 3–4, p. 265-284.
1313 Pascoe, R., Hooper, R., Storhaug, K., and Harper, H., 1999, Evolution of extensional styles at
1314 the southern termination of the Nordland Ridge, Mid-Norway: a response to variations
1315 in coupling above Triassic salt: Petroleum Geology Conference Series, v. 5, p. 83-90.
1316 Patton, T. L., Logan, J. M., and Friedman, M., 1998, Experimentally generated normal faults in
1317 single-layer and multilayer limestone specimens at confining pressure: Tectonophysics,
1318 v. 295, no. 1, p. 53-77.
1319 Patton, T. L., 2004, Numerical models of growth-sediment development above an active
1320 monocline: Basin Research, v. 16, p. 25-39.
1321 Paul, D., and Mitra, S., 2015, Fault patterns associated with extensional fault-propagation
1322 folding: Marine and Petroleum Geology, v. 67, p. 120-143.
1323 Peacock, D. C. P., and Parfitt, E. A., 2002, Active relay ramps and normal fault propagation on
1324 Kilauea Volcano, Hawaii: Journal of Structural Geology, v. 24, no. 4, p. 729-742.
1325 Podolsky, D. M., and Roberts, G. P., 2008, Growth of the volcano-flank Koa'e fault system,
1326 Hawaii: Journal of Structural Geology, v. 30, no. 10, p. 1254-1263.
1327 Putz-Perrier, M. W., and Sanderson, D. J., 2009, Distribution of faults and extensional strain in
1328 fractured carbonates of the North Malta Graben: AAPG bulletin, v. 94, no. 4, p. 435-
1329 456.

1330 Resor, P. G., 2008, Deformation associated with a continental normal fault system, western
1331 Grand Canyon, Arizona: Geological Society of America Bulletin, v. 120, p. 414-430.
1332 Richard, P., 1989, Champs de failles au dessus d'un décrochement de socle : modélisation
1333 expérimentale: Université Rennes 1.
1334 Richard, P., 1991, Experiments on faulting in a two-layer cover sequence overlying a
1335 reactivated basement fault with oblique-slip: Journal of Structural Geology, v. 13, no. 4,
1336 p. 459-469.
1337 Richardson, N. J., Underhill, J. R., and Lewis, G., 2005, The role of evaporite mobility in
1338 modifying subsidence patterns during normal fault growth and linkage, Halten Terrace,
1339 Mid-Norway: Basin Research, v. 17, no. 2, p. 203-223.
1340 Ringnér, M., 2008, What is principal component analysis?: Nature Biotechnology, v. 26, p. 303.
1341 Roche, V., Homberg, C., and Rocher, M., 2012, Fault displacement profiles in multilayer
1342 systems: from fault restriction to fault propagation: Terra Nova, v. 24, no. 6, p. 499-504.
1343 Rotevatn, A., and Jackson, C. A. L., 2014, 3D structure and evolution of folds during normal
1344 fault dip linkage: Journal of the Geological Society, v. 171, no. 6, p. 821-829.
1345 Rowan, M. G., and Kligfield, R., 1989, Cross section restoration and balancing as aid to seismic
1346 interpretation in extensional terranes: AAPG bulletin, v. 73, no. 8, p. 955-966.
1347 Rowan, M. G., and Ratliff, R. A., 2012, Cross-section restoration of salt-related deformation:
1348 Best practices and potential pitfalls: Journal of Structural Geology, v. 41, p. 24-37.
1349 Schellart, W. P., and Strak, V., 2016, A review of analogue modelling of geodynamic processes:
1350 Approaches, scaling, materials and quantification, with an application to subduction
1351 experiments: Journal of Geodynamics, v. 100, p. 7-32.
1352 Schöpfer, M. P., Childs, C., and Walsh, J. J., 2007, Two-dimensional distinct element modeling
1353 of the structure and growth of normal faults in multilayer sequences: 2. Impact of

confining pressure and strength contrast on fault zone geometry and growth: Journal of Geophysical Research: Solid Earth (1978–2012), v. 112, no. B10.

Schreurs, G., Buiter, S. J. H., Boutelier, D., Corti, G., Costa, E., Cruden, A. R., Daniel, J.-M., Hoth, S., Koyi, H. A., Kukowski, N., Lohrmann, J., Ravaglia, A., Schlische, R. W., Withjack, M. O., Yamada, Y., Cavozzi, C., Del Ventisette, C., Brady, J. A. E., Hoffmann-Rothe, A., Mengus, J.-M., Montanari, D., and Nilforoushan, F., 2006, Analogue benchmarks of shortening and extension experiments: Geological Society, London, Special Publications, v. 253, no. 1, p. 1-27.

Serck, CS, and Braathen, A., 2019, Extensional fault and fold growth: Impact on accommodation evolution and sedimentary infill: Basin Research. p. 1– 24. https://doi.org/10.1111/bre.12353

Sharp, I., Gawthorpe, R., Armstrong, B., and Underhill, J., 2000a, Propagation history and passive rotation of mesoscale normal faults: implications for synrift stratigraphic development: Basin Research, v. 12, no. 3-4, p. 285-305.

Sharp, I. R., Gawthorpe, R. L., Underhill, J. R., and Gupta, S., 2000b, Fault-propagation folding in extensional settings: Examples of structural style and synrift sedimentary response from the Suez rift, Sinai, Egypt: Geological Society of America Bulletin, v. 112, no. 12, p. 1877-1899.

Skuce, A. G., 1996, Forward modelling of compaction above normal faults: an example from the Sirte Basin, Libya: Geological Society, London, Special Publications, v. 99, no. 1, p. 135-146.

Smart, K.J., Ferrill, D.A., Morris, A.P., Bichon, B.J., Riha, D.S. and Huyse, L., 2010, Geomechanical modeling of an extensional fault-propagation fold: Big Brushy Canyon monocline, Sierra Del Carmen, Texas: American Association of Petroleum Geologists (AAPG) bulletin, v. 94, p. 221-240.

1379 Smart, K. J., and Ferrill, D. A., 2018, Discrete element modeling of extensional fault-related
1380 monocline formation: Journal of Structural Geology, v. 115, p. 82-90.
1381 Soliva, R., and Benedicto, A., 2005, Geometry, scaling relations and spacing of vertically
1382 restricted normal faults: Journal of Structural Geology, v. 27, no. 2, p. 317-325.
1383 Soliva, R., Schultz, R. A., and Benedicto, A., 2005, Three-dimensional displacement-length
1384 scaling and maximum dimension of normal faults in layered rocks: Geophysical
1385 Research Letters, v. 32, no. 16.
1386 Spahic, D., Grasemann, B. and Exner, U., 2013, Identifying fault segments from 3D fault drag
1387 analysis (Vienna Basin, Austria): Journal of Structural Geology, v. 55, p. 182-195.
1388 Stearns, D. W., 1978, Faulting and forced folding in the Rocky Mountains foreland: Geological
1389 Society of America Memoirs, v. 151, p. 1-38.
1390 Stewart, I. S. and Hancock, P. L., 1991, Scales of structural heterogeneity within neotectonic
1391 normal fault zones in the Aegean region: Journal of Structural Geology, v. 13, p. 191-
1392 204.
1393 Stewart, S., and Argent, J., 2000, Relationship between polarity of extensional fault arrays and
1394 presence of detachments: Journal of Structural Geology, v. 22, no. 6, p. 693-711.
1395 Stewart, S., 2007, Salt tectonics in the North Sea Basin: a structural style template for seismic
1396 interpreters: Geological Society, London, Special Publications, v. 272, p. 361.
1397 Stewart, S. A., Harvey, M. J., Otto, S. C., and Weston, P. J., 1996, Influence of salt on fault
1398 geometry: examples from the UK salt basins: Geological Society, London, Special
1399 Publications, v. 100, no. 1, p. 175-202.
1400 Stewart, S. A., Ruffell, A. H., and Harvey, M. J., 1997, Relationship between basement-linked
1401 and gravity-driven fault systems in the UKCS salt basins: Marine and Petroleum
1402 Geology, v. 14, no. 5, p. 581-604.

1403 Stewart, S. A., 1999, Geometry of thin-skinned tectonic systems in relation to detachment layer
1404 thickness in sedimentary basins: Tectonics, v. 18, no. 4, p. 719-732.
1405 Tankard, A., and Welsink, H., 1987, Extensional tectonics and stratigraphy of Hibernia oil field,
1406 Grand Banks, Newfoundland: AAPG Bulletin, v. 71, no. 10, p. 1210-1232.
1407 Tavani, S., Carola, E., Granado, P., Quintà, A., and Muñoz, J. A., 2013, Transpressive inversion
1408 of a Mesozoic extensional forced fold system with an intermediate décollement level in
1409 the Basque-Cantabrian Basin (Spain): Tectonics, v. 32, no. 2, p. 146-158.
1410 Tavani, S., and Granado, P., 2015, Along-strike evolution of folding, stretching and breaching
1411 of supra-salt strata in the Plataforma Burgalesa extensional forced fold system (northern
1412 Spain): Basin Research, p. 1-13.
1413 Tavani, S., Balsamo, F., and Granado, P., 2018, Petroleum system in supra-salt strata of
1414 extensional forced-folds: A case-study from the Basque-Cantabrian basin (Spain):
1415 Marine and Petroleum Geology, v. 96, p. 315 - 330.
1416 Thomson, K. and Underhill, J., 1993, Controls on the development and evolution of structural
1417 styles in the Inner Moray Firth Basin: Geological Society, London, Petroleum Geology
1418 Conference series, 1993. Geological Society of London, p. 1167-1178.
1419 Trippanera, D., Acocella, V., Ruch, J., and Abebe, B., 2015, Fault and graben growth along
1420 active magmatic divergent plate boundaries in Iceland and Ethiopia: Tectonics, v. 34,
1421 no. 11, p. 2318-2348.
1422 Tsuneishi, Y., 1978, Geological and Experimental Studies on Mechanism of Block Faulting.
1423 Turner, J. P. and Williams, G. A., 2004, Sedimentary basin inversion and intra-plate shortening.
1424 Earth-Science Reviews, v. 65, p. 277-304.
1425 Tvedt, A. B. M., Rotevatn, A., and Jackson, C. A. L., 2016, Supra-salt normal fault growth
1426 during the rise and fall of a diapir: Perspectives from 3D seismic reflection data,
1427 Norwegian North Sea: Journal of Structural Geology, v. 91, p. 1-26.

1428 Uphoff, T. L., 2005, Subsalt (pre-Jurassic) exploration play in the northern Lusitanian basin of
1429 Portugal: AAPG bulletin, v. 89, no. 6, p. 699-714.
1430 van Gent, H., Urai, J. L., and de Keijzer, M., 2011, The internal geometry of salt structures – A
1431 first look using 3D seismic data from the Zechstein of the Netherlands: Journal of
1432 Structural Geology, v. 33, no. 3, p. 292-311.
1433 Vasquez, L., Nalpas, T., Ballard, J.-F., De Veslud, C. L. C., Simon, B., Dauteuil, O., and Du
1434 Bernard, X., 2018, 3D geometries of normal faults in a brittle-ductile sedimentary cover:
1435 Analogue modelling: Journal of Structural Geology, v. 112, p. 29-38.
1436 Vendeville, B., 1987, Champs de failles et tectonique en extension: Modélisation
1437 expérimentale: Université Rennes 1.
1438 Vendeville, B. C., Ge, H., and Jackson, M. P. A., 1995, Scale models of salt tectonics during
1439 basement-involved extension: Petroleum Geoscience, v. 1, no. 2, p. 179-183.
1440 Vita-Finzi, C., and King, G., 1985, The seismicity, geomorphology and structural evolution of
1441 the Corinth area of Greece: Philosophical Transactions of the Royal Society of London
1442 A: Mathematical, Physical and Engineering Sciences, v. 314, no. 1530, p. 379-407.
1443 Walker, R., Holdsworth, R., Imber, J., Faulkner, D., and Armitage, P., 2013, Fault zone
1444 architecture and fluid flow in interlayered basaltic volcaniclastic-crystalline sequences:
1445 Journal of Structural Geology, v. 51, p. 92-104.
1446 Walker, R. J., Holdsworth, R. E., Imber, J., and Ellis, D., 2012, Fault-zone evolution in layered
1447 basalt sequences: A case study from the Faroe Islands, NE Atlantic margin: Geological
1448 Society of America Bulletin, v. 124, no. 7-8, p. 1382-1393.
1449 Walsh, J. J., and Watterson, J., 1988, Analysis of the relationship between displacements and
1450 dimensions of faults: Journal of Structural geology, v. 10, no. 3, p. 239-247.

1451 Walsh, J. J., Childs, C., Imber, J., Manzocchi, T., Watterson, J., and Nell, P. A. R., 2003, Strain
1452 localisation and population changes during fault system growth within the Inner Moray
1453 Firth, Northern North Sea: Journal of Structural Geology, v. 25, no. 2, p. 307-315.
1454 Warsitzka, M., Kley, J., and Kukowski, N., 2015, Analogue experiments of salt flow and pillow
1455 growth due to basement faulting and differential loading: Solid Earth, v. 6, no. 1, p. 9.
1456 Warsitzka, M., Kley, J., Jähne-Klingberg, F., and Kukowski, N., 2017, Dynamics of prolonged
1457 salt movement in the Glückstadt Graben (NW Germany) driven by tectonic and
1458 sedimentary processes: International Journal of Earth Sciences, v. 106, no. 1, p. 131-
1459 155.
1460 Weinberg, D. M., 1979, Experimental folding of rocks under confining pressure: Part VII.
1461 Partially scaled models of drape folds: Tectonophysics, v. 54, no. 1, p. 1-24.
1462 Wheeler, G., 1939, Triassic fault-line deflections and associated warping: The Journal of
1463 Geology, p. 337-370.
1464 White, I. R., and Crider, J. G., 2006, Extensional fault-propagation folds: mechanical models
1465 and observations from the Modoc Plateau, northeastern California: Journal of Structural
1466 Geology, v. 28, no. 7, p. 1352-1370.
1467 Wibberley, C. A. J., Yielding, G., and Di Toro, G., 2008, Recent advances in the understanding
1468 of fault zone internal structure: a review: Geological Society, London, Special
1469 Publications, v. 299, no. 1, p. 5-33.
1470 Wilkins, S. J., and Gross, M. R., 2002, Normal fault growth in layered rocks at Split Mountain,
1471 Utah: influence of mechanical stratigraphy on dip linkage, fault restriction and fault
1472 scaling: Journal of Structural Geology, v. 24, no. 9, p. 1413-1429.
1473 Willsey, S. P., Umhoefer, P. J., and Hilley, G. E., 2002, Early evolution of an extensional
1474 monocline by a propagating normal fault: 3D analysis from combined field study and
1475 numerical modeling: Journal of Structural Geology, v. 24, no. 4, p. 651-669.

1476 Wilson, P., Elliott, G. M., Gawthorpe, R. L., Jackson, C. A.-L., Michelsen, L., and Sharp, I. R.,
1477 2013, Geometry and segmentation of an evaporite-detached normal fault array: 3D
1478 seismic analysis of the southern Bremstein Fault Complex, offshore mid-Norway:
1479 Journal of Structural Geology, v. 51, p. 74-91.
1480 Wilson, P., Elliott, G. M., Gawthorpe, R. L., Jackson, C. A.-L., Michelsen, L., and Sharp, I. R.,
1481 2015, Lateral variation in structural style along an evaporite-influenced rift fault system
1482 in the Halten Terrace, Norway: Influence of basement structure and evaporite facies:
1483 Journal of Structural Geology, v. 79, p. 110-123.
1484 Withjack, M. O., Meisling, K. E., and Russell, L. R., 1989, Forced Folding and Basement-
1485 Detached Normal Faulting in the Haltenbanken Area, Offshore Norway: Chapter 37:
1486 North Sea and Barents Shelf, *in* Tankard, A. J., and Balkwill, H. R., eds., Extensional
1487 Tectonics and Stratigraphy of the North Atlantic Margins, AAPG Memoir 46, p. 567-
1488 575.
1489 Withjack, M. O., Olson, J., and Peterson, E., 1990, Experimental models of extensional forced
1490 folds: AAPG Bulletin, v. 74, no. 7, p. 1038-1054.
1491 Withjack, M. O., and Callaway, S., 2000, Active normal faulting beneath a salt layer: an
1492 experimental study of deformation patterns in the cover sequence: AAPG bulletin, v.
1493 84, no. 5, p. 627-651.
1494 Withjack, M. O., Schlische, R. W., and Olsen, P. E., 2002, Rift-basin structure and its influence
1495 on sedimentary systems: Society for Sedimentary Geology Special Publication, v. 73,
1496 p. 57-81.

Fold type	3D Geometry	Section (with synkinematic strata)	Map	Refs
Forced fold	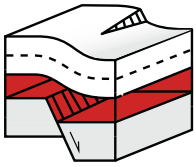	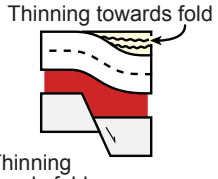		[1 - 4]
Fault-prop. fold	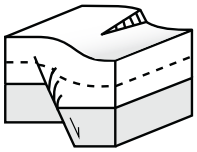	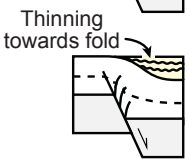		[5 -8]
Fault-prop. fold (breached)	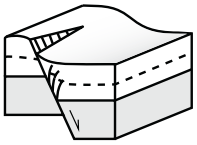	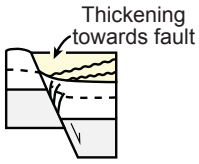		[5 - 8]
Compactional drape	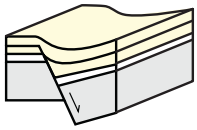	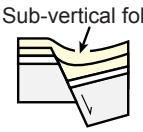		[9 - 11]
Withdrawal drape	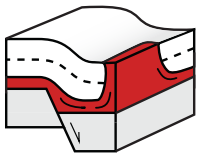			[2]
Frictional drag	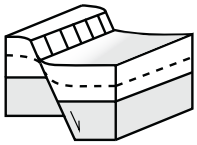	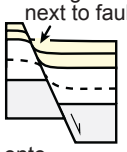	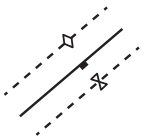	[13 - 14]
Inversion	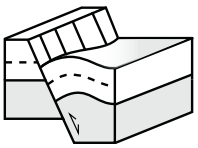	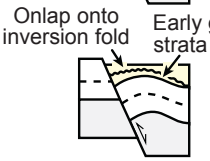		[16 - 20]
Fault-line deflection (recess)	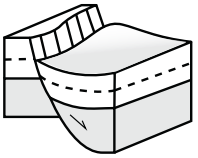	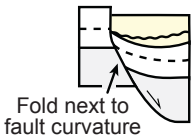	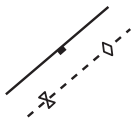	[21 - 23]
Fault-line deflection (salient)	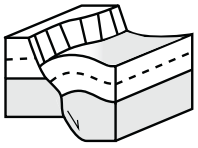	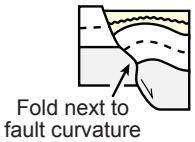	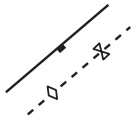	[21 - 24]

Synkinematic | Prekinematic | Detachment | Basement

Figure 1 - Fault-related folds in extensional settings. See Appendix A for brief description of how each fold is developed. References are as follows: 1 – Laubscher, 1982; 2 – Withjack and Callaway, 2000; 3 - Ford et al., 2007; 4 – Lewis et al., 2013; 5 – Withjack et al., 1990; 6 – Gawthorpe et al., 1997; 7 – Sharp et al., 2000b; 8 – Jackson et al., 2006; 9 – Thomson and Underhill, 1993; 10 - Skuce, 1996; 11- Faerseth and Lien, 2002; 12 – Billings, 1972; 13 – Resor, 2008; 14- Davis et al., 2011; 15 – Spahic et al., 2013; 16 – Badley et al., 1989; 17 – Mitra, 1993; 18 – Mitra and Islam, 1994; 19 – Turner and Williams, 2004; 20 – Jackson and Rotevatn, 2013; 21 – Wheeler, 1939; 22 – Stewart and Hancock, 1991; 23 - Ehrlich and Gabrielsen, 2004; 24 – Machette et al., 1991. Synkinematic and prekinematic strata are also shown. Example detachments could include but are not limited to, salt (or evaporitic sequences) and overpressured shale.

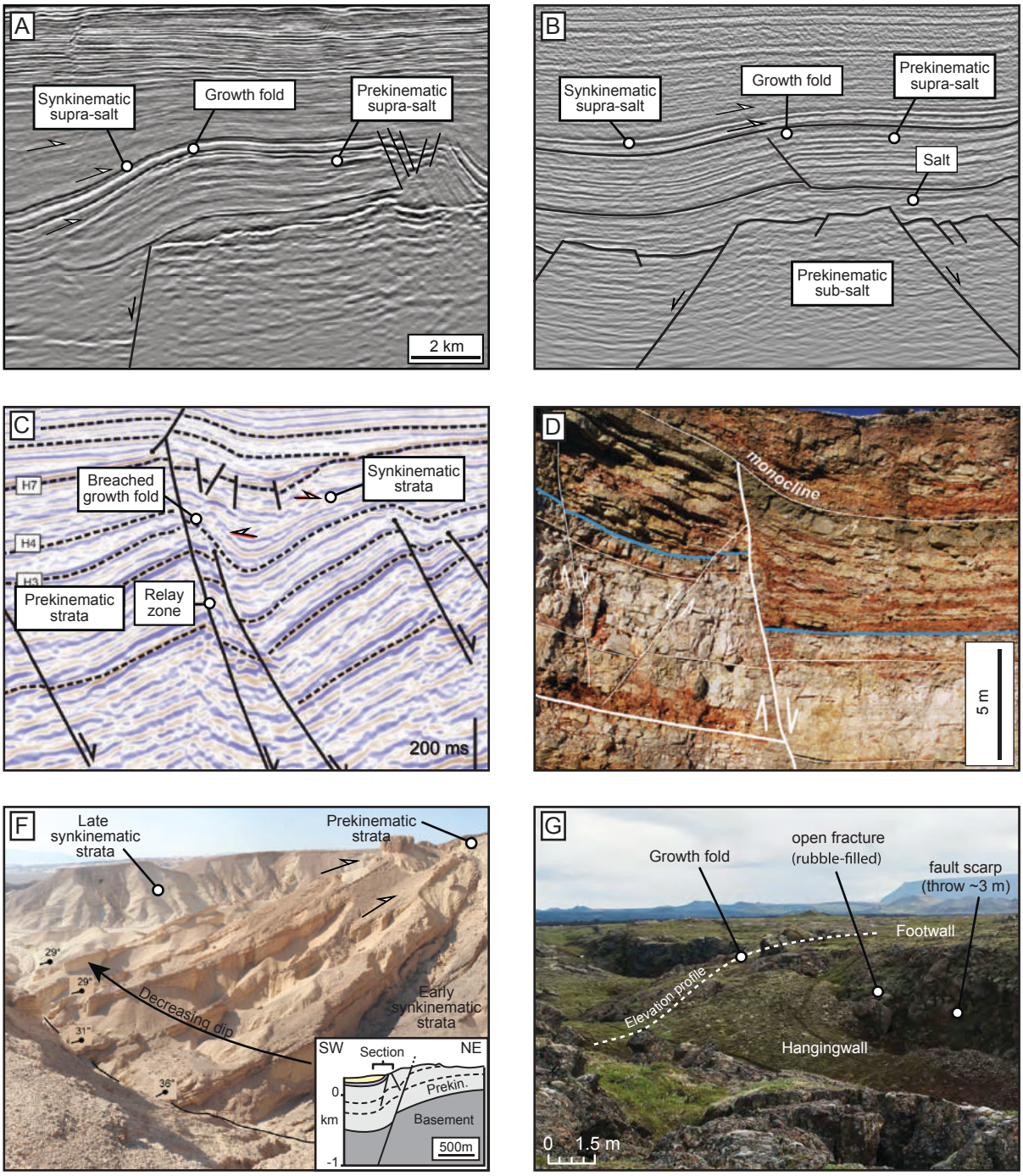

Figure 2 - Examples of growth folds from outcrop and seismic from Lewis et al., 2013 (A), Marsh et al., 2008 (B), Lapadat et al., 2016 (C), Ferrill et al., 2010 (D), Lewis et al., 2015 (E) and Bubeck et al., 2018 (F).

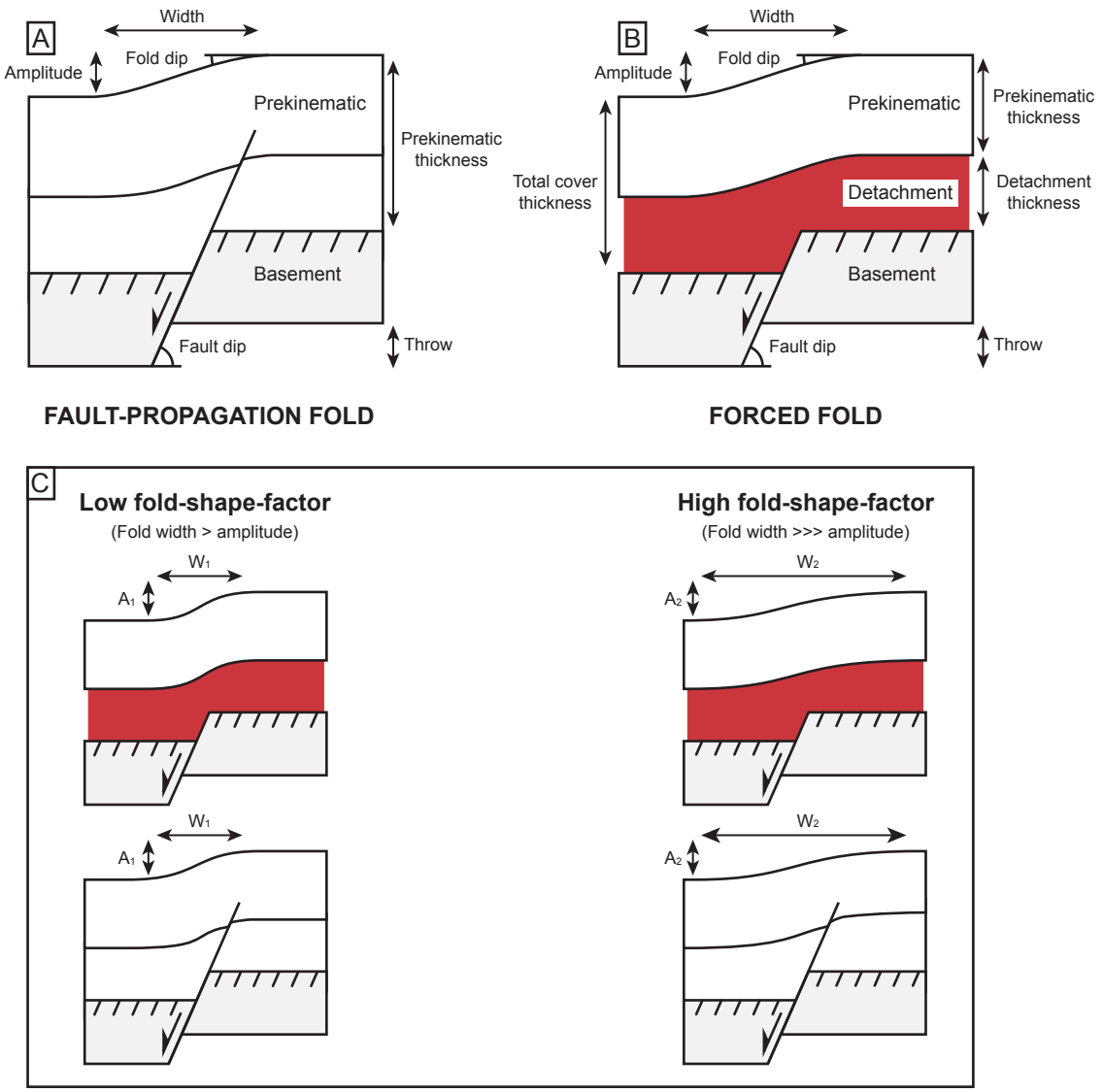

Figure 3 - Schematic, nomenclature and measured parameters for fault-propagation folds (A) and forced folds (B), showing the transition between faulting and folding. Modified after Withjack et al. (1990) and Stewart et al. (1996). Fold-shape-factor (FSF) = fold width/fold amplitude. Wide folds with small amplitudes have large FSF values, narrow folds with large amplitudes have low FSF values. Cover-detachment ratio (C:D) = prekinematic thickness/detachment thickness. Sequences with thick prekinematic strata and thin detachments have high C:D ratios. Sequences with very thin prekinematic strata and thick detachments have low C:D ratios. (C) Examples of low (FSF $\leq$ 1) and high fold-shape-factor growth folds (FSF > 1) are also shown. A_1 - A_2 and W_1 - W_2 are amplitudes and widths for the different folds. Note that $A_1 = A_2$, but $W_1 < W_2$.

A Growth fold above blind fault (lower wedge)

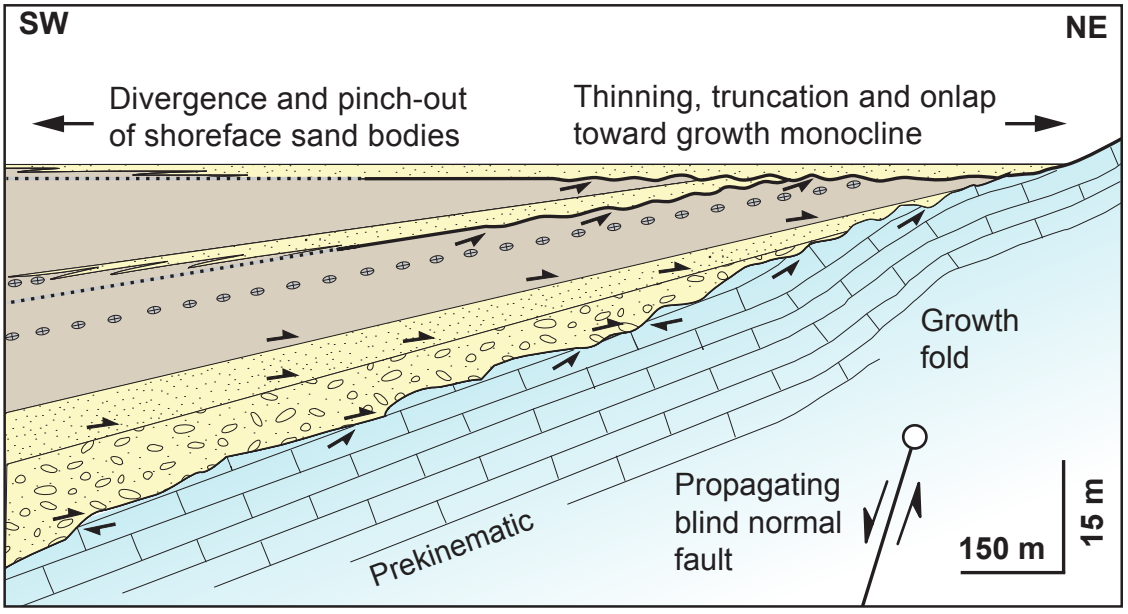

B Surface-breaking fault (upper wedge)

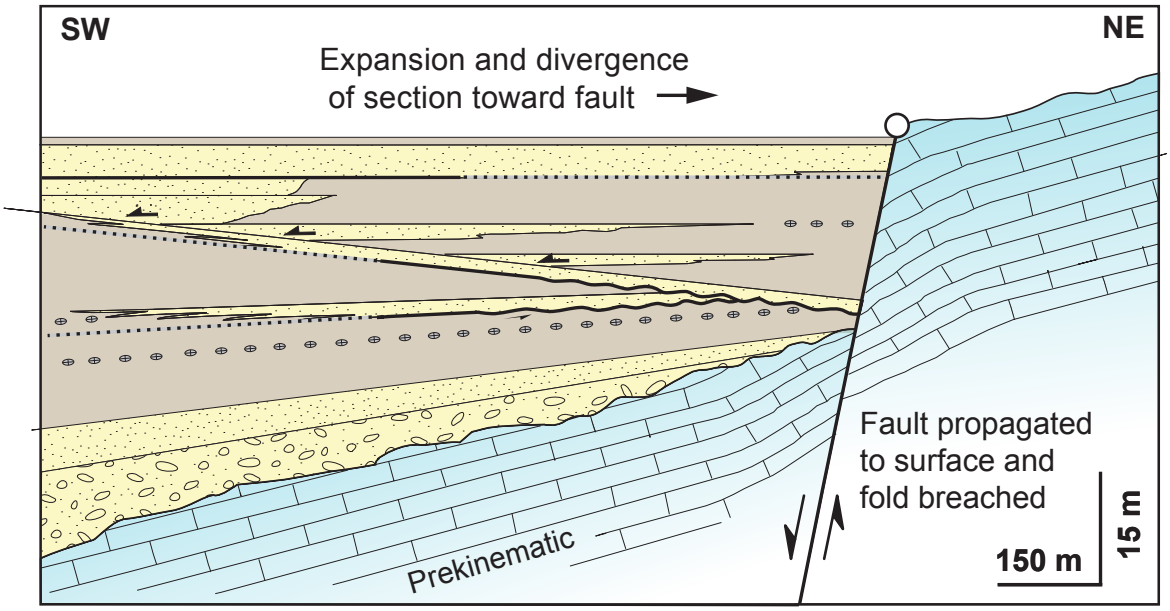

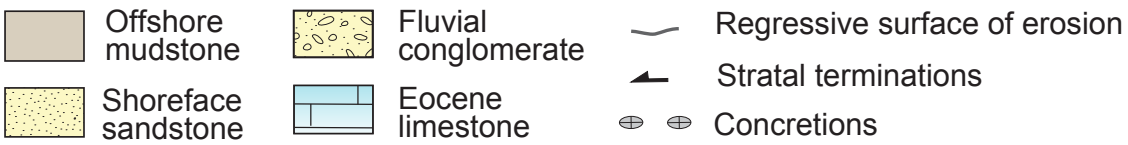

Figure 4 - Tectonostratigraphic evolution of the Baba-Sidri fault zone, Gulf of Suez. (A) Synkinematic sediments onlap onto the fault-propagation fold above a blind fault tip and thickening basinwards. (B) The fold is breached by the propagating normal fault and sediments thicken towards the fault. Modified from Gawthorpe et al. 1997.

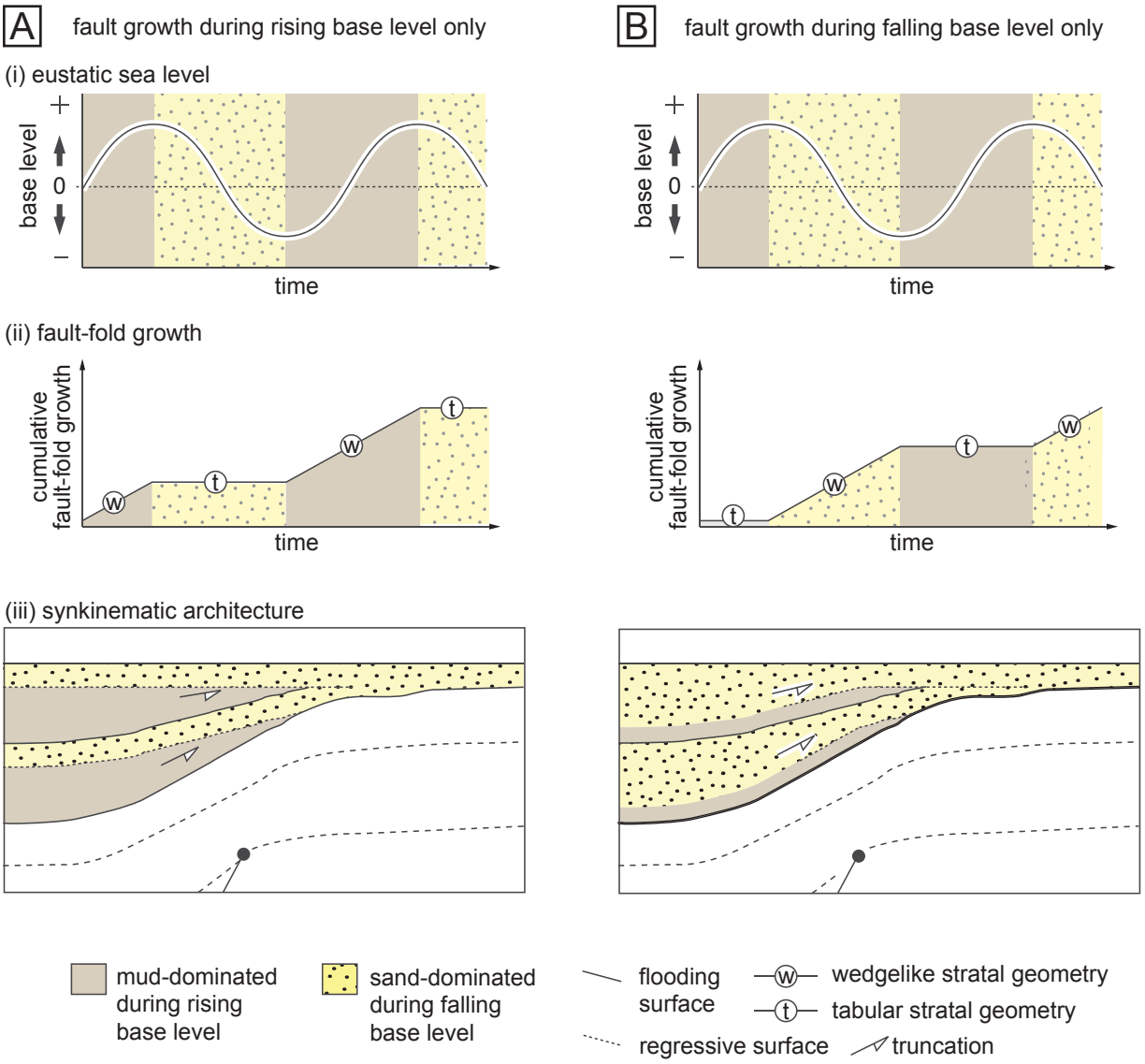

Figure 5 - How growth folds and eustasy interact to control synkinematic stratal architecture. Two end-member scenarios, depicting shallow marine shoreface sandstone deposition during falling base level (forced regression) are illustrated. (A) Surfaceward fault propagation and fold amplification during rising base level only results in basinward thickening of mudstone-dominated sediments. Shoreface sands are deposited during times of tectonic quiescence, hence are tabular and truncate underlying mudstones. (B) Surfaceward fault propagation and fold amplification during falling base level results in basinward thickening of the sandstone units. Mudstones are deposited during times of tectonic quiescence, hence are tabular and are truncated near the fold crest. Unconformities near the fold may pass basinward into correlative conformities. Modified from Lewis et al. (2015).

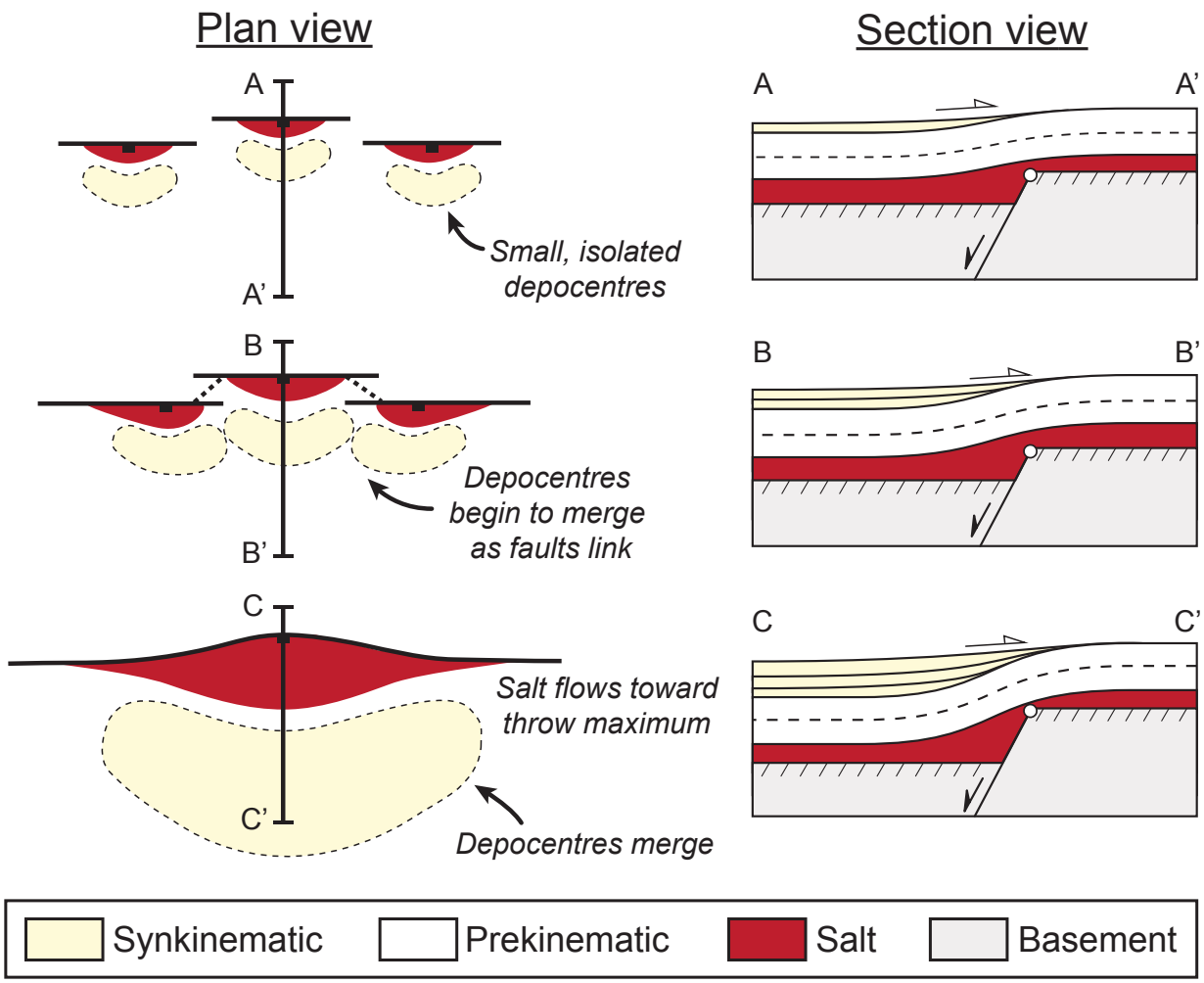

Figure 6 - Schematic diagram illustrating the evolution of salt-influenced fault-fold systems and their associated sedimentary depocentres. Modified from Richardson et al., 2005.

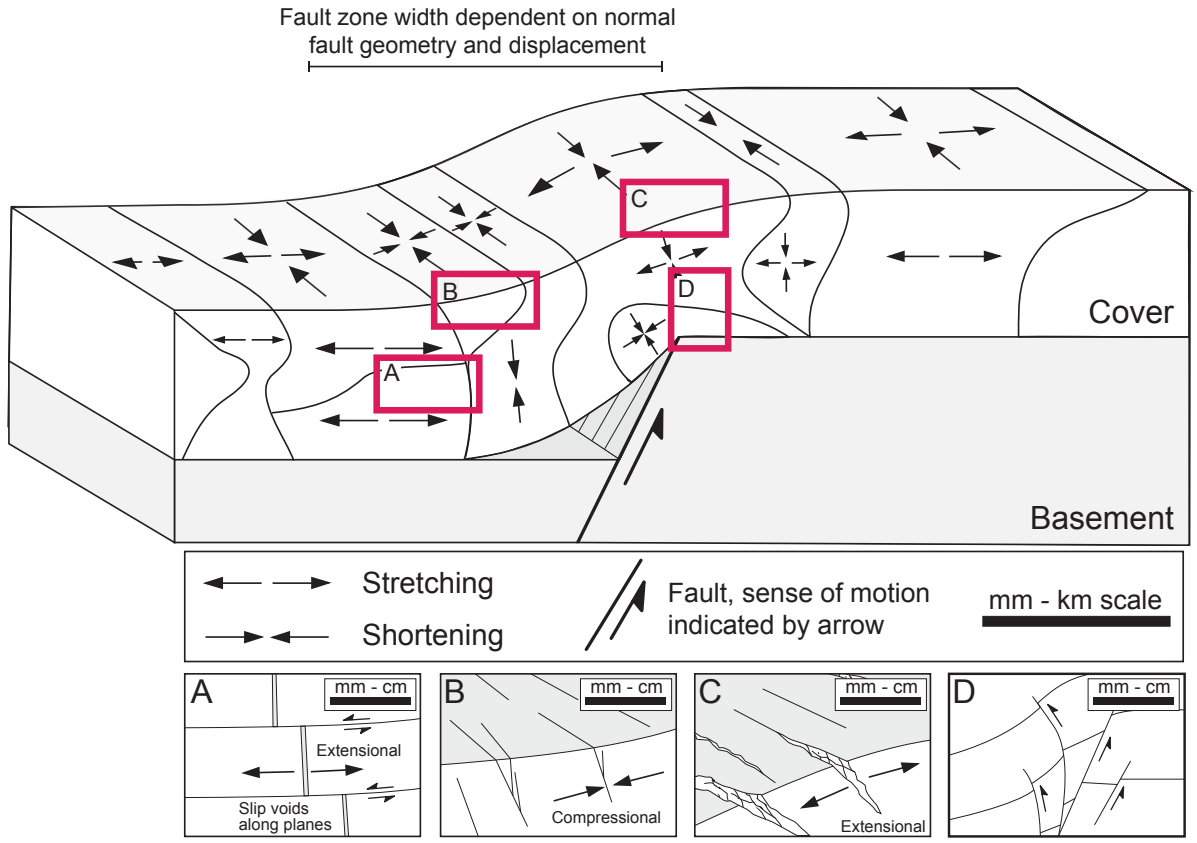

Figure 7 - Block diagram of a growth fold developed above a basement normal fault. The fold has been divided into zones according to shortening or stretching, modified from Ameen, 1988 and Ameen, 1990. Idealised secondary deformation features are superimposed: (A) layer-parallel slip surfaces and slip voids, (B) compaction bands and closed fractures, (C) dilational fractures, and (D) secondary reverse faults. Secondary deformation inspired by observations from field studies, including the Gulf of Suez (e.g. Sharp et al., 2000a; b; Jackson et al., 2006), Brushy Canyon (e.g. Ferrill et al., 2007; Smart et al., 2010), and the Pyrenees (e.g. Tavani et al., 2018), and physical models (e.g. Withjack et al., 1990; Withjack and Callaway, 2000; Jin and Groshong, 2006; Paul and Mitra, 2015). Along-strike strain is zero or extensional. This is not an exhaustive list of possible features, just of those traditionally reported from field studies – see text for details.

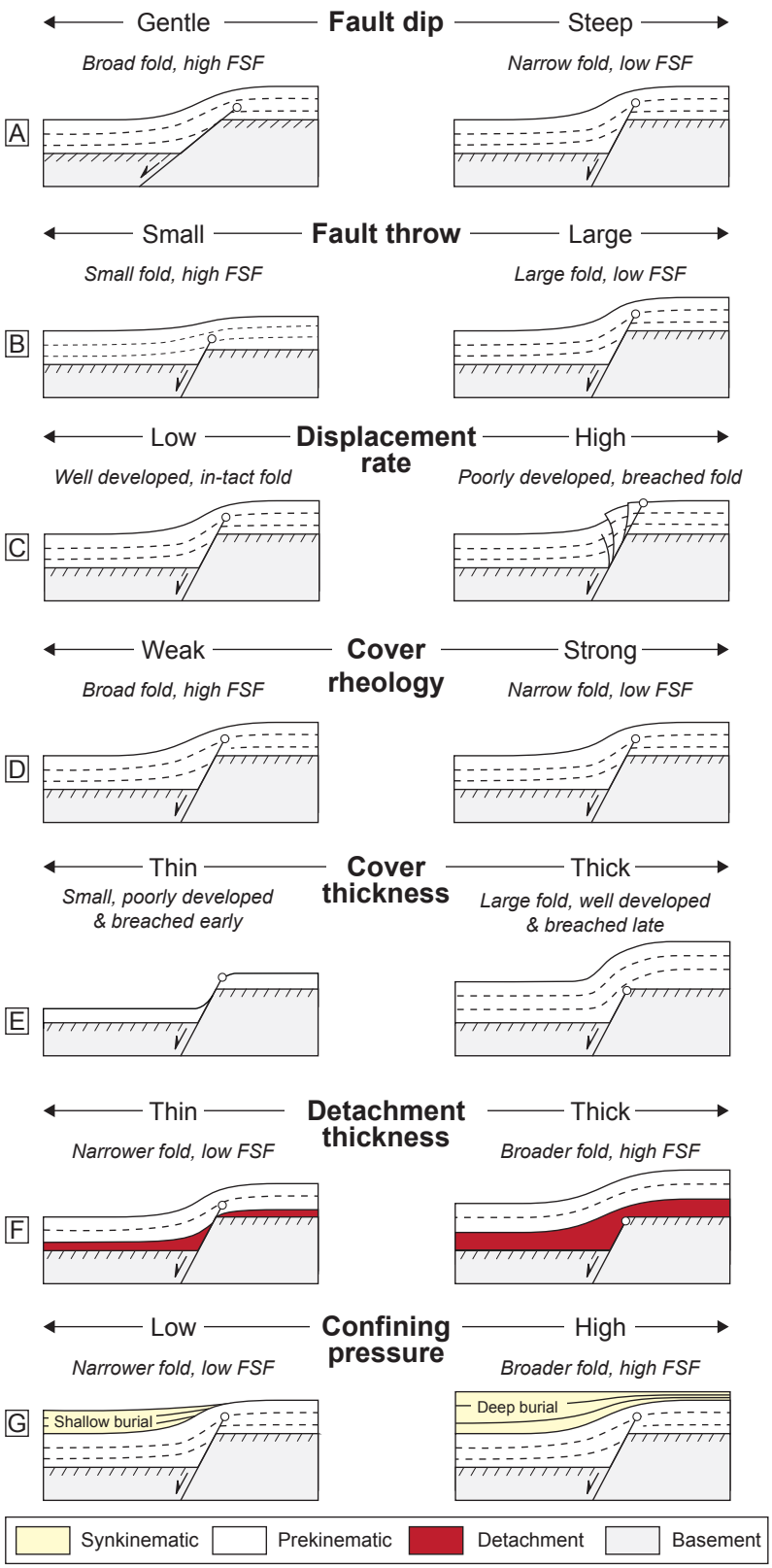

Key references

Mitra, 1993 - Fig. 4 & 9
Withjack & Callaway, 2000 - Fig. 3
Finch et al., 2004 - Fig. 7 & 8
Hardy, 2018 - Fig. 6

Mitra, 1993 - Fig. 4
Withjack & Callaway, 2000 - Fig. 7
Miller & Mitra, 2011 - Fig. 9 - 11

Hardy & McClay, 1999 - Fig. 5
Withjack & Callaway, 2000 - Fig. 14

Withjack & Callaway, 2000 - Fig. 5a & Fig. 11a
Finch et al., 2004 - Fig. 9 - 11

Withjack & Callaway, 2000 - Fig. 14

Richard, 1989 - Fig. 4.8
Withjack & Callaway, 2000 - Fig. 5
Finch et al., 2004 - Fig. 13
Hardy, 2018 - Fig. 7

Patton et al., 1998 - Fig. 7

Figure 8 - Controls on growth fold shape and size as identified by physical and numerical models. Displacement rate (C), is also linked to the strain rate and propagation rate of the upper fault tip in Withjack and Callaway (2000).

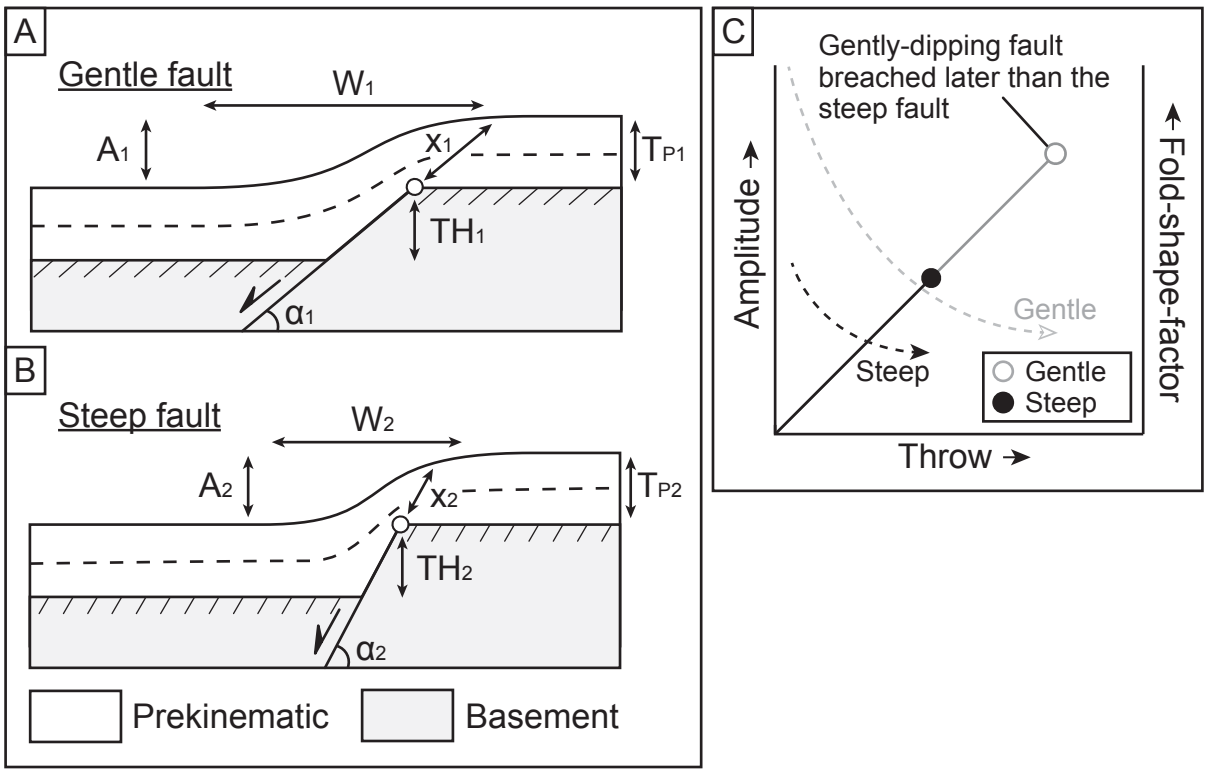

Figure 9 - Schematic showing the rapid breach of growth folds above a gently-dipping fault (A) compared to a steeply-dipping fault (B). The idealized geometry of the developing fold is also shown. (C) The amplitude (solid lines) for a gentle and steep fault increase with throw. Where faults breach the fold, a circle is plotted. The steeply-dipping fault breaches its associated fold more quickly than for a gently-dipping fault as there is a larger rock volume infront of the propagating upper normal fault tip i.e. $x_1 >> x_2$. The fold-shape-factor is shown by the dashed lines, and both decrease with increasing throw on the basement fault. Symbology for the parameters are also shown. Note how the fold associated with the steeply-dipping fault is breached earlier than the gently-dipping fault, and how the FSF decreases as the fold grows.

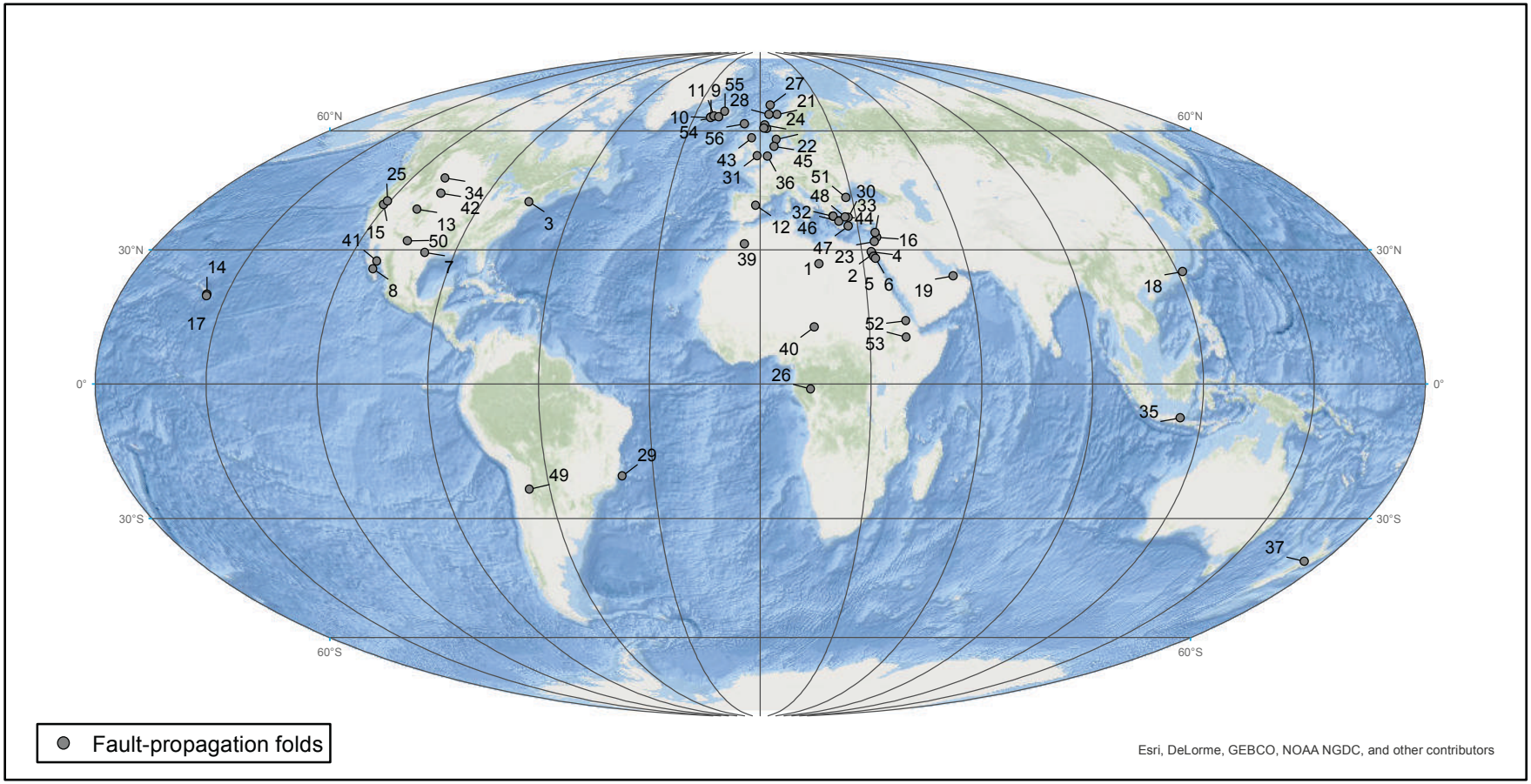

Figure 10 - Distribution of fault-propagation folds. See Appendix B for locations.

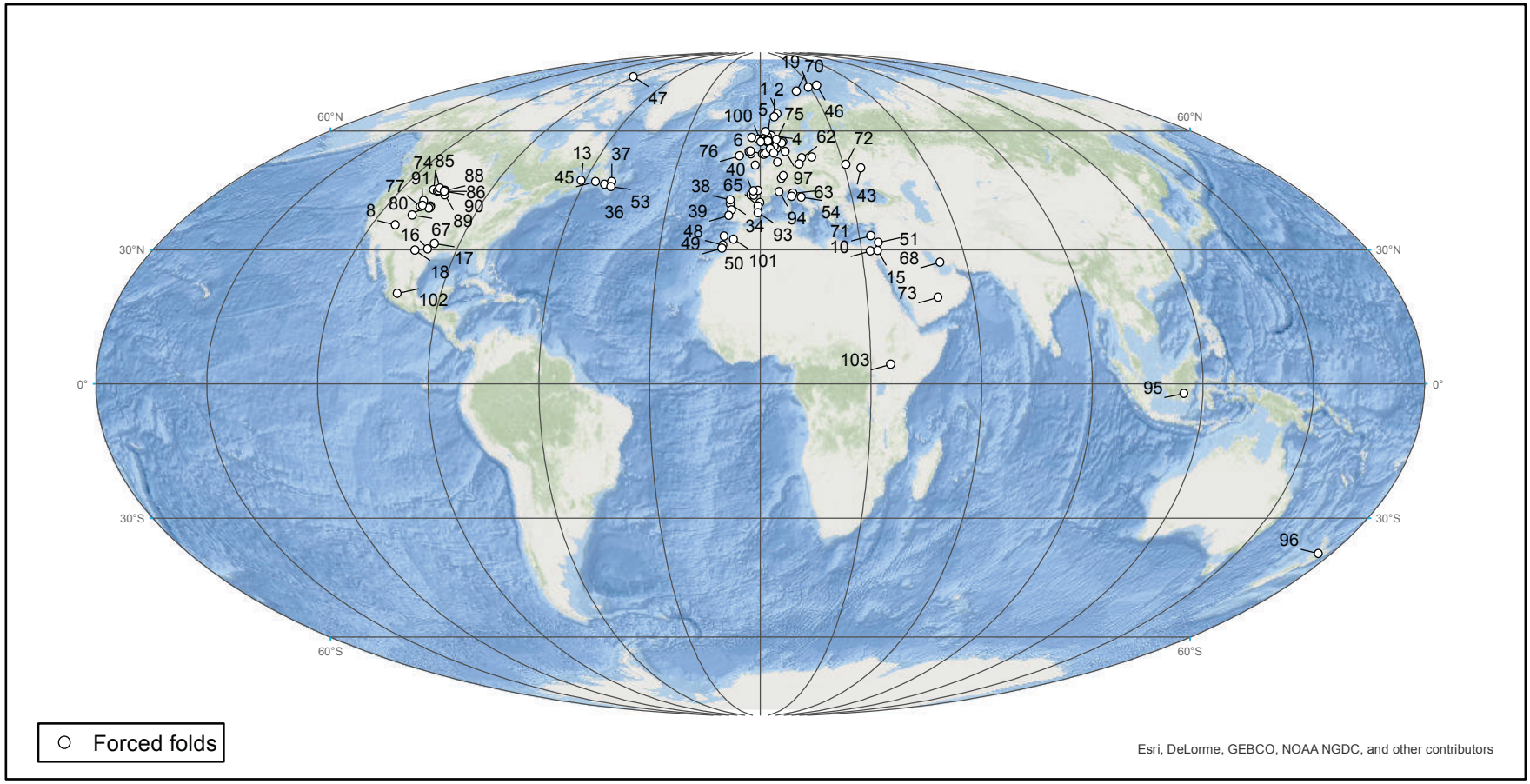

Figure 11 - Distribution of forced folds. See Appendix C for locations.

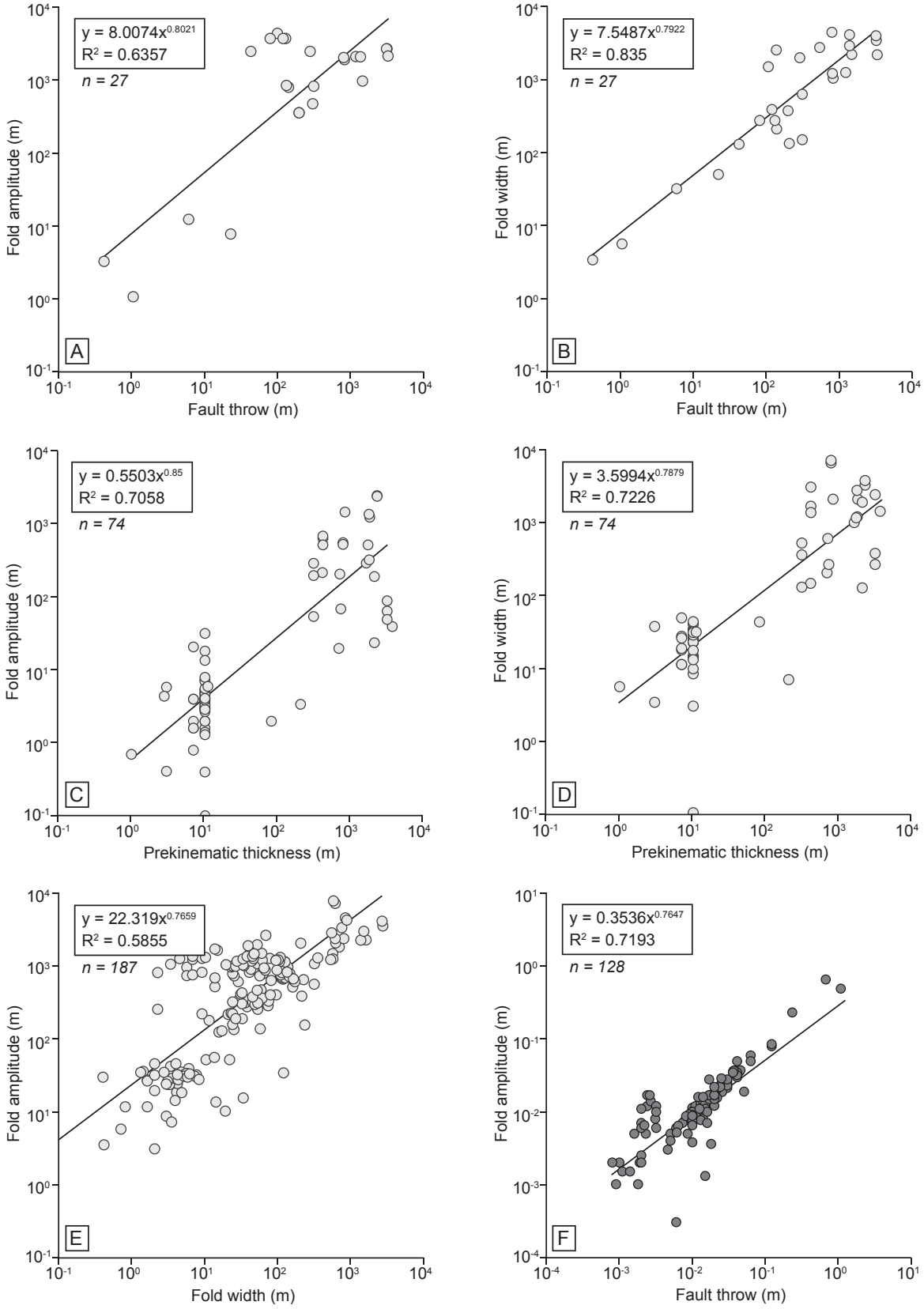
y = 8.0074x^0.8021
R² = 0.6357
n = 27
Fold amplitude (m)
Fault throw (m)
A
y = 7.5487x^0.7922
R² = 0.835
n = 27
Fold width (m)
Fault throw (m)
B
y = 0.5503x^0.85
R² = 0.7058
n = 74
Fold amplitude (m)
Prekinematic thickness (m)
C
y = 3.5994x^0.7879
R² = 0.7226
n = 74
Fold width (m)
Prekinematic thickness (m)
D
y = 22.319x^0.7659
R² = 0.5855
n = 187
Fold amplitude (m)
Fold width (m)
E
y = 0.3536x^0.7647
R² = 0.7193
n = 128
Fold amplitude (m)
Fault throw (m)
F

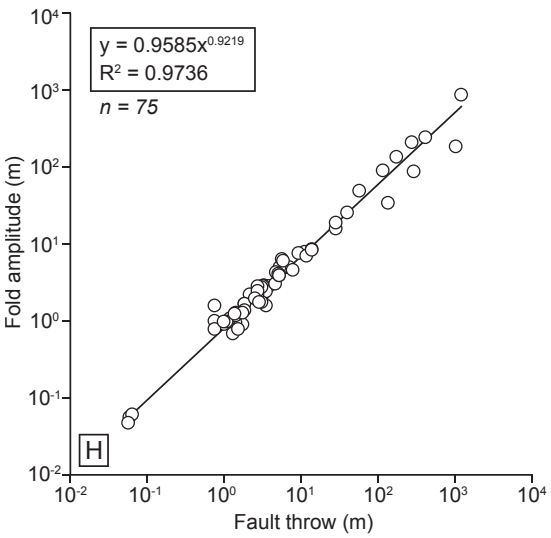
y = 0.9585x^0.9219
R² = 0.9736
n = 75
Fold amplitude (m)
Fault throw (m)
H

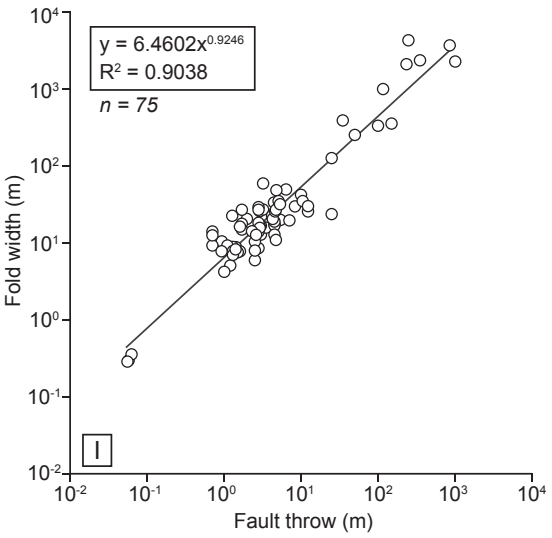
y = 6.4602x^0.9246
R² = 0.9038
n = 75
Fold width (m)
Fault throw (m)
I

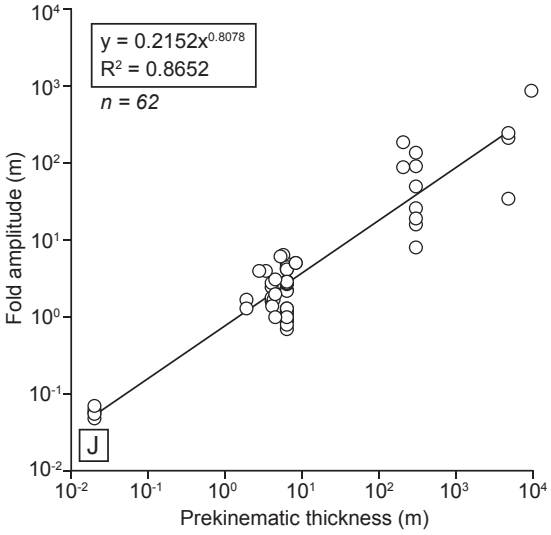
y = 0.2152x^0.8078
R² = 0.8652
n = 62
Fold amplitude (m)
Prekinematic thickness (m)
J

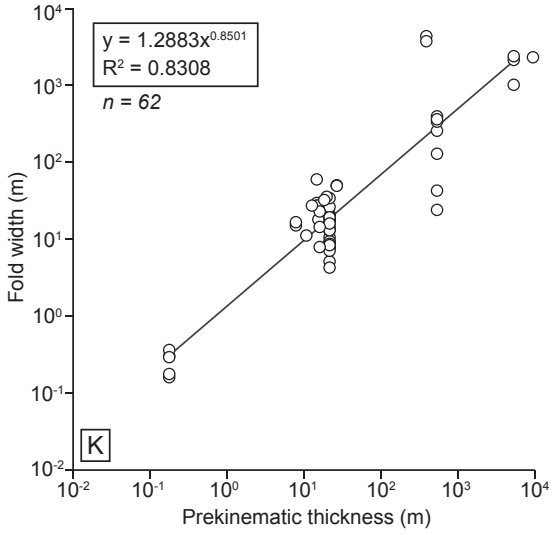
y = 1.2883x^0.8501
R² = 0.8308
n = 62
Fold width (m)
Prekinematic thickness (m)
K

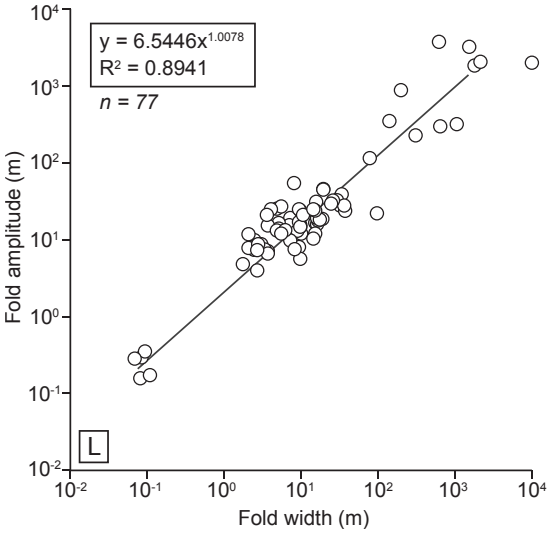
y = 6.5446x^1.0078
R² = 0.8941
n = 77
Fold amplitude (m)
Fold width (m)
L

Figure 12 - Moderate-to-strong correlations for fault-propagation folds in nature (A – E; light grey circles), physical models (F; dark grey circles) and numerical models (H-L; white circles). The best-fit regression, correlation coefficient (R_2) and number of observations (n) are also shown. See Table 2 for further details. See Fig. 2 for parameter descriptions.

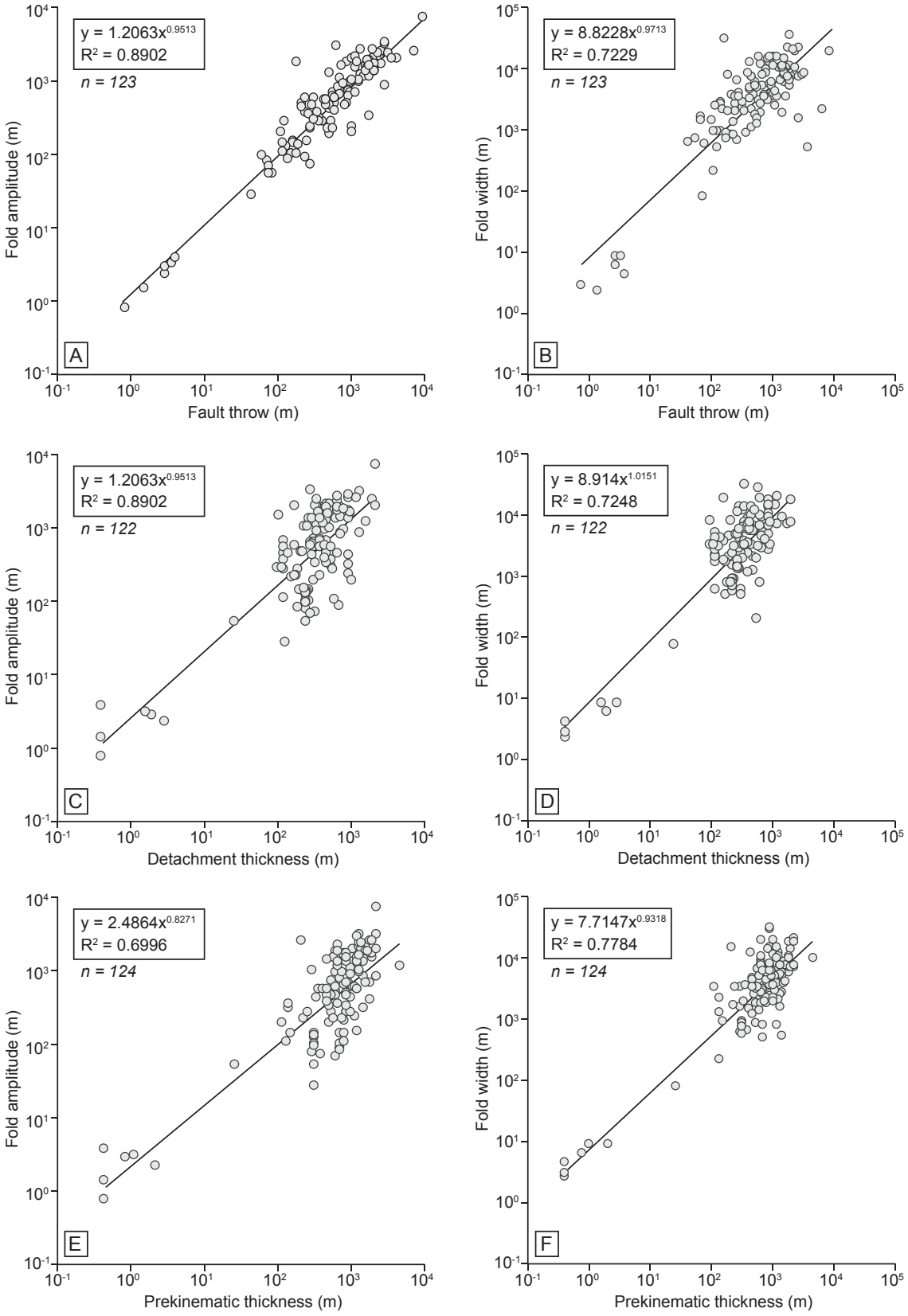
y = 1.2063x^0.9513
R² = 0.8902
n = 123
Fold amplitude (m)
Fault throw (m)
A
y = 8.8228x^0.9713
R² = 0.7229
n = 123
Fold width (m)
Fault throw (m)
B
y = 1.2063x^0.9513
R² = 0.8902
n = 122
Fold amplitude (m)
Detachment thickness (m)
C
y = 8.914x^1.0151
R² = 0.7248
n = 122
Fold width (m)
Detachment thickness (m)
D
y = 2.4864x^0.8271
R² = 0.6996
n = 124
Fold amplitude (m)
Prekinematic thickness (m)
E
y = 7.7147x^0.9318
R² = 0.7784
n = 124
Fold width (m)
Prekinematic thickness (m)
F

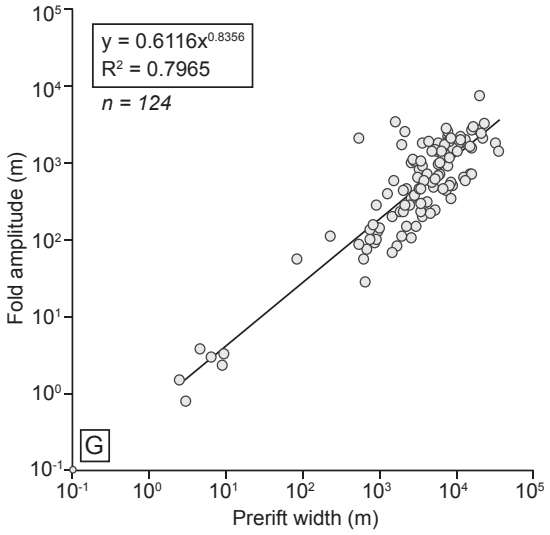

Figure 13 - Moderate-to-strong correlations for forced folds in nature (A – G; light grey circles). The best-fit regression, correlation coefficient (R_2) and number of observations (n) are also shown. Physical models lacked any moderate-to-strong correlations. See Table 2 for further details. See Fig. 2 for parameter descriptions. Analysis was not undertaken for numerical models of forced folds.

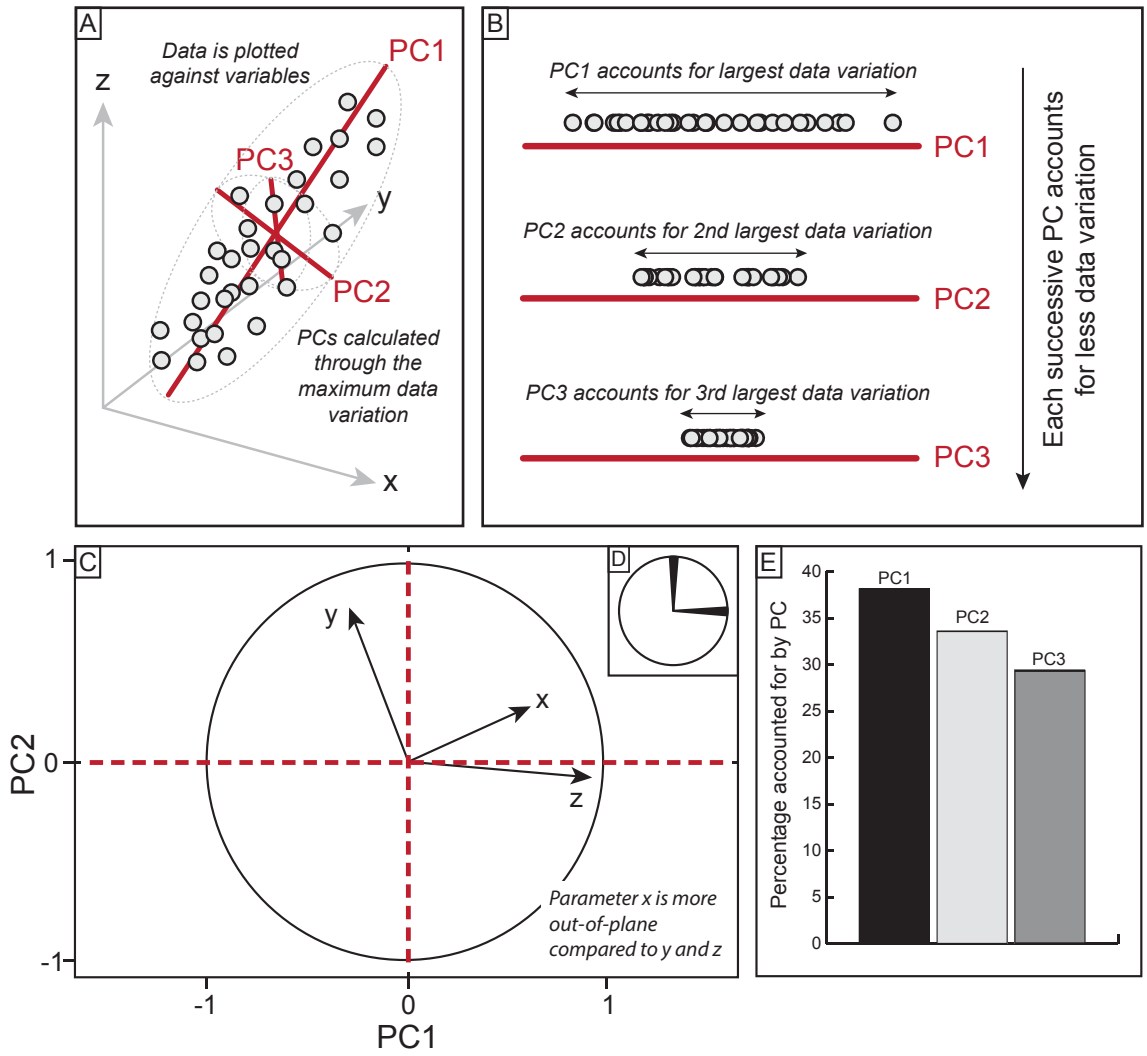

Figure 14 - Principal Component Analysis (PCA) reduces the dimensionality of multi-variate data. Data with parameters x, y and z, are plotted and a principal component (PC) may then calculated for the data to account for the maximum amount of data variation or spread (A). Successive PCs are then calculated, until all of the data variation is accounted for (B). The data may then be projected onto a loadings plot with PCs as axes (C). The parameters are displayed as arrows depending on how they relate to the PCs. Where arrows are sub-parallel to a PC, the parameter is strongly correlated with the PC. Where arrows are sub-perpindicular to a PC, the parameter is uncorrelated to the PC. Arrows that are at an angle to a PC, the parameter may be only slightly correlated to the PC. As the data is projected, the length of the arrow simply describes whether the parameter is in- or out-of- plane; the arrow is shorter when the parameter is out-of-plane relative to the PCs. The uncertainty associated with the position of the PCs is also shown (D). Where the shaded region in D is small, the higher certainty in the position of the PCs. The percentage of the data accounted for by each PC is also shown (E). We use plates C - E as a standard throughout, see Fig. 13 - 14.

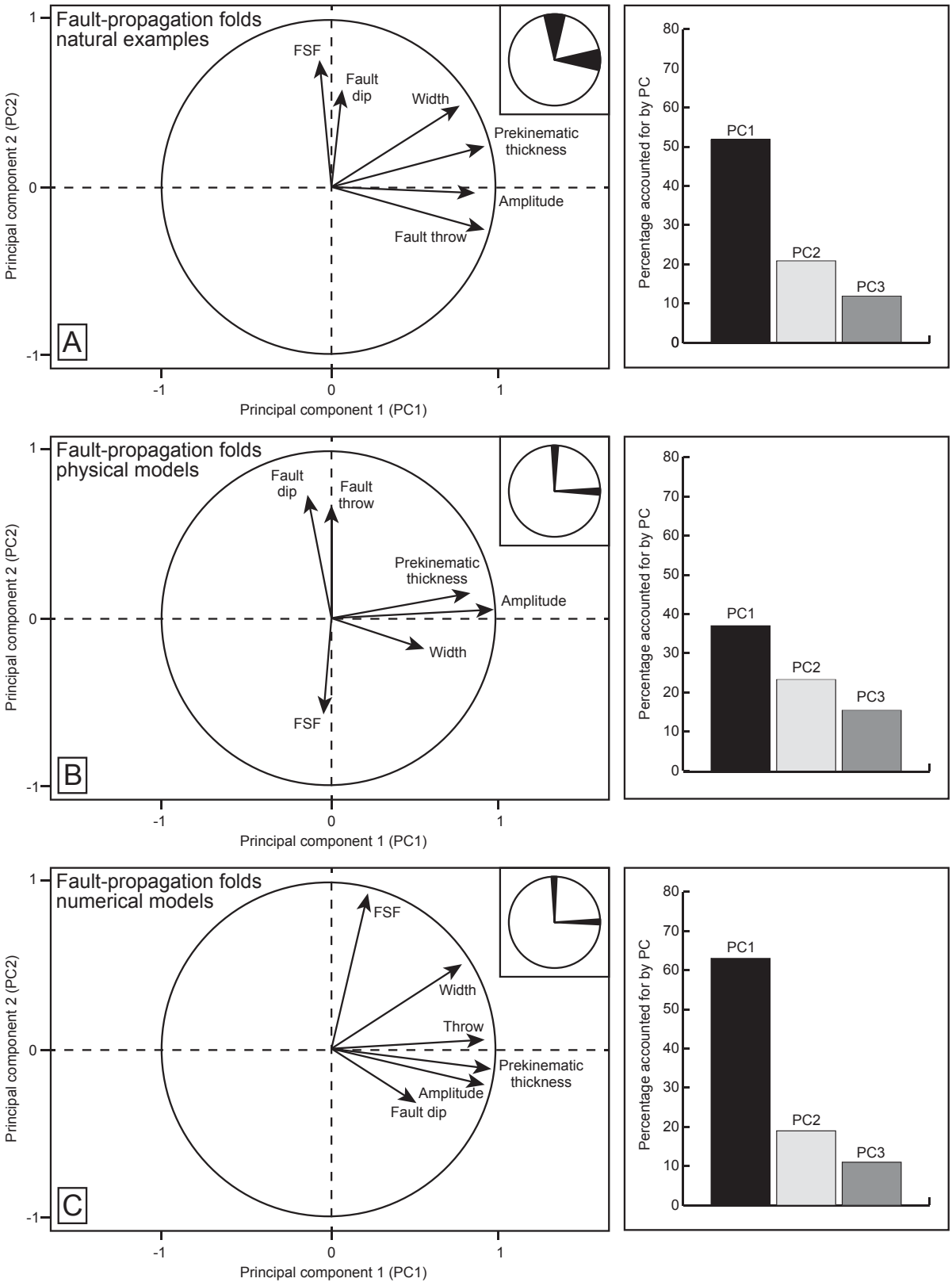

Figure 15 - Principal component analysis (PCA) for fault-propagation folds in nature (A), physical models (B) and numerical models (C). The percentage of the data variation accounted for by each principal component (PC) and uncertainty associated with missing values is shown in each case. See Fig. 2 for parameters.

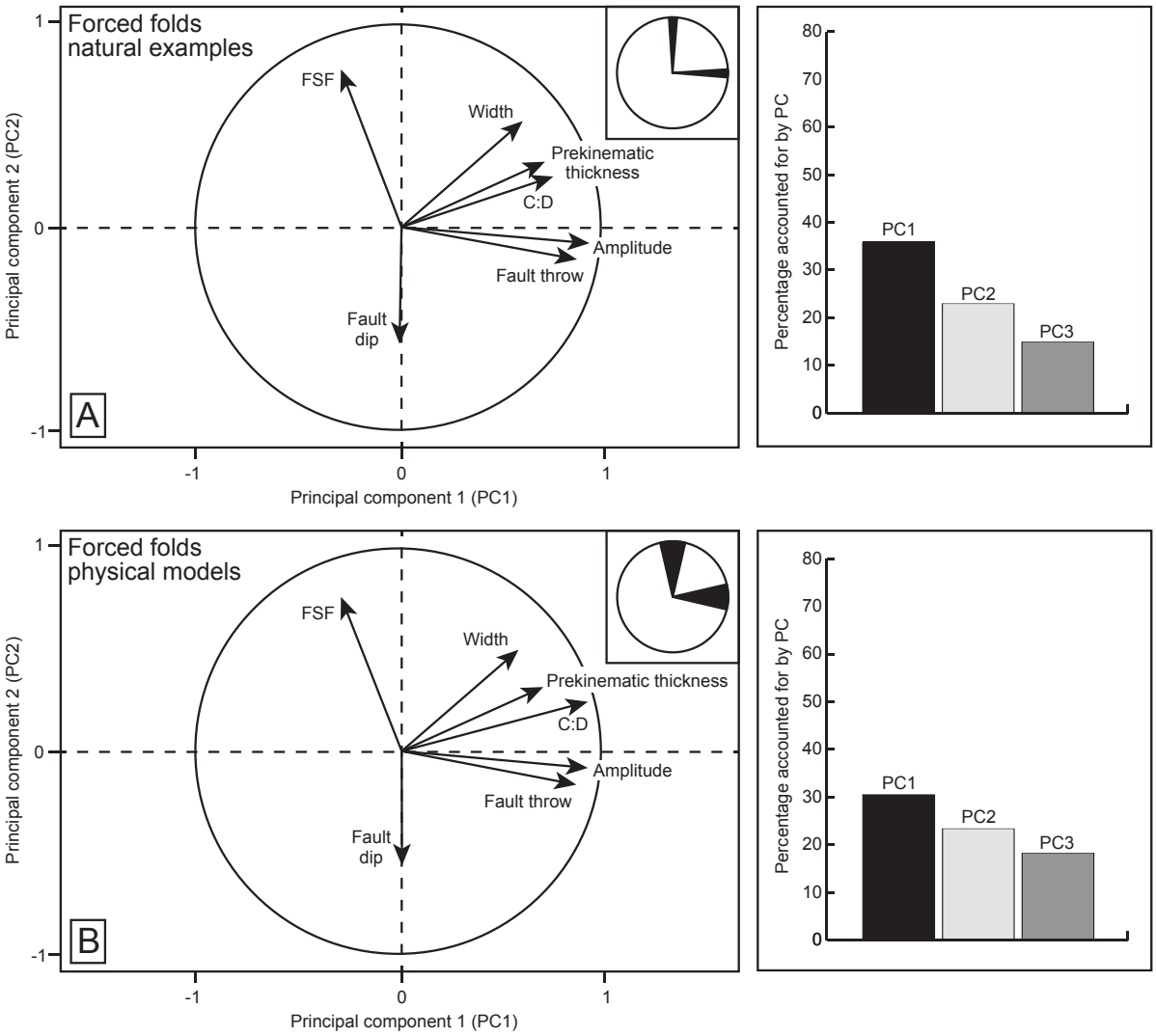

Figure 16 - Principal component analysis (PCA) for forced folds in nature (A) and physical models (B). The percentage of the data variation accounted for by each principal component (PC) and uncertainty associated with missing values is shown in each case. PCA was not undertaken for numerical models as there only Hardy (2018) explicitly model a forced fold. See Fig. 2 for parameters.

IS THIS ACTUALLY KOOPMAN ET AL. FIG. 7???

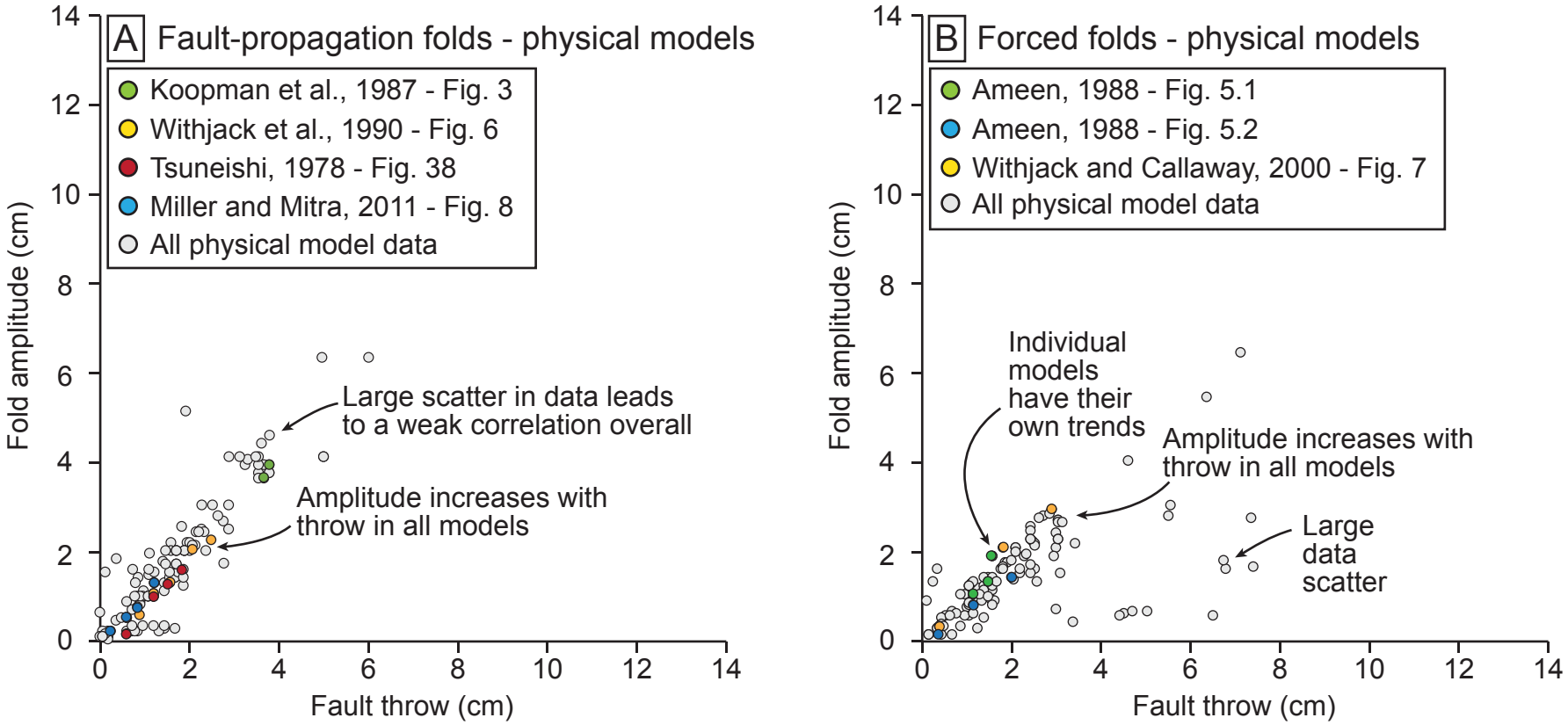

Figure 17 - Physical models of fault-propagation and forced folds show an overall weak-to-moderate correlation between fault throw and fold amplitude. However, individual models in isolation, show similar trends as observed in nature e.g. increased amplitude with throw. These relationships are often hidden within the data are likely due to the large amount of variance introduced by different model setups and material properties.

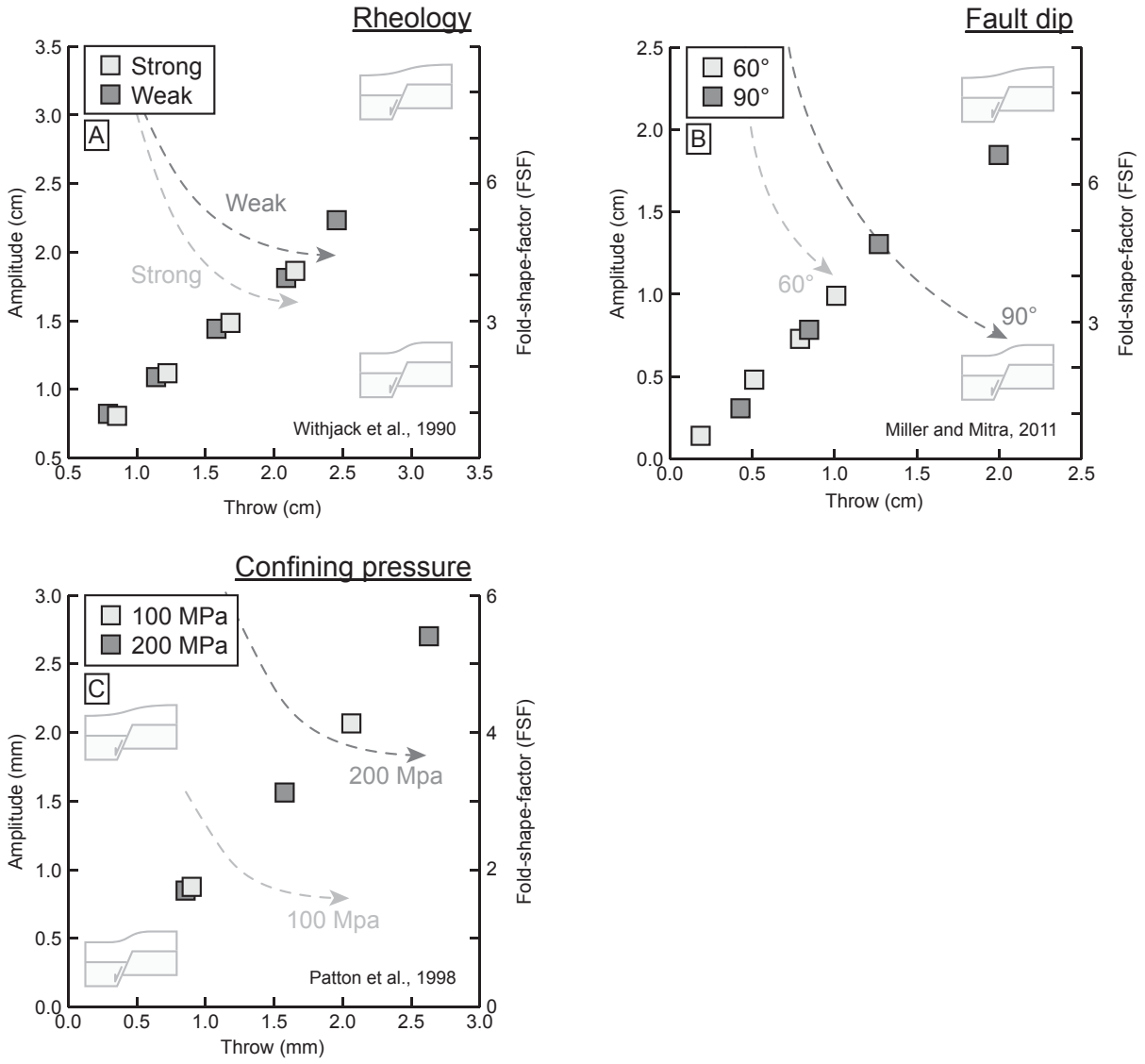

Figure 18 - Predictions of fault-propagation fold growth from physical models due to changes in (A) cover rheology, (B) fault dip, and (C) confining pressure. Fold-shape-factor (FSF) is represented by the dashed line and decreases with increased throw. A schematic drawing of the fold shape is also shown. Amplitude is on the left-y-axis, while FSF is on the right-y-axis for panels A - C. The squares are amplitude-throw points. Only measurements from intact folds, that are not breached by the underlying fault, are plotted. FSF and amplitude values are taken from the same model at the same time. The reference for each plot is also shown.

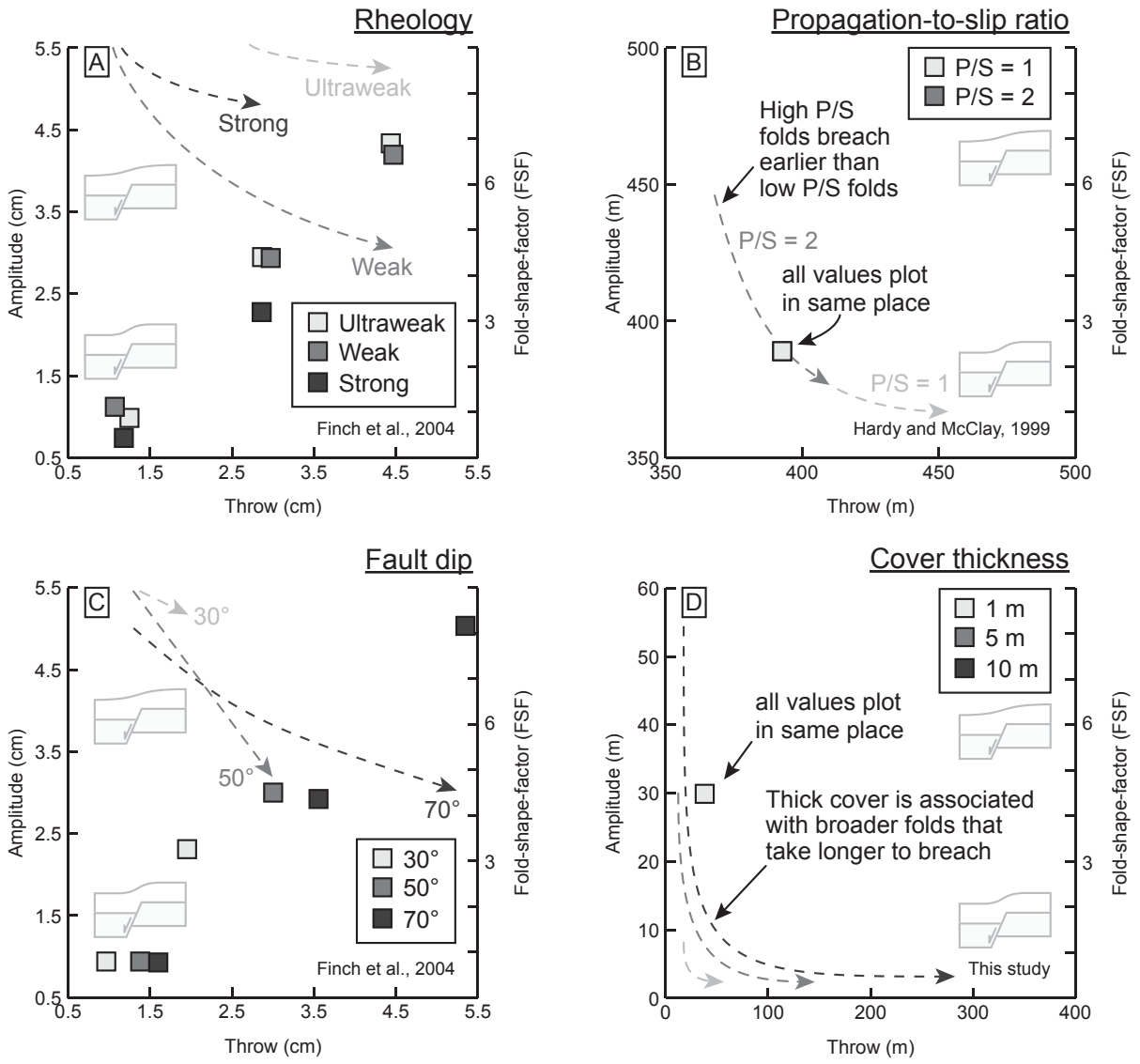

Figure 19 - Predictions of fault-propagation fold growth from numerical models due to changes in (A) cover rheology, (B) propagation-to-slip ratio, (C) fault dip, (D) cover thickness. Fold-shape-factor (FSF) is represented by the dashed line and decreases with increased throw. A schematic drawing of the fold shape is also shown. Amplitude is on the left-y-axis, while FSF is on the right-y-axis for panels A - D. The squares are amplitude-throw points. Only measurements from intact folds, that are not breached by the underlying fault, are plotted. The reference for each plot is also shown. Cover thickness (D) was calculated in this study using forward trishear models (after Allmendinger, 1998).

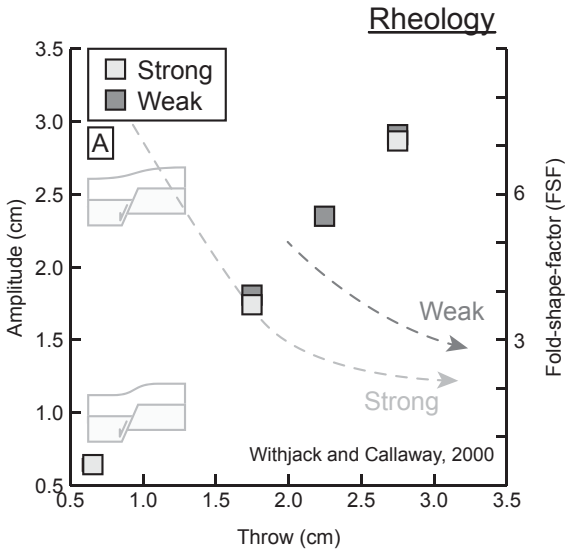
Rheology
Strong
Weak
A
Weak
Strong
Withjack and Callaway, 2000
Amplitude (cm)
Fold-shape-factor (FSF)
Throw (cm)

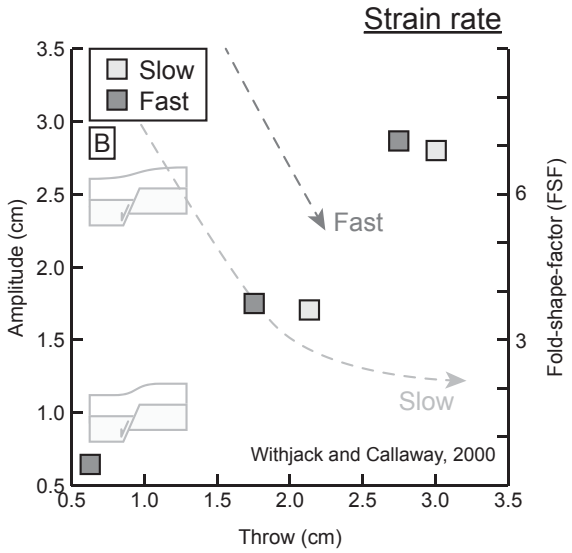
Strain rate
Slow
Fast
B
Fast
Slow
Withjack and Callaway, 2000
Amplitude (cm)
Fold-shape-factor (FSF)
Throw (cm)

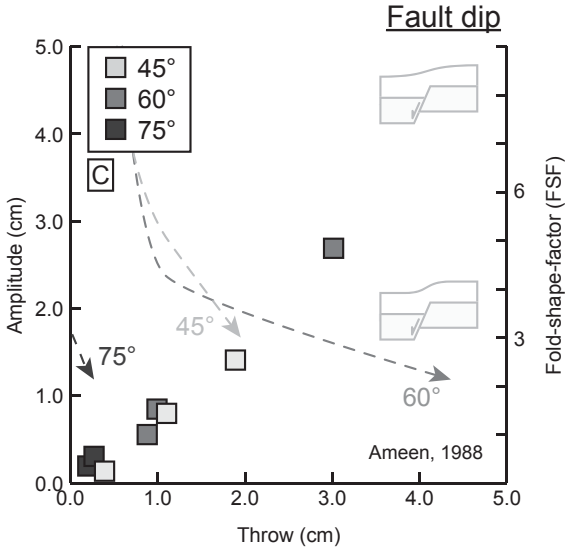
Fault dip
45°
60°
75°
C
45°
75°
60°
Ameen, 1988
Amplitude (cm)
Fold-shape-factor (FSF)
Throw (cm)

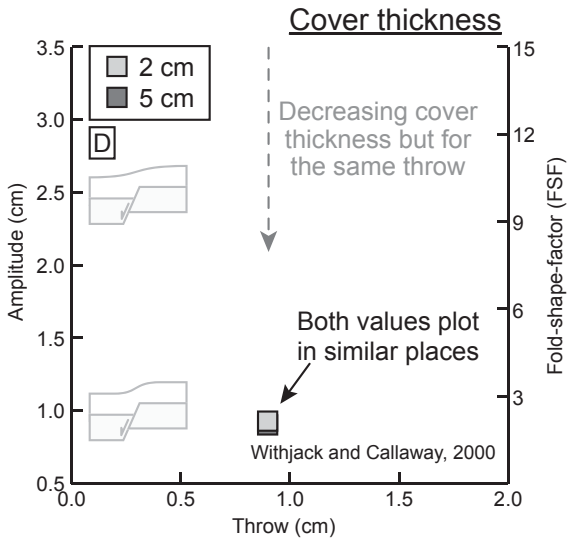
Cover thickness
2 cm
5 cm
D
Decreasing cover thickness but for the same throw
Both values plot in similar places
Withjack and Callaway, 2000
Amplitude (cm)
Fold-shape-factor (FSF)
Throw (cm)

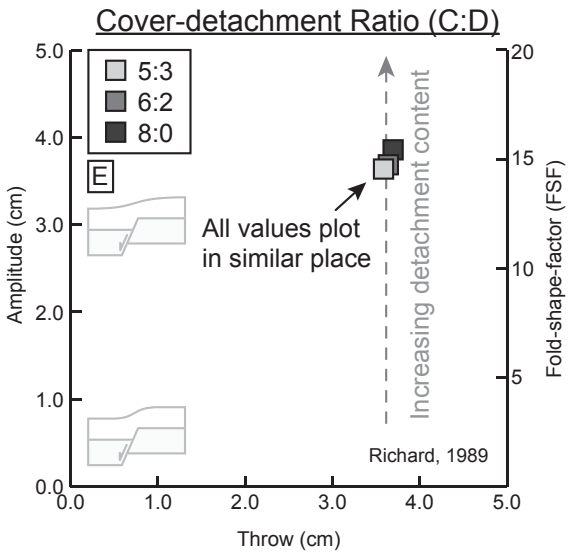
Cover-detachment Ratio (C:D)
5:3
6:2
8:0
E
All values plot in similar place
Increasing detachment content
Richard, 1989
Amplitude (cm)
Fold-shape-factor (FSF)
Throw (cm)

Figure 20 (previous page) - Predictions of forced fold growth from physical models due to changes in (A) cover rheology, (B) strain rate, (C) fault dip, (D) cover thickness, and (E) cover-detachment ratio. Fold-shape-factor (FSF) is represented by the dashed line and decreases with increased throw. A schematic drawing of the fold shape is also shown. Amplitude is on the left-y-axis, while FSF is on the right-y-axis for panels A - E. The squares are amplitude-throw points. Fold amplitude data on panels D – E are largely similar but the fold width and hence the FSF, is different. Only measurements from intact folds, that are not breached by the underlying fault, are plotted. References for each plot are also shown. FSF and amplitude values are taken from the same model at the same time. Note that the strain rate and displacement rate are linked in Withjack and Callaway (2000).

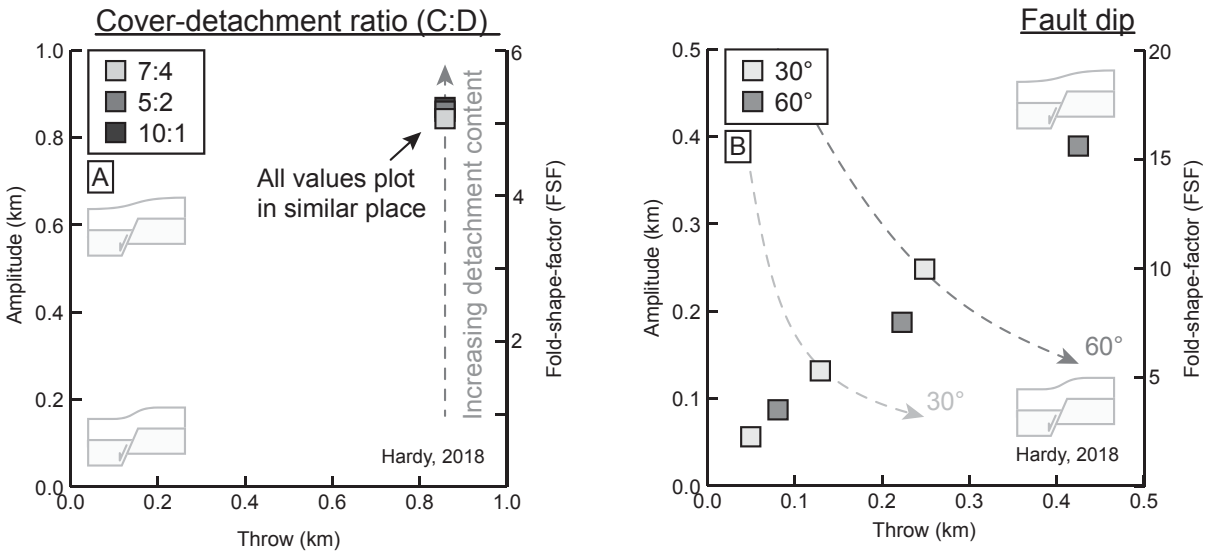

Figure 21 - Predictions of forced fold growth from numerical models (from Hardy, 2018) due to changes in (A) cover-detachment ratio, (B) fault dip. Fold-shape-factor (FSF) is represented by the dashed line and decreases with increased throw. Amplitude is on the left-y-axis, while FSF is on the right-y-axis for panels A - B. A schematic drawing of the fold shape is also shown. The squares are amplitude-throw points. Only measurements from intact folds, that are not breached by the underlying fault, are plotted.

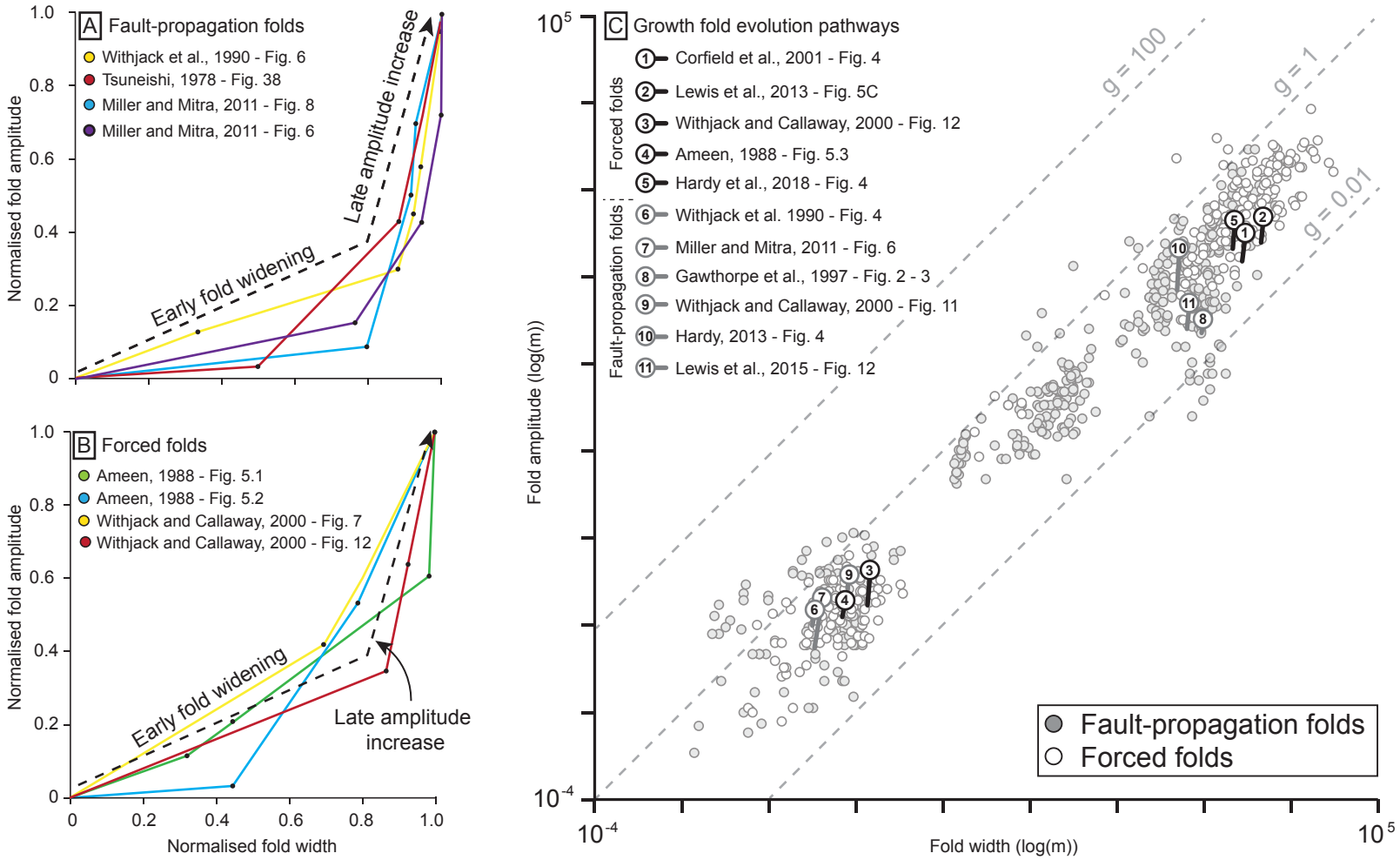

Figure 22 - Normalised fold amplitude versus normalised fold width for physical models of fault-propagation (A) and forced folds (B). The approximate growth pathways for 5 forced (folds 1 - 5 on C) and 6 fault-propagation (folds 6 - 11 on C) folds are also shown relative to the growth fold database - see Appendix D - E for the data. The pathways have been inferred from growth strata or snapshots for models at regular increments. Note how the fold widths are established early during folding, before amplifying as throw is accrued. As the fold width is initially greater than the amplitude, the fold-shape-factor (FSF) is initially large and then decreases as the fold grows.

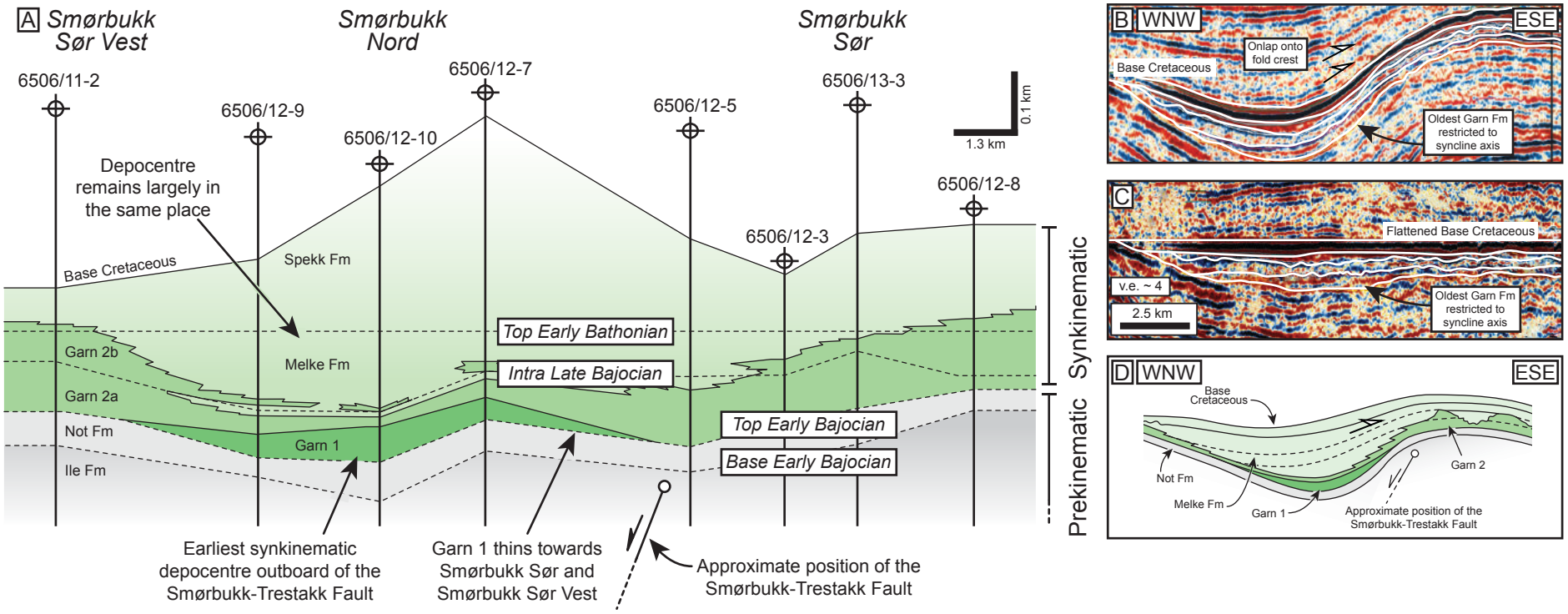

Figure 23 - Simplified correlation panel flattened on the Top Early Bathonian time-line (A). The earliest synkinematic unit (Garn 1) is restricted to the synclinal axis in the vicinity of Smørbukk Nord, and thins towards Smørbukk Sør Vest and Smørbukk Sør. The Late Bajocian to Early Bathonian package is thickest in the vicinity of Smørbukk Nord. Seismic reflection dip line from the footwall crest of Smørbukk Nord to Smørbukk Sør (B). Same seismic flattened on the Base Cretaceous (C). Schematic of the growth fold above the Smørbukk-Trestakk Fault (D). Modified from Corfield et al. (2001).

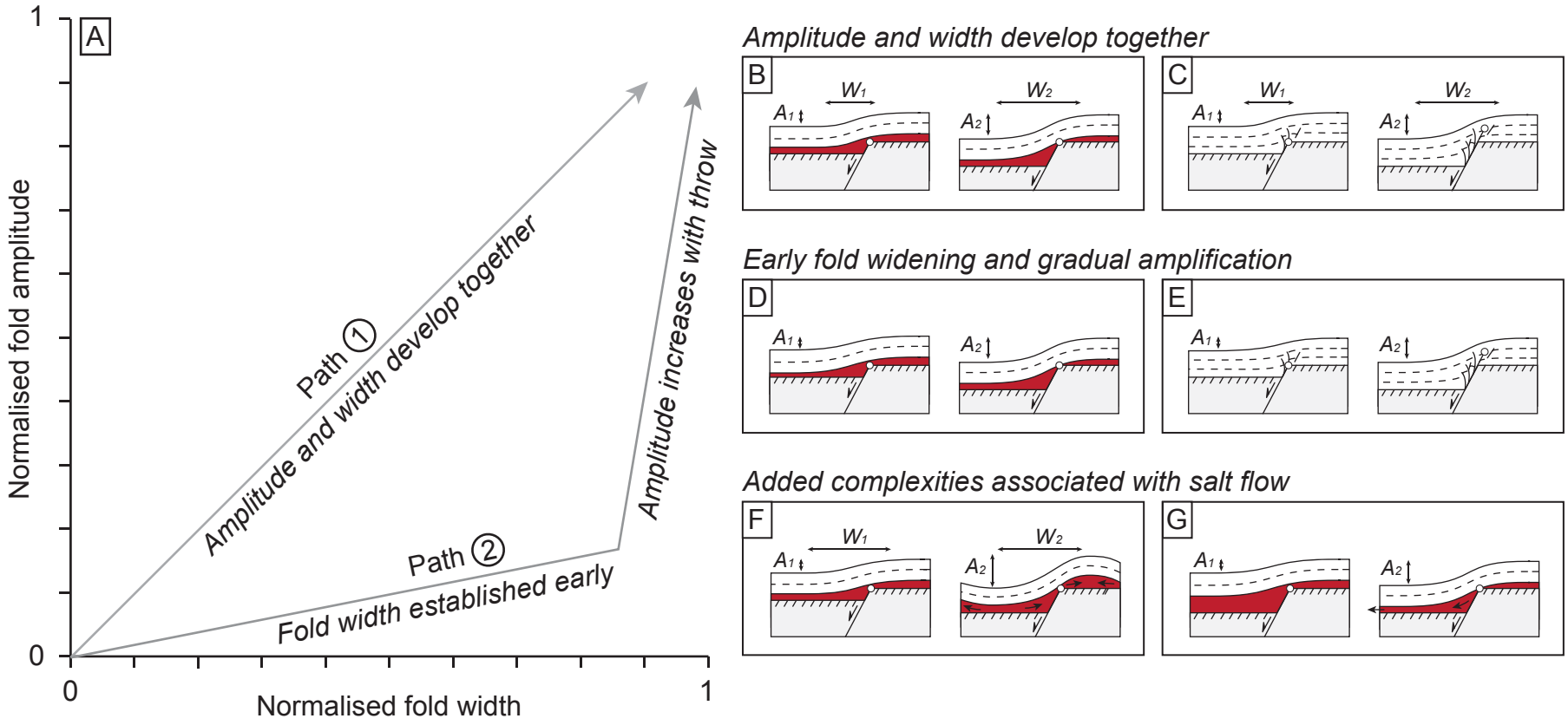

Figure 24 - Growth of fault-propagation and forced folds (A). Two schematic paths for the growth fold evolution are plotted (Path 1 and Path 2). Folds following Path 1 amplify and widen at a similar, gradual rate (B - C). Folds following path 2 widen early and amplify relatively late during fold growth (D - E). Amplitude and width variations due to salt flow are also shown (F - G). Changes in the fold amplitude or width changes in cross-section is shown, all other parameters remain the same (B - G).

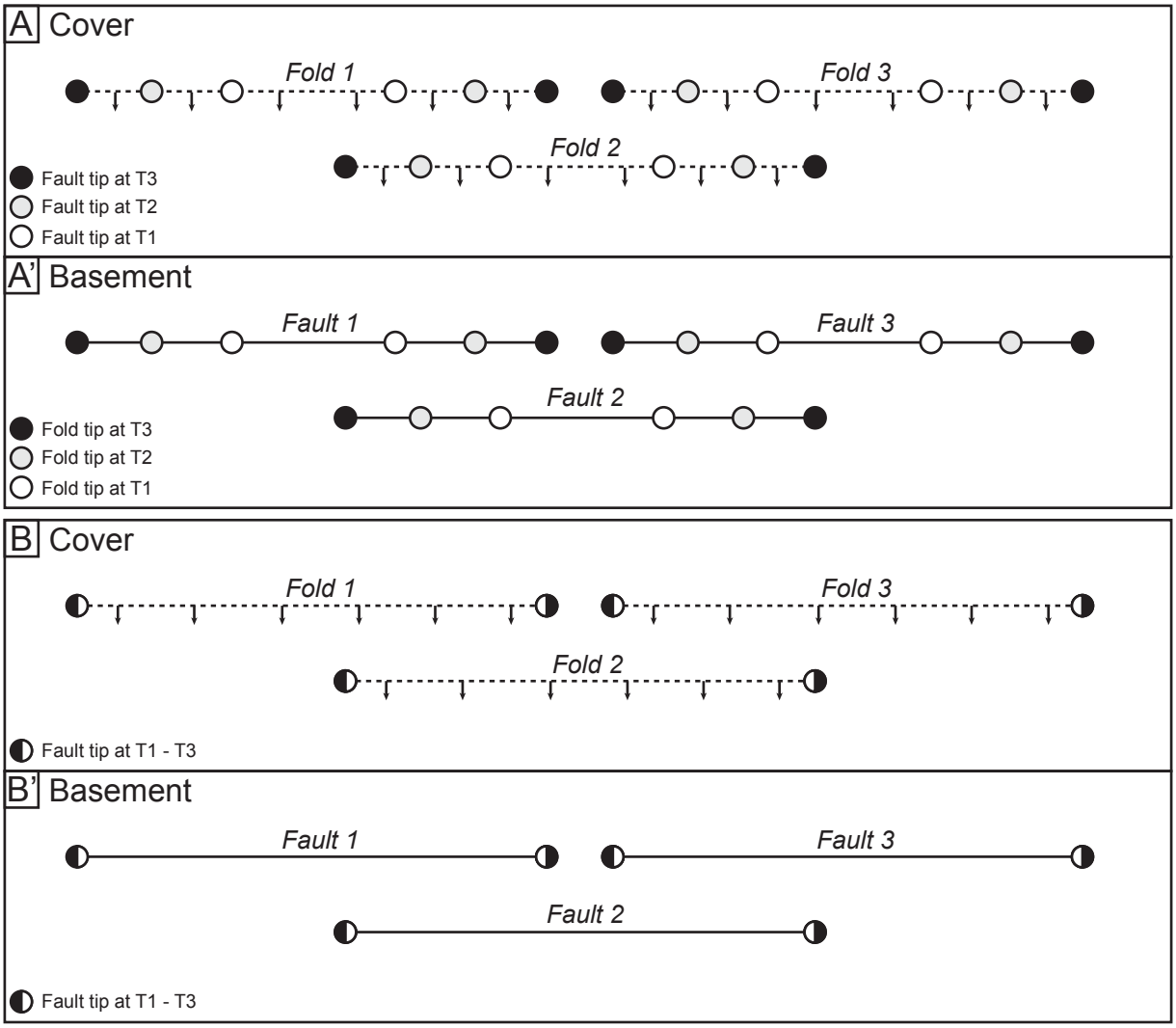

Figure 25 - Evolution of cover growth folds above growing basement-involved normal faults. (A) Isolated fault growth model. The basement normal faults get incrementally longer through time and accumulate displacement gradually; growth folds develop their along-strike width gradually and attain their amplitude as displacement is accrued. (B) Coherent fault growth model. The basement normal faults establish their lengths very rapidly before attaining displacement gradually; growth folds attain their along-strike width rapidly and then amplify as displacement is accrued. The across-strike width of fold is established early during fold growth in both models, and increases very slowly. Modified from Jackson and Rotevatn, 2013; Jackson et al. 2017. The direction of the dipping growth fold limb is indicated by the direction of the black arrows in (A) and (B).

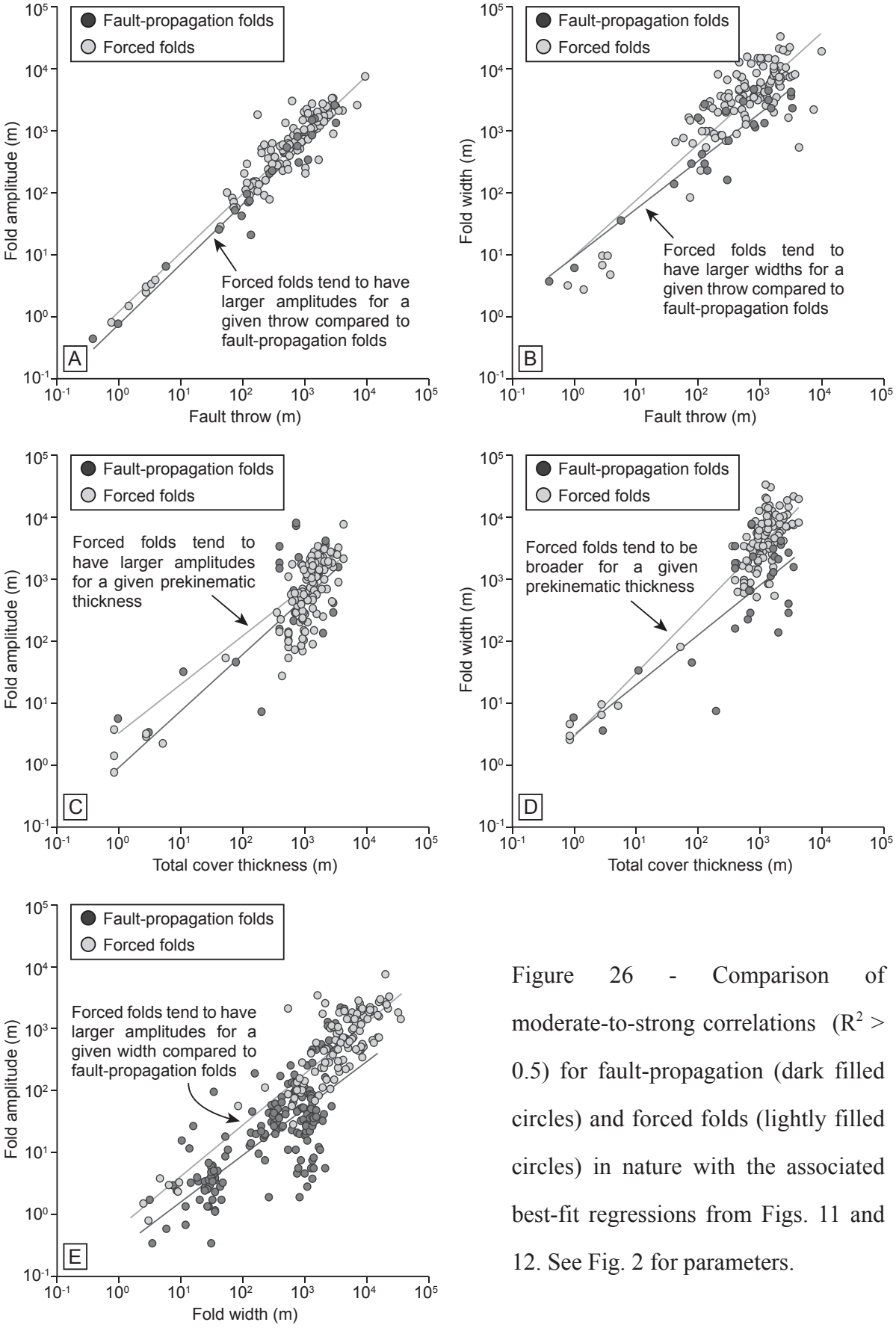

Figure 26 - Comparison of moderate-to-strong correlations ($R^2 > 0.5$) for fault-propagation (dark filled circles) and forced folds (lightly filled circles) in nature with the associated best-fit regressions from Figs. 11 and 12. See Fig. 2 for parameters.

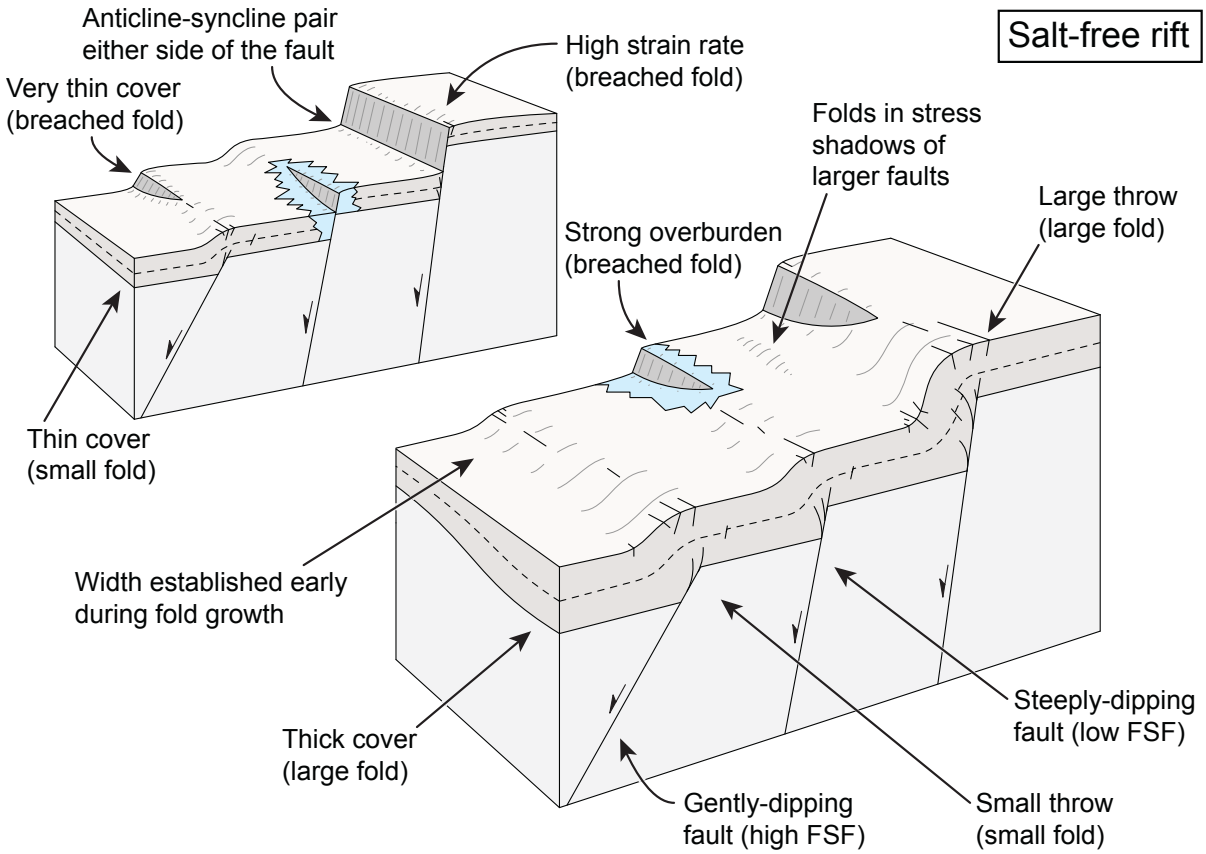
Salt-free rift
Anticline-syncline pair either side of the fault
Very thin cover (breached fold)
High strain rate (breached fold)
Folds in stress shadows of larger faults
Large throw (large fold)
Strong overburden (breached fold)
Thin cover (small fold)
Width established early during fold growth
Thick cover (large fold)
Steeply-dipping fault (low FSF)
Gently-dipping fault (high FSF)
Small throw (small fold)

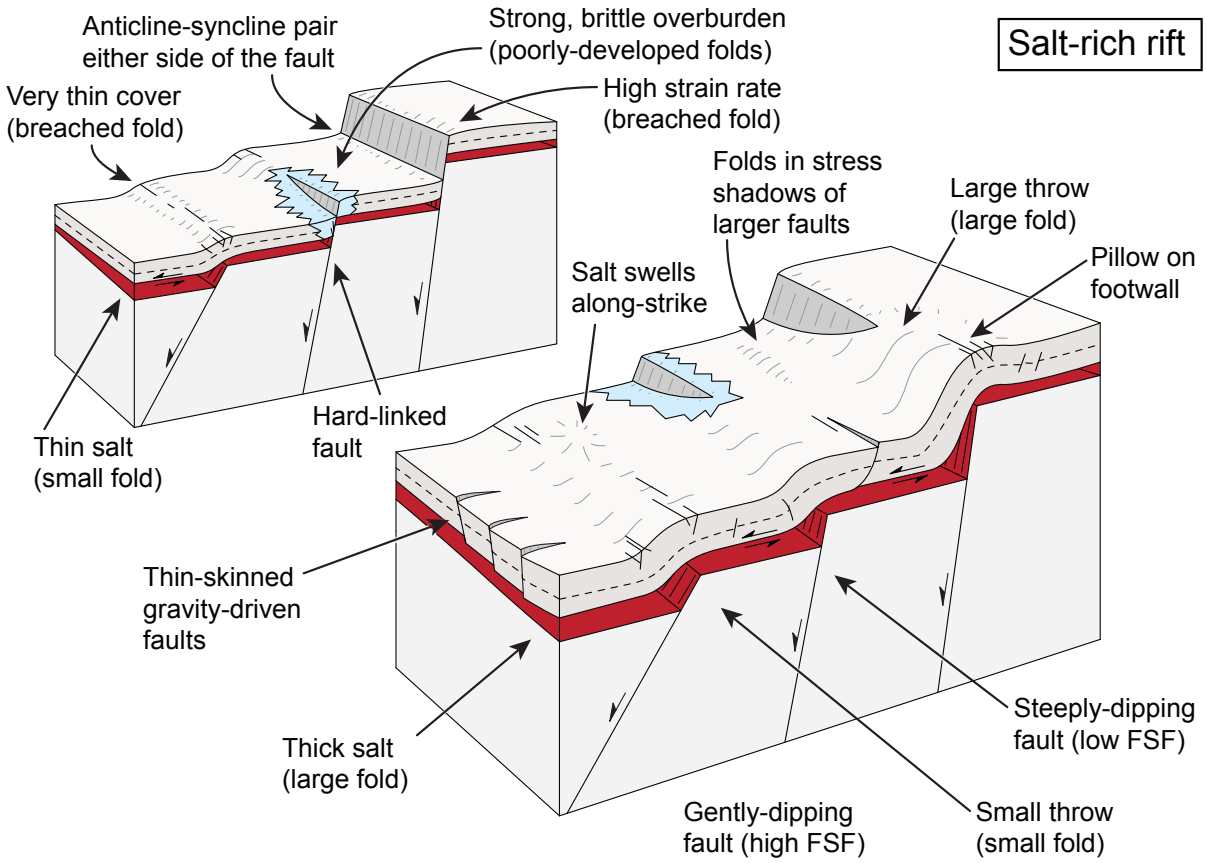
Salt-rich rift
Anticline-syncline pair either side of the fault
Strong, brittle overburden (poorly-developed folds)
Very thin cover (breached fold)
High strain rate (breached fold)
Folds in stress shadows of larger faults
Large throw (large fold)
Pillow on footwall
Salt swells along-strike
Thin salt (small fold)
Hard-linked fault
Thin-skinned gravity-driven faults
Thick salt (large fold)
Steeply-dipping fault (low FSF)
Gently-dipping fault (high FSF)
Small throw (small fold)

Figure 27 (previous page) - Growth fold geometry in salt-free (top) and salt-rich (bottom) sedimentary basins. Brittle, rheologically strong cover is shown in blue. Note how the width and amplitude of growth folds in salt-rich settings may be considerably different to those developed in salt-free settings. Salt may also create additional fault and fracture populations related to diapirism, independent of regional extension. Cover thickness decreases towards the background in both salt-free and salt-rich settings, which in turn, affects fold geometry.

Parameter	Fault-propagation folds (FPF)			Forced folds (FF)		
	Natural examples	**Physical models**	**Numerical models**	**Natural examples**	**Physical models**	**Numerical models**
Fold amplitude (A)	10 cm – 2.5 km	3 mm – 8.6 cm	4 mm – 965 m	75 cm – 3.2 km	7 mm – 6.6 cm	50 m – 820 m
Fold width (W)	10 cm – 7.5 km	1.5 mm – 16 cm	7 mm – 4.6 km	2.4 m – 20 km	6 mm – 38 cm	2 km – 3.4 km
Fold-shape-factor (FSF)	0.3 – 357	0.2 – 79	1.2 – 50	0.25 - 24	0.93 - 25	2.8 – 14
Fault throw (TH)	41 cm – 3.3 km	6 mm – 12 cm	4 mm – 1km	81 cm – 9.8 km	1 mm – 7 cm	50 m – 910 m
Fault dip (fd)	45° - 85°	45° - 90°	30° - 90°	13° – 90°	30° - 90°	30° – 65°
Prekinematic thickness (T_P)	2.8 m – 3.5 km	1 cm – 26 cm	6 cm – 9.7 km	43 cm – 2.3 km	3.5 mm – 7 cm	1.75 km – 2.75 km
Detachment thickness (T_D)	-	-	-	42 cm – 2.1 km	5 mm – 7 cm	250 m – 1 km
Cover-detachment ratio (C:D)	-	-	-	0.6 - 9	0.9 - 26	1.5 - 10

Table 1 – Ranges for the growth fold parameters identified in Fig. 2 Values are approximate based on measurements from global data compilation in Appendix D and E.

Correlation	Fault-propagation folds (FPF)			Forced folds (FF)	
	Natural examples	Physical models	Numerical models	Natural examples	Physical models
Fold amplitude vs fold width	$A=22.319(W)^{0.7659}$ $[R^2 = 0.63]$	No correlation $[R^2 < 0.1]$	$A=6.5446(W)^{1.0078}$ $[R^2 = 0.8941]$	$A=0.6116(W)^{0.8356}$ $[R^2 = 0.7965]$	*Weak correlation* $[R^2 = 0.3451]$
Fold amplitude vs fault dip	*Weak correlation* $[R^2 = 0.1024]$	No correlation $[R^2 < 0.1]$	*Weak correlation* $[R^2 = 0.2566]$	No correlation $[R^2 < 0.1]$	No correlation $[R^2 < 0.1]$
Fold amplitude vs fault throw	$A=8.0074(TH)^{0.8.021}$ $[R^2 = 0.63]$	$A=0.3536(TH)^{0.7647}$ $[R^2 = 0.72]$	$A=0.9585(TH)^{0.9219}$ $[R^2 = 0.8912]$	$A=1.2063(TH)^{0.9513}$ $[R^2 = 0.8912]$	*Weak correlation* $[R^2 = 0.4355]$
Fold amplitude vs prekinematic thickness	$A=0.7508(T_P)^{0.85}$ $[R^2 = 0.71]$	*Weak correlation* $[R^2 = 0.1658]$	$A=0.2152(T_P)^{0.8076}$ $[R^2 = 0.8652]$	$A=2.4864(T_P)^{0.8271}$ $[R^2 = 0.6996]$	*Weak correlation* $[R^2 = 0.1032]$
Fold width vs fault dip	*Weak correlation* $[R^2 = 0.1063]$	No correlation $[R^2 < 0.1]$	*Weak correlation* $[R^2 = 0.1125]$	No correlation $[R^2 < 0.1]$	No correlation $[R^2 < 0.1]$
Fold width vs fault throw	$W=7.5487(TH)^{0.7922}$ $[R^2 = 0.835]$	No correlation $[R^2 < 0.1]$	$W=6.4602(T_P)^{0.9246}$ $[R^2 = 0.9038]$	$W=8.8228(TH)^{0.9178}$ $[R^2 = 0.7229]$	*Weak correlation* $[R^2 = 0.3061]$
Fold width vs prekinematic thickness	$W=3.5994(T_P)^{0.7879}$ $[R^2 = 0.7226]$	*Weak correlation* $[R^2 = 0.1567]$	$W=0.2883(T_P)^{0.8501}$ $[R^2 = 0.8303]$	$W=7.7147(T_P)^{0.9318}$ $[R^2 = 0.7784]$	*Weak correlation* $[R^2 = 0.2485]$
Fold-shape-factor vs fault dip	No correlation $[R^2 < 0.1]$	No correlation $[R^2 < 0.1]$	No correlation $[R^2 < 0.1]$	No correlation $[R^2 < 0.1]$	No correlation $[R^2 < 0.1]$

Table 2 - Correlations for for fault-propagation and forced folds in nature, physical models and numerical models. Where Moderate-to-strong correlations ($R_2 > 0.5$) are present, the best-fit parametric equation has been provided. The R_2 value is shown in all cases. A = fold amplitude. W = fold width. TH = fault throw. T_P = prekinematic cover thickness. T_D = detachment thickness. Regression analysis was not undertaken for numerical models of forced folds.

Correlation	Fault-propagation folds (FPF)			Forced folds (FF)	
	Natural examples	Physical models	Numerical models	Natural examples	Physical models
Fold-shape-factor vs fault throw	*Weak correlation* *[$R^2 = 0.1214$]*	*Weak correlation* *[$R^2 = 0.3898$]*	No correlation *[$R^2 < 0.1$]*	No correlation *[$R^2 < 0.1$]*	No correlation *[$R^2 < 0.1$]*
Fold-shape-factor vs prekinematic thickness	*Weak correlation* *[$R^2 = 0.1488$]*	No correlation *[$R^2 < 0.1$]*	No correlation *[$R^2 < 0.1$]*	No correlation *[$R^2 < 0.1$]*	No correlation *[$R^2 < 0.1$]*
Detachment thickness vs fold amplitude	-	-	-	$A=2.6853(T_D)^{0.9065}$ *[$R^2 = 0.6226$]*	*Weak correlation* *[$R^2 = 0.1179$]*
Detachment thickness vs fold width	-	-	-	$W=8.914(T_D)^{1.0151}$ *[$R^2 = 0.7248$]*	*Weak correlation* *[$R^2 = 0.4058$]*
Detachment thickness vs fold-shape-factor	-	-	-	No correlation *[$R^2 < 0.1$]*	*Weak correlation* *[$R^2 = 0.133$]*
Cover-detachment ratio vs fold amplitude	-	-	-	No correlation *[$R^2 < 0.1$]*	No correlation *[$R^2 < 0.1$]*
Cover-detachment ratio vs fold width	-	-	-	No correlation *[$R^2 < 0.1$]*	No correlation *[$R^2 < 0.1$]*
Cover-detachment ratio vs fold-shape-factor	-	-	-	No correlation *[$R^2 < 0.1$]*	No correlation *[$R^2 < 0.1$]*

Table 2 continued - Correlations for for fault-propagation and forced folds in nature, physical models and numerical models. Where Moderate-to-strong correlations ($R_2 > 0.5$) are present, the best-fit parametric equation has been provided. The R_2 value is shown in all cases. A = fold amplitude. W = fold width. TH = fault throw. T_P = prekinematic cover thickness. T_D = detachment thickness. Regression analysis was not undertaken for numerical models of forced folds.

Appendix A - Genesis of fault-related folds

Forced fold – As a fault propagates towards the surface, folding occurs above the upper fault. Deformation is principally faulted at depth, but abruptly transitions to folding at shallower levels. This abrupt change between faulting below and folding above is facilitated due to a detachment or ductile lithology, such as salt or overpressured shale (e.g. Laubscher, 1982; Withjack and Callaway, 2000; Ford et al., 2007; Duffy et al., 2013; Lewis et al., 2013; Jackson and Lewis, 2016; Coleman et al., 2017). A breached forced fold resembles that of a breached fault-propagation fold.

Fault-propagation fold – As a fault propagates towards the surface, folding occurs above the upper fault tip. Deformation is manifested as faulting at depth but gradually transitions to folding at shallow levels (e.g. Withjack et al., 1990; Gawthorpe et al., 1997; Sharp et al., 2000; Jackson et al., 2006; Lewis et al., 2015).

Fault-propagation folds (breached) – Following fault-propagation folding, the underlying fault may propagate through its cover and folding ceases. The fold may then be preserved in the footwall and hangingwall, typically as an anticline and syncline, respectively (e.g. Withjack et al., 1990; Gawthorpe et al., 1997; Lewis et al., 2015). Forced folds that are breached appear similar to breached fault-propagation folds (e.g. Withjack and Callaway, 2000; Ford et al., 2007; Lewis et al., 2013).

Compactional drape – Differential compaction either side of a fault plane creates folding with sub-vertical fold axes (e.g. Thomson and Underhill, 1993; Skuce, 1996; Faerseth and Lien, 2002).

Withdrawal drape – Prekinematic strata may become folded above a pre-existing basement fault step as an underlying mobile unit, such as salt or shale, is evacuated. The withdrawal drape fold is geometrically similar to a forced fold, however, is *not* due to a propagating upper fault tip (e.g. Withjack and Callaway, 2000). Withdrawal drape folds are typically associated with nearby 'leakage points' such as salt or shale diapirs.

Frictional drag – The deflection of beds adjacent to a fault into folds that are convex in the direction of relative slip due to frictional sliding along a fault and progressive tilting of beds

with increased amount of sliding along a fault (e.g. Billings, 1972; Resor, 2008; Spahic et al., 2013). Their origin has been recently called into question (cf. Reches and Eidelman, 1995; Graseman et al., 2005; Ferril et al., 2012).

Inversion – The compressional reactivation of pre-existing extensional structures, so that an initial structural low is uplifted, and subsequently inverted, to form a structural high (e.g. Badley et al., 1989; Mitra, 1993; Mitra and Islam, 1994; Turner and Williams, 2004; Jackson et al., 2013).

Fault-line deflection (recess) – Folding due to along-strike corrugations in fault plane geometry. Recess features are created at concave fault segments (e.g. Wheeler, 1939; Stewart and Hancock, 1991; Ehrlich and Gabrielsen, 2004).

Fault-line deflection (salient) – Folding due to along-strike corrugations in fault plane geometry. Salient features are created at convex fault segments (e.g. Wheeler, 1939; Machette et al., 1991; Stewart and Hancock, 1991; Ehrlich and Gabrielsen, 2004; cf. Claringbould et al., 2017).

References for Appendix A

BADLEY, M. E., PRICE, J. D. and BACKSHALL, L. C. 1989. Inversion, reactivated faults and related structures: seismic examples from the southern North Sea. Geological Society, London, Special Publications, 44, 201-219.

BILLINGS, M. P. and BILLINGS, M. 1972. Structural geology, Prentice-Hall Englewood Cliffs, NJ.

CLARINGBOULD, J. S., BELL, R. E., JACKSON, C. A. L., GAWTHORPE, R. L. and ODINSEN, T. 2017. Pre-existing normal faults have limited control on the rift geometry of the northern North Sea. Earth and Planetary Science Letters, 475, 190-206.

COLEMAN, A. J., JACKSON, C. A. L. and DUFFY, O. B. 2017. Balancing sub- and supra-salt strain in salt-influenced rifts: Implications for extension estimates. Journal of Structural Geology, 102, 208-225..

DUFFY, O. B., GAWTHORPE, R. L., DOCHERTY, M. and BROCKLEHURST, S. H. 2013. Mobile evaporite controls on the structural style and evolution of rift basins: Danish Central Graben, North Sea. Basin Research, 25, 310-330.

EHRLICH, R. and GABRIELSEN, R. H. 2004. The complexity of a ramp–flat–ramp fault and its effect on hanging-wall structuring: an example from the Njord oil field, offshore mid-Norway. Petroleum Geoscience, 10, 305-317.

FÆRSETH, R. B. and LIEN, T. 2002. Cretaceous evolution in the Norwegian Sea—a period characterized by tectonic quiescence. Marine and Petroleum Geology, 19, 1005-1027.

FERRILL, D. A., MORRIS, A. P. and MCGINNIS, R. N. 2012. Extensional fault-propagation folding in mechanically layered rocks: The case against the frictional drag mechanism. Tectonophysics, 576-577, 78-85.

FORD, M., LE CARLIER DE VESLUD, C. and BOURGEOIS, O. 2007. Kinematic and geometric analysis of fault-related folds in a rift setting: The Dannemarie basin, Upper Rhine Graben, France. Journal of Structural Geology, 29, 1811-1830.

GAWTHORPE, R. L., SHARP, I., UNDERHILL, J. R. and GUPTA, S. 1997. Linked sequence stratigraphic and structural evolution of propagating normal faults. Geology, 25, 795.

GRASEMANN, B., MARTEL, S. and PASSCHIER, C. 2005. Reverse and normal drag along a fault. Journal of Structural Geology, 27, 999-1010.

JACKSON, C. A. L., CHUA, S. T., BELL, R. E. and MAGEE, C. 2013. Structural style and early stage growth of inversion structures: 3D seismic insights from the Egersund Basin, offshore Norway. Journal of Structural Geology, 46, 167-185.

JACKSON, C. A. L. and LEWIS, M. M. 2016. Structural style and evolution of a salt-influenced rift basin margin; the impact of variations in salt composition and the role of polyphase extension. Basin Research, 28, 81-102.

LAUBSCHER, H. 1982. Die Sudostecke des Rheingrabens-ein kinematisches und dynamisches problem. Eclogae Geologicae Helvetiae, 75, 101-116.

LEWIS, M. M., JACKSON, C. A., GAWTHORPE, R. L. and WHIPP, P. S. 2015. Early synrift reservoir development on the flanks of extensional forced folds: A seismic-scale outcrop analog from the Hadahid Fault System, Suez Rift, Egypt. AAPG Bulletin.

LEWIS, M. M., JACKSON, C. A. L. and GAWTHORPE, R. L. 2013. Salt-influenced normal fault growth and forced folding: The Stavanger Fault System, North Sea. Journal of Structural Geology, 54, 156-173.

MACHETTE, M.N., PERSONIUS, S.F., NELSON, A.R., SCHWARTZ, D.P. and LUND, W.R. 1991. The Wasatch fault zone, Utah—Segmentation and history of Holocene earthquakes. Journal of Structural Geology, 13, 137-149.

MITRA, S. 1993. Geometry and kinematic evolution of inversion structures. AAPG Bulletin, 77, 1159-1191.

MITRA, S. and ISLAM, Q. T. 1994. Experimental (clay) models of inversion structures. Tectonophysics, 230, 211-222.

RECHES, Z. E. and EIDELMAN, A. 1995. Drag along faults. Tectonophysics, 247, 145-156.

RESOR, P. G. 2008. Deformation associated with a continental normal fault system, western Grand Canyon, Arizona. Geological Society of America Bulletin, 120, 414-430.

SHARP, I. R., GAWTHORPE, R. L., UNDERHILL, J. R. and GUPTA, S. 2000. Fault-propagation folding in extensional settings: Examples of structural style and synrift sedimentary response from the Suez rift, Sinai, Egypt. Geological Society of America Bulletin, 112, 1877-1899.

SKUCE, A. G. 1996. Forward modelling of compaction above normal faults: an example from the Sirte Basin, Libya. Geological Society, London, Special Publications, 99, 135-146.

SPAHIĆ, D., GRASEMANN, B. and EXNER, U. 2013. Identifying fault segments from 3D fault drag analysis (Vienna Basin, Austria). Journal of Structural Geology, 55, 182-195.

STEWART, I. S. and HANCOCK, P. L. 1991. Scales of structural heterogeneity within neotectonic normal fault zones in the Aegean region. Journal of Structural Geology, 13, 191-204.

THOMSON, K. and UNDERHILL, J. Controls on the development and evolution of structural styles in the Inner Moray Firth Basin. Geological Society, London, Petroleum Geology Conference series, 1993. Geological Society of London, 1167-1178.

TURNER, J. P. and WILLIAMS, G. A. 2004. Sedimentary basin inversion and intra-plate shortening. Earth-Science Reviews, 65, 277-304.

WHEELER, G. 1939. Triassic fault-line deflections and associated warping. The Journal of Geology, 337-370.

WITHJACK, M. O., OLSON, J. and PETERSON, E. 1990. Experimental models of extensional forced folds. AAPG Bulletin, 74, 1038-1054.

WITHJACK, M. O. and CALLAWAY, S. 2000. Active normal faulting beneath a salt layer: an experimental study of deformation patterns in the cover sequence. AAPG bulletin, 84, 627-651.

Appendix B - Fault-propagation fold locations

Locality	Country	Fault System	Basin	Reference(s)	Published	Confidence
1	Libya		Sirte Basin	Fodor et al., 2005; Skuce, 1996	Yes	High
2	Egypt		Gulf of Suez	Jackson et al., 2006; Khalil and McClay, 2002; Khalil and McClay, 2016	Yes	High
3	US		Newark Basin	Olsen et al., 1996; Schlische et al., 1992	Yes	Low
4	Egypt		Northern Gulf of Suez	Jackson et al., 2006; Sharp et al., 2000a; b; Garfunkel and Bartov, 1977; Moustafa, 1993	Yes	High
5	Egypt		Central Gulf of Suez	Sharp et al., 2000b; Garfunkel and Bartov, 1977; Moustafa, 1993	Yes	High
6	Egypt		Southern Gulf of Suez	Sharp et al., 2000a; Garfunkel and Bartov, 1977; Moustafa, 1993	Yes	High
7	US	Balcones Fault System	Gulf Coast Basin	Ferrill et al., 2011; Ferril et al., 2012	Yes	High
8	US	Nopolo Fault	Loreto Basin	Willsey et al., 2002	Yes	High
9	Iceland		Vogar	Grant and Kattenhorn, 2004; Hardy et al., 2013; Trippanera et al., 2015	Yes	High
10	Iceland		Grindavik	Grant and Kattenhorn, 2004; Hardy et al., 2013	Yes	High
11	Iceland		Thingvellir	Grant and Kattenhorn, 2004; Hardy et al., 2013; Trippanera et al., 2015; Smart and Ferrill, 2018	Yes	High
12	Spain		Jiloca Graben	Lafuente et al., 2011	Yes	High

13	US		Canyonlands Graben	Cartwright and Mansfield, 1998	Yes	High
14	US	Koa'e Fault System	Kilauea Southwest and East Rift Zone	Martel and Langley, 2006; Kaven and Martel, 2007; Bubeck et al., 2018	Yes	High
15	US	Hat Creek System	Hat Creek Graben	Blakeslee and Kattenhorn, 2013	Yes	High
16	Israel	Galilee and Zurim Escarpment	Dead Sea	Matmon et al., 2010	Yes	High
17	US	White Rabbit Fault System	Kilauea Southwest Rift Zone	Podolsky and Roberts, 2008	Yes	High
18	Taiwan	Shanchiao Fault System	Taipei Basin	Chu et al., 2015	Yes	High
19	Saudi Arabia		Jebel Hafeet	van Gent et al., 2010	Yes	High
20	Norway	Oseburg East	Horda Platform	Finch et al., 2004; Jackson et al., 2017	Yes/No	High
21	Norway	Smorbukk	Halten Terrace	Corfield and Sharp, 2000; Bell et al., 2014; Færseth and Lien, 2002	Yes	High
22	Norway	Fjerritslev Fault System	Farsund Basin	Phillips et al., 2018	No	High
23	Israel		Levant Basin	Baudon and Cartwright, 2008a; b; c	Yes	Low
24	Norway	Strathspey-Brent-Statfjord Fault Zone	Eastern Shetland Basin	McLeod et al., 2000	Yes	Mid
25	US		Modoc Plateau	White and Crider, 2006	Yes	High
26	Gabon	Mikouloungou; Kiene; Mounana; Kaya; Magna faults	Franceville Basin	Ndongo et al., 2016	Yes	High
27	Norway		Vøring Basin	Færseth and Lien, 2002	Yes	Mid

28	Norway		Møre Basin	Færseth and Lien, 2002	Yes	Mid
29	Brazil		Espirito Santo Basin	Omosanya and Alves, 2014	Yes	High
30	Turkey	Yavansu Fault Zone	Menderes Graben	Hancock and Barka, 1987	Yes	High
31	UK	East Pennine Coalfield	Welbeck Low	Walsh and Watterson, 1987	Yes	High
32	Greece	Southern Corinth Fault System	Corinth Rift	Vita-Finzi and King, 1985	Yes	High
33	Israel		Levant Basin	Ghalayini et al., 2016	Yes	High
34	US	Sandy Creek Fault System	Cat Creek	Mitra, 1993	Yes	High
35	Java	Java	Kangean Basin	Mitra, 1993; Badley, 1989	Yes	High
36	UK		South Hewett Zone	Badley et al., 1989; Mitra, 1993	Yes	Mid
37	New Zealand	Manaia Fault System, Kupe Structure	Southern Taranaki Basin	Mitra, 1993; Knox, 1982; Conneally, 2017	Yes	High
38	UK	Heather; Ninian Structure	North Viking Graben	Paul and Mitra, 2015	Yes	High
39	Morocco		Anti-Atlas Basin	Robert-Charrue and Burkhard, 2008	Yes	Low
40	Nigeria		Maiduguri Basin	Avbovbo et al., 1986	Yes	Mid
41	US	Central Transform Fault	Guaymas Basin	Lonsdale and Lawver, 1980	Yes	High
42	US	Robinson's Bend Coalbed; Taylor Creek	Black Warrior Basin	Groshong et al., 2010	Yes	High
43	UK		Inner Moray Firth	Lapadat et al., 2016; http://www.seismicatlas.org/uploaded/image/200802/ e1d2ebbb-18d7	Yes	High

				-4f9f-a677-7511d521e7aa.jpg		
44	Greece	Western Corinth Canal	Isthmia Graben	Sletten, 2016	No	High
45	Denmark	Coffee-Soil Fault	Tail-End Graben	Duffy et al., 2013	Yes	High
46	Greece	Milos Fault Zone	Southern Aegian Sea	Angelier, 1979	Yes	Mid
47	Greece	Karpathos Fault Zone	Southern Aegian Sea	Angelier, 1979	Yes	Mid
48	Greece	Samos Fault Zone	Southern Aegian Sea	Angelier, 1979	Yes	Mid
49	Argentina	Tres Cruces	Salta Rift	Monaldi et al., 2008	Yes	Mid
50	US	Slaughter Canyon	Permian Basin	Koša and Hunt, 2005	Yes	High
51	Bulgaria	Emine Fault System	Burgas Basin	Doglioni et al., 1996	Yes	High
52	Ethiopia	Fantale Magmatic System	Ethiopian Rift	Trippanera et al., 2015	Yes	High
53	Ethiopia	Manda Hararo Rift	Ethiopian Rift	Trippanera et al., 2015	Yes	High
54	Iceland	Eldgjá	Erdja Fissure Swarm	Trippanera et al., 2015	Yes	High
55	Iceland	Sveinar-Sveinagja	Sveinar Graben	Trippanera et al., 2015	Yes	High
56	Faroe Islands		Faroe-Shetland Basin	Walker et al., 2012; Walker et al., 2013	Yes	High

References for Appendix B

ANGELIER, J. 1979. Recent quaternary tectonics in the hellenic arc: Examples of geological observations on land. Tectonophysics, 52, 267-275.

AVBOVBO, A., AYOOLA, E. & OSAHON, G. 1986. Depositional and structural styles in Chad Basin of Northeastern Nigeria. AAPG Bulletin, 70, 1787-1798.

BADLEY, M. E., PRICE, J. D. & BACKSHALL, L. C. 1989. Inversion, reactivated faults and related structures: seismic examples from the southern North Sea. Geological Society, London, Special Publications, 44, 201-219.

BAUDON, C. & CARTWRIGHT, J. 2008a. Early stage evolution of growth faults: 3D seismic insights from the Levant Basin, Eastern Mediterranean. Journal of Structural Geology, 30, 888-898.

BAUDON, C. & CARTWRIGHT, J. 2008b. The kinematics of reactivation of normal faults using high resolution throw mapping. Journal of Structural Geology, 30, 1072-1084.

BAUDON, C. & CARTWRIGHT, J. A. 2008c. 3D seismic characterisation of an array of blind normal faults in the Levant Basin, Eastern Mediterranean. Journal of Structural Geology, 30, 746-760.

BELL, R. E., JACKSON, C. A. L., ELLIOTT, G. M., GAWTHORPE, R. L., SHARP, I. R. & MICHELSEN, L. 2014. Insights into the development of major rift-related unconformities from geologically constrained subsidence modelling: Halten Terrace, offshore mid Norway. Basin Research, 26, 203-224.

BLAKESLEE, M. W. & KATTENHORN, S. A. 2013. Revised earthquake hazard of the Hat Creek fault, northern California: A case example of a normal fault dissecting variable-age basaltic lavas. Geosphere, 9, 1397-1409.

BUBECK, A., WALKER, R. J., IMBER, J., and MACLEOD, C. J., 2018, Normal fault growth in layered basaltic rocks: The role of strain rate in fault evolution. Journal of Structural Geology, 115, 103-120.

CARTWRIGHT, J. & MANSFIELD, C. 1998. Lateral displacement variation and lateral tip geometry of normal faults in the Canyonlands National Park, Utah. Journal of Structural Geology, 20, 3-19.

CHU, S.-S., LIN, M.-L., HUANG, W.-C., NIEN, W.-T., LIU, H.-C. & CHAN, P.-C. 2015. Simulation of growth normal fault sandbox tests using the 2D discrete element method. Computers & Geosciences, 74, 1-12.

CONNEALLY, J., CHILDS, C. & NICOL, A. 2017. Monocline formation during growth of segmented faults in the Taranaki Basin, offshore New Zealand. Tectonophysics, 721, 310-321.

CORFIELD, S. & SHARP, I. 2000. Structural style and stratigraphic architecture of fault propagation folding in extensional settings: a seismic example from the Smørbukk area, Halten Terrace, Mid-Norway. Basin Research, 12, 329-341.

DUFFY, O. B., GAWTHORPE, R. L., DOCHERTY, M. & BROCKLEHURST, S. H. 2013. Mobile evaporite controls on the structural style and evolution of rift basins: Danish Central Graben, North Sea. Basin Research, 25, 310-330.

DOGLIONI, C., BUSATTA, C., BOLIS, G., MARIANNA, L. & ZANELLA, M. 1996. Structural evolution of the eastern Balkans. Marine and Petroleum Geology, 13, 225 – 251.

FÆRSETH, R. B. & LIEN, T. 2002. Cretaceous evolution in the Norwegian Sea—a period characterized by tectonic quiescence. Marine and Petroleum Geology, 19, 1005-1027.

FERRILL, D. A., MORRIS, A. P. & MCGINNIS, R. N. 2012. Extensional fault-propagation folding in mechanically layered rocks: The case against the frictional drag mechanism. Tectonophysics, 576-577, 78-85.

FERRILL, D. A., MORRIS, A. P., MCGINNIS, R. N., SMART, K. J. & WARD, W. C. 2011. Fault zone deformation and displacement partitioning in mechanically layered carbonates: The Hidden Valley fault, central Texas. AAPG Bulletin, 95, 1383-1397.

FINCH, E., HARDY, S. & GAWTHORPE, R. 2004. Discrete-element modelling of extensional fault-propagation folding above rigid basement fault blocks. Basin Research, 16, 467-488.

FODOR, L., TURKI, S., DALUB, H. & AL GERBI, A. 2005. Fault-related folds and along-dip segmentation of breaching faults: syn-diagenetic deformation in the south-western Sirt basin, Libya. Terra Nova, 17, 121-128.

GARFUNKEL, Z. & BARTOV, Y. 1977. The tectonics of the Suez rift, Bull. Geol. Surv. Isr.

GHALAYINI, R., HOMBERG, C., DANIEL, J. M. & NADER, F. H. 2016. Growth of layer-bound normal faults under a regional anisotropic stress field. Geological Society, London, Special Publications, 439.

GRANT, J. V. & KATTENHORN, S. A. 2004. Evolution of vertical faults at an extensional plate boundary, southwest Iceland. Journal of Structural Geology, 26, 537-557.

GROSHONG, R. H., HAWKINS, W. B., PASHIN, J. C. & HARRY, D. L. 2010. Extensional structures of the Alabama promontory and Black Warrior foreland Basin: Styles and relationship to the Appalachian fold-thrust belt. Geological Society of America Memoirs, 206, 579-605.

HANCOCK, P. L. & BARKA, A. A. 1987. Kinematic indicators on active normal faults in Western Turkey. Journal of Structural Geology, 9, 573-584.

HARDY, S. 2013. Propagation of blind normal faults to the surface in basaltic sequences: Insights from 2D discrete element modelling. Marine and Petroleum Geology, 48, 149-159.

HARDY, S., 2018, Coupling a frictional-cohesive cover and a viscous substrate in a discrete element model: First results of application to thick- and thin-skinned extensional tectonics. Marine and Petroleum Geology, 97, 32-44.

JACKSON, C. A. L., GAWTHORPE, R. L. & SHARP, I. R. 2006. Style and sequence of deformation during extensional fault-propagation folding: examples from the Hammam Faraun and El-Qaa fault blocks, Suez Rift, Egypt. Journal of Structural Geology, 28, 519-535.

JACKSON, C. A. L., CORFIELD, S. & DREYER, T. 2017. Temporal evolution of extensional fault-propagation folds. EarthArXiv. Doi: 10.31223/osf.io/v9p8e.

KAVEN, J. O. & MARTEL, S. J. 2007. Growth of surface-breaching normal faults as a three-dimensional fracturing process. Journal of Structural Geology, 29, 1463-1476.

KHALIL, S. & MCCLAY, K. 2002. Extensional fault-related folding, northwestern Red Sea, Egypt. Journal of Structural Geology, 24, 743-762.

KHALIL, S. M. & MCCLAY, K. R. 2016. 3D geometry and kinematic evolution of extensional fault-related folds, NW Red Sea, Egypt. Geological Society, London, Special Publications, 439, 1-11.

KNOX, G. 1982. Taranaki Basin, structural style and tectonic setting. New Zealand journal of geology and geophysics, 25, 125-140.

KOSA, E. & HUNT, D. 2005. Growth of syndepositional faults in carbonate strata: Upper Permian Capitan platform, New Mexico, USA.

LAFUENTE, P., ARLEGUI, L., LIESA, C. & SIMÓN, J. 2011. Paleoseismological analysis of an intraplate extensional structure: the Concud fault (Iberian Chain, eastern Spain). International Journal of Earth Sciences, 100, 1713-1732.

LĂPĂDAT, A., IMBER, J., YIELDING, G., IACOPINI, D., MCCAFFREY, K. J. W., LONG, J. J. & JONES, R. R. 2016. Occurrence and development of folding related to normal faulting within a mechanically heterogeneous sedimentary sequence: a case study from Inner Moray Firth, UK. Geological Society, London, Special Publications, 439.

LONSDALE, P. & LAWVER, L. 1980. Immature plate boundary zones studied with a submersible in the Gulf of California. Geological Society of America Bulletin, 91, 555-569.

MARTEL, S. J. & LANGLEY, J. S. 2006. Propagation of normal faults to the surface in basalt, Koae fault system, Hawaii. Journal of Structural Geology, 28, 2123-2143.

MATMON, A., KATZ, O., SHAAR, R., RON, H., PORAT, N. & AGNON, A. 2010. Timing of relay ramp growth and normal fault linkage, Upper Galilee, northern Israel. Tectonics, 29, 2, 1-13.

MCLEOD, A. E., DAWERS, N. H. & UNDERHILL, J. R. 2000. The propagation and linkage of normal faults: insights from the Strathspey–Brent–Statfjord fault array, northern North Sea. Basin Research, 12, 263-284.

MITRA, S. 1993. Geometry and kinematic evolution of inversion structures. AAPG Bulletin, 77, 1159-1191.

MONALDI, C.R., SALFITY, J.A. and KLEY, J., 2008. Preserved extensional structures in an inverted Cretaceous rift basin, northwestern Argentina: Outcrop examples and implications for fault reactivation. Tectonics, 27, 1-21.

MOUSTAFA, A. R. 1993. Structural characteristics and tectonic evolution of the east-margin blocks of the Suez rift. Tectonophysics, 223, 381-399.

NDONGO, A., GUIRAUD, M., VENNIN, E., MBINA, M., BUONCRISTIANI, J.-F., THOMAZO, C. & FLOTTÉ, N. 2016. Control of fluid-pressure on early deformation structures in the Paleoproterozoic extensional Franceville Basin (SE Gabon). Precambrian Research, 277, 1-25.

OLSEN, P. E., KENT, D. V., CORNET, B., WITTE, W. K. & SCHLISCHE, R. W. 1996. High-resolution stratigraphy of the Newark rift basin (early Mesozoic, eastern North America). Geological Society of America Bulletin, 108, 40-77.

OMOSANYA, K. D. O. & ALVES, T. M. 2014. Mass-transport deposits controlling fault propagation, reactivation and structural decoupling on continental margins (Espírito Santo Basin, SE Brazil). Tectonophysics, 628, 158-171.

PAUL, D. & MITRA, S. 2015. Fault patterns associated with extensional fault-propagation folding. Marine and Petroleum Geology, 67, 120-143.

PHILLIPS, T. B., JACKSON, C. A., BELL, R. E. & DUFFY, O. B. 2018. Oblique reactivation of lithosphere-scale lineaments controls rift physiography–the upper-crustal expression of the Sorgenfrei–Tornquist Zone, offshore southern Norway. Solid Earth, 9, 403.

PODOLSKY, D. M. & ROBERTS, G. P. 2008. Growth of the volcano-flank Koa'e fault system, Hawaii. Journal of Structural Geology, 30, 1254-1263.

ROBERT-CHARRUE, C. & BURKHARD, M. 2008. Inversion tectonics, interference pattern and extensional fault-related folding in the Eastern Anti-Atlas, Morocco. Swiss Journal of Geosciences, 101, 397-408.

SCHLISCHE, R. W. 1992. Structural and stratigraphic development of the Newark extensional basin, eastern North America: Evidence for the growth of the basin and its bounding structures. Geological Society of America Bulletin, 104, 1246-1263.

SHARP, I., GAWTHORPE, R., ARMSTRONG, B. & UNDERHILL, J. 2000a. Propagation history and passive rotation of mesoscale normal faults: implications for synrift stratigraphic development. Basin Research, 12, 285-305.

SHARP, I. R., GAWTHORPE, R. L., UNDERHILL, J. R. & GUPTA, S. 2000b. Fault-propagation folding in extensional settings: Examples of structural style and synrift sedimentary response from the Suez rift, Sinai, Egypt. Geological Society of America Bulletin, 112, 1877-1899.

SLETTEN, S. H. 2016. Normal fault growth and fault zone architecture of normal faults exposed in the Corinth Canal, central Greece. MSc thesis, University of Bergen. Available at http://bora.uib.no/handle/1956/12783.

SKUCE, A. G. 1996. Forward modelling of compaction above normal faults: an example from the Sirte Basin, Libya. Geological Society, London, Special Publications, 99, 135-146.

SMART, K. J., and FERRILL, D. A., 2018, Discrete element modeling of extensional fault-related monocline formation. Journal of Structural Geology, 115, 82-90.

TRIPPANERA, D., ACOCELLA, V., RUCH, J., and ABEBE, B., 2015, Fault and graben growth along active magmatic divergent plate boundaries in Iceland and Ethiopia. Tectonics, 34, 11, 2318-2348.

VAN GENT, H. W., HOLLAND, M., URAI, J. L. & LOOSVELD, R. 2010. Evolution of fault zones in carbonates with mechanical stratigraphy – Insights from scale models using layered cohesive powder. Journal of Structural Geology, 32, 1375-1391.

VITA-FINZI, C. & KING, G. 1985. The seismicity, geomorphology and structural evolution of the Corinth area of Greece. Philosophical Transactions of the Royal Society of London A: Mathematical, Physical and Engineering Sciences, 314, 379-407.

WALKER, R. J., HOLDSWORTH, R. E., IMBER, J., and ELLIS, D., 2012, Fault-zone evolution in layered basalt sequences: A case study from the Faroe Islands, NE Atlantic margin. Geological Society of America Bulletin, 124, 7-8, 1382-1393.

WALKER, R., HOLDSWORTH, R., IMBER, J., FAULKNER, D., and ARMITAGE, P., 2013, Fault zone architecture and fluid flow in interlayered basaltic volcaniclastic-crystalline sequences. Journal of Structural Geology, 51, 92-104.

WALSH, J. J. & WATTERSON, J. 1987. Distributions of cumulative displacement and seismic slip on a single normal fault surface. Journal of Structural Geology, 9, 1039-1046.

WHITE, I.R. and CRIDER, J.G., 2006. Extensional fault-propagation folds: Mechanical models and observations from the Modoc Plateau, northeastern California. Journal of Structural Geology, 28, 1352-1370.

WILLSEY, S. P., UMHOEFER, P. J. & HILLEY, G. E. 2002. Early evolution of an extensional monocline by a propagating normal fault: 3D analysis from combined field study and numerical modeling. Journal of Structural Geology, 24, 651-669.

Appendix C - Forced fold locations

Locality	Country	Fault System	Basin	Reference(s)	Published	Confidence
1	Norway	Revfallet	Halten Terrace	Dooley et al., 2003; Dooley et al., 2005; Pascoe et al., 1999; Faerseth and Lien, 2002; Gabrielsen et al., 1999; Grunnaleite and Gabrielsen, 1995	Yes	High
2	Norway	Bremstein	Halten Terrace	Wilson et al., 2013; Wilson et al., 2015; Coleman et al. 2017; Faerseth and Lien, 2002; Gabrielsen et al., 1999; Grunnaleite and Gabrielsen, 1995	Yes	High
3	France	Illfurth	Dannemarie Basin, Rhine Graben	Ford et al., 2007; Maurin and Niviere, 1999	Yes	High
4	Norway	Stavanger	Egersund Basin	Jackson and Lewis, 2016	Yes	High
5	Norway	Sele High	Egersund Basin	Lewis et al., 2013	Yes	High
6	UK	Dowsing Fault Zone	Sole Pit Trough	Coward and Stewart, 1995	Yes	High
7	Belguim	Southern Roer Valley	Roer Valley, Rhine Graben	Deckers, 2015; Deckers et al., 2014	Yes	High
8	US	Jackpot - Tamurian Block	Basin and Range	Howard and John, 1997	Yes	High
9	UK	Buchan Graben	Buchan Graben	Stewart and Clark, 1999; Stewart, 2014	Yes	High
10	Egypt	Ramadan Oil Field	Gulf of Suez	Brown, 1980; Abdine et al., 1992; Withjack et al., 2000	Yes	High
11	Denmark	Horn Graben	Horn Graben	Stewart and Clark, 1999	Yes	High
12	UK	Wright-Bray	Channel Basin	Harvey and Stewart, 1998	Yes	High

13	Canada	Creignish; Hollow Fault	Maritimes Basin	Keller and Lynch, 1999; Lynch et al., 1998	Yes	High
14	Spain	Ubierna; Saltacaballos	Basque-Cantabrian Basin	Tavani et al., 2018; Tavani et al., 2011; 2013; Tavani and Granado, 2014; Quintana et al., 2006	Yes	High
15	Israel	Ma'aleh Gerofit	Central Dead Sea Rift	Gross et al., 1997	Yes	High
16	US	Balcones	Gulf of Mexico Basin	Ferrill et al., 2012; Ferrill and Morris, 2008	Yes	High
17	US	Balcones	Gulf of Mexico Basin	Ferrill and Morris, 2008	Yes	High
18	US	Big Brushy Canyon	Big Brushy Canyon	Ferrill et al., 2007	Yes	High
19	Norway	Nordkapp Basin	Nordkapp Basin	Nilsen et al., 1995; Koyi et al., 1993; Koyi et al., 1995; Gudlaugson et al., 1998	Yes	High
20	UK	Keys Graben	Keys Graben	Jackson and Mulholland, 1993; Stewart et al., 1997; Penge et al., 1999	Yes	High
21	Denmark	East North Sea High	Norwegian-Danish Basin	Geil, 1991; Petersen et al., 1992; Stewart et al., 1996	Yes	High
22	Norway	Sleipner Basin	South Viking Graben	Kane et al., 2010	Yes	High
23	UK	Fisher Bank Basin	Fisher Bank Basin	Penge et al., 1999	Yes	High
24	UK	Forties-Montrose High	Forties-Montrose High	Penge et al., 1999	Yes	High
25	UK	East Deemster Graben	East Deemster Graben	Penge et al., 1999	Yes	High
26	UK	Dowsing Fault Zone	Swarte Bank Hinge	Stewart and Coward, 1995; Stewart et al., 1996	Yes	High

27	UK	Machar and Median Diapirs	East Central Trough	Stewart et al., 1996	Yes	High
28	UK	Cleaver Bank High	Cleaver Bank High	Oudmayer and de Jager, 1993	Yes	High
29	Denmark	Hyllebjerg Basin	Hyllebjerg Basin	Koyi and Petersen, 1993	Yes	High
30	Denmark	RÃ¸ddung Graben	RÃ¸ddung Graben	Koyi and Petersen, 1993	Yes	High
31	UK	Lagman Fault	Lagman Basin	Jackson and Mulholland, 1993	Yes	High
32	UK	Tynwald Fault	Tynwald Basin	Jackson and Mulholland, 1993	Yes	High
33	Denmark	Coffee-Soil Fault	Tail-End Graben	Duffy et al., 2013	Yes	High
34	Portugal		Northern Lusitanian Basin	Alves et al., 2002; Alves et al., 2003	Yes	High
35	Portugal	Arruda subbasin and Bombarral-Alcobaca subbasin	Central Lusitanian Basin	Alves et al., 2002; Alves et al., 2003	Yes	High
36	Canada		Whale Basin	Balkwill and Legall, 1989; Vendeville et al., 1995; Withjack and Callaway, 2000	Yes	High
37	Canada		Jeanne D'Arc Basin	Sinclair, 1995; Withjack and Callaway, 2000; Serano-Saurez et al., 2013	Yes	High
38	Portugal	Porto Basin	Porto Basin	Alves et al., 2006	Yes	High
39	Portugal	Alentejo Basin	Alentejo Basin	Alves et al., 2006	Yes	High
40	Spain	Zarate Fault	Lasarte Basin	Bodego and Agirrezabala, 2013	Yes	High
41	France	Aquitaine Basin	Aquitaine Basin	Bourrouilh et al., 1995	Yes	High

42	France	Parentis Basin	Parentis Basin	Ferrer et al., 2012; Ferrer et al., 2014	Yes	High
43	Ukraine		Dniepr-Donets Basin	Stovba and Stephenson, 2002; Brown et al., 2012	Yes	Low
44	Poland		Mid Polish Trough	Burliga et al., 2012; Krzywiec, 2010; Lamarche and Scheck-Wenderoth, 2005	Yes	High
45	Canada		Orpheus Basin	Durcanin, 2009; Zulfitriadi, 2011; Hanafi, 2013	No	High
46	Norway		Haapet Dome		No	High
47	Canada		Sverdrup Basin	Harrison and Jackson, 2014	Yes	Low
48	Morocco		Essaquira Basin	Tari et al., 2000; Tari and Jabour, 2013	Yes	Low
49	Morocco		Agadir Basin	Tari et al., 2000; Tari and Jabour, 2013	Yes	Low
50	Morocco		Safi Basin	Tari et al., 2000; Tari and Jabour, 2013	Yes	Low
51	Israel	Sedom Fault	Southern Dead Sea Rift	Smit et al., 2008	Yes	High
52	Spain		Ebro Basin	Salas and Casas, 1993; Alvaro et al., 1979	Yes	Low
53	Canada		Carson Basin	Enachescu, 1992.	Yes	Low
54	Italy		Po Basin	Cardello and Doglioni, 2015	Yes	High
55	Norway		Feda Graben	Ge et al., 2016	Yes	High
56	Norway		Steinbit Terrace	Ge et al., 2016	Yes	High
57	Norway		Breiflabb Graben	Ge et al., 2016	Yes	High
58	Norway		Cod Terrace	Ge et al., 2016	Yes	High
59	UK		Josephine High	Ge et al., 2016; Vendeville et al., 1995	Yes	High
60	Norway		Sorvestlandet High	Ge et al., 2016; Stewart, 1993; Vendeville et al., 1995	Yes	High
61	Norway		Hidra High	Ge et al., 2016	Yes	High

62	Poland		Lower Silesian Basin	Mejia-Herrera et al., 2015	Yes	Mid
63	Italy		Radicondoli Radicondoli Basin	Brogi and Liotta, 2008	Yes	Low
64	Czech Republic		Most Basin	Rajchl and Uličný, 2001; Rajchl et al., 2008; 2009	Yes	High
65	Spain	Gargallo Fault	Maestrazgo Basin	Rodriguez-Lopez et al., 2007	Yes	High
66	France	Rhenish Fault	Soult-sous-Forets Area	Place et al., 2010	Yes	High
67	US	Moab Fault Splay	Paradox Basin	Berg and Skar, 2005	Yes	High
68	Iran		Southern Salt Basin	Perotti et al., 2016	Yes	Low
69	UK	Beatrice Fault System	Inner Moray Firth	Lapadat et al., 2016	Yes	High
70	Norway		Hammerfest Basin	Gabrielsen et al., 2016	Yes	High
71	Israel		Levant Basin	Reiche et al., 2014	Yes	Low
72	Russia		Pripyat Basin	Garetskii et al., 2004	Yes	High
73	Saudi Arabia		Rub' Al-Khali Basin	Stewart, 2016	Yes	Low
74	US		Rattlesnake Mountain	Stearns, 1978; Weinberg, 1979	Yes	High
75	Norway	Fjerritslev Fault System	Farsund Basin	Phillips et al., 2018	No	High
76	Ireland		Central Ireland Carboniferous Basin	Lewis and Couples, 1999	Yes	Low
77	US		Uinta Mountains	Stearns, 1978	Yes	High
78	US		West Powder River Basin	Sacrison, 1978; Stearns, 1978	Yes	High
79	US		Brady Structure	Sacrison, 1978	Yes	High

80	US		Carter Lake Anticline	Matthews and Work, 1978	Yes	Low
81	US		Bellview Dome	Matthews and Work, 1978	Yes	Mid
82	US		Milner Mountain Anticline	Matthews and Work, 1978	Yes	Mid
83	US		Dowe Pass Anticline	Matthews and Work, 1978	Yes	Mid
84	US	Horn Fault; Tensleep-Beaver Creek Fault	Horn Block	Palmquist, 1978	Yes	Mid
85	US		Piney Creek	Palmquist, 1978	Yes	Low
86	US		Fanny Peak Monocline	Lisenbee, 1978	Yes	Low
87	US		Rapid City Structure	Lisenbee, 1978	Yes	Low
88			Rockerville Quadrangle Area	Lisenbee, 1978	Yes	Low
89	US		Cascade Springs Anticline	Lisenbee, 1978	Yes	Mid
90	US		Stockade Beaver Creek Monocline	Lisenbee, 1978	Yes	Mid
91	US		Red Rock Fold	Cook, 1978	Yes	Low
92	Italy	Zuccale Fault	Elba Basin	Smith et al., 2007	Yes	High
93	Spain		Prebetic Basin	Rubinat et al., 2013	Yes	High
94	France	St Benoit Fault	Annot Basin	Tomasso and Sinclair, 2004	Yes	Mid
95	Borneo		East Barito Fordeep	Satyana and Silitonga, 1994	Yes	Mid
96	New Zealand		Taupo Volcanic Zone	Milner et al., 2002	Yes	Low

97	Germany		Gluckstadt Graben	Best et al., 1983; Warsitzka et al., 2017	Yes	Mid
98	Denmark		Step Graben	Remmelts, 1995	Yes	High
99	Denmark	Rifgronden Fault Zone	Terschelling Basin	Remmelts, 1995	Yes	Low
100	UK		West Central Graben	Weston et al., 1993; Hossack, 1995	Yes	High
101	Morocco		Essaouira Basin	Hafid et al., 2000	Yes	Mid
102	Mexico	Rincon de Parangueo Maar	Rincon de Parangueo	Aranda-Gomez et al., 2017	Yes	High
103	Tanzania	Lokichar	Usangu Basin	Morley, 2002	Yes	High

References for Appendix C

ABDINE, A. S., MESHREF, W., SHAHIN, A. N., GAROSSINO, P. & SHAZLY, S. 1992. Ramadan Field--Egypt Gulf of Suez Basin.

ALVARO, M., CAPOTE, R. & VEGAS, R. 1979. Un modelo de evolución geotectónica para la Cadena Celtibérica. Acta Geológica Hispánica, 14, 172-177.

ALVES, T. M., GAWTHORPE, R. L., HUNT, D. W. & MONTEIRO, J. H. 2002. Jurassic tectono-sedimentary evolution of the Northern Lusitanian Basin (offshore Portugal). Marine and Petroleum Geology, 19, 727-754.

ALVES, T. M., MANUPPELLA, G., GAWTHORPE, R. L., HUNT, D. W. & MONTEIRO, J. H. 2003. The depositional evolution of diapir- and fault-bounded rift basins: examples from the Lusitanian Basin of West Iberia. Sedimentary Geology, 162, 273-303.

ALVES, T. M., MOITA, C., SANDNES, F., CUNHA, T., MONTEIRO, J. H. & PINHEIRO, L. M. 2006. Mesozoic–Cenozoic evolution of North Atlantic continental-slope basins: The Peniche basin, western Iberian margin. AAPG bulletin, 90, 31-60.

ARANDA-GÓMEZ, J. J., CERCA, M., ROCHA-TREVIÑO, L., CARRERA-HERNÁNDEZ, J. J., LEVRESSE, G., PACHECO, J., YUTSIS, V., ARZATE-FLORES, J. A., CHACÓN, E. & BERALDI-CAMPESI, H. 2017. Structural evidence of enhanced active subsidence at the bottom of a maar: Rincón de Parangueo, México. Geological Society, London, Special Publications, 446, 225-254.

BALKWILL, H. & LEGALL, F. 1989. Whale Basin, Offshore Newfoundland: Extension and Salt Diapirism: Chapter 15: North American Margins.

BERG, S.S. and SKAR, T., 2005. Controls on damage zone asymmetry of a normal fault zone: outcrop analyses of a segment of the Moab fault, SE Utah. Journal of Structural Geology, 27, 1803-1822.

BEST, G., KOCKEL, F. & SCHÖNEICH, H. 1983. Geological history of the southern Horn Graben. Petroleum Geology of the Southeastern North Sea and the Adjacent Onshore Areas in: Kaasschieter, J. P. H., and Reijers, T. J. A., eds., Petroleum geology of the southeastern North Sea and the adjacent onshore areas, Geol. Mijnbouw 62, 25-33.

BODEGO, A. & AGIRREZABALA, L. M. 2013. Syn-depositional thin- and thick-skinned extensional tectonics in the mid-Cretaceous Lasarte sub-basin, western Pyrenees. Basin Research, 25, 594-612.

BOURROUILH, R., RICHERT, J.-P. & ZOLNAI, G. 1995. The north Pyrenean Aquitaine basin, France: evolution and hydrocarbons. AAPG Bulletin, 79, 831-853.

BROGI, A. & LIOTTA, D. 2008. Highly extended terrains, lateral segmentation of the substratum, and basin development: The middle-late Miocene Radicondoli Basin (inner northern Apennines, Italy). Tectonics, 27, n/a-n/a.

BROWN, J., BOWYER, M. & ZOLOTARENKO, V. 2012. Wedges and buffers: some new structural observations from the Dnieper–Donets Basin, onshore Ukraine. Geological Society, London, Special Publications, 363, 431-448.

BROWN, R. N. 1980. History of exploration and discovery of Morgan, Ramadan and July oilfields, Gulf of Suez, Egypt.

BROWN, W. G. 1988. Deformational style of Laramide uplifts in the Wyoming foreland. Interaction of the Rocky Mountain foreland and the Cordilleran thrust belt: Geological Society of America Memoir, 171, 1-25.

BURLIGA, S., KOYI, H. A. & CHEMIA, Z. 2012. Analogue and numerical modelling of salt supply to a diapiric structure rising above an active basement fault. Geological Society, London, Special Publications, 363, 395-408.

CARDELLO, G. L. & DOGLIONI, C. 2015. From Mesozoic rifting to Apennine orogeny: The Gran Sasso range (Italy). Gondwana Research, 27, 1307-1334.

COLEMAN, A. J., JACKSON, C. A. L. & DUFFY, O. B. 2017. Balancing sub- and supra-salt strain in salt-influenced rifts: Implications for extension estimates. Journal of Structural Geology, 102, 208-225.

COOK, R. A. 1978. A relationship between strike-slip faults and the process of drape folding of layered rocks. In: MATHEWS, V. III (ed.) Laramide folding associated with basement block faulting in the western United States. GSA Memoir, 197-214.

COWARD, M. & STEWART, S. 1995. Salt-influenced structures in the Mesozoic-Tertiary cover of the southern North Sea, UK, In: JACKSON, M.P.A., ROBERTS, D.G., SNELSON, S., eds., Salt Tectonics: A Global Perspective, AAPG Memoir, 65, 229-250.

DECKERS, J. 2015. Decoupled extensional faulting and forced folding in the southern part of the Roer Valley Graben, Belgium. Journal of Structural Geology, 81, 125-134.

DECKERS, J., BROOTHAERS, M., LAGROU, D. & MATTHIJS, J. 2014. The late Maastrichtian to Late Paleocene tectonic evolution of the southern part of the Roer Valley Graben (Belgium). Netherlands Journal of Geosciences, 93, 83-93.

DOOLEY, T., MCCLAY, K. & PASCOE, R. 2003. 3D analogue models of variable displacement extensional faults: applications to the Revfallet Fault system, offshore mid-Norway. Geological Society, London, Special Publications, 212, 151-167.

DOOLEY, T., MCCLAY, K. R., HEMPTON, M. & SMIT, D. 2005. Salt tectonics above complex basement extensional fault systems: results from analogue modelling. Geological Society, London, Petroleum Geology Conference series, 6, 1631-1648.

DUFFY, O.B., GAWTHORPE, R.L., DOCHERTY, M. and BROCKLEHURST, S.H., 2013. Mobile evaporite controls on the structural style and evolution of rift basins: Danish Central Graben, North Sea. Basin Research, 25, 310-330.

DURCANIN, M. A. 2009. Influence of synrift salt on rift-basin development. MSc Thesis. Rutgers University. doi:10.7282/T39P31T3.

ENACHESCU, M.E., 1992. Basement extension on the Newfoundland continental margin (Canadian east coast), In: MASON, R., eds., Basement Tectonics, 7, Springer, Dordrecht.

FÆRSETH, R. B. & LIEN, T. 2002. Cretaceous evolution in the Norwegian Sea—a period characterized by tectonic quiescence. Marine and Petroleum Geology, 19, 1005-1027.

FERRER, O., JACKSON, M.P.A., ROCA, E. and RUBINAT, M., 2012. Evolution of salt structures during extension and inversion of the Offshore Parentis Basin (Eastern Bay of Biscay). Geological Society, London, Special Publications, 363, 361-380.

FERRER, O., ROCA, E. and VENDEVILLE, B.C., 2014. The role of salt layers in the hangingwall deformation of kinked-planar extensional faults: insights from 3D analogue models and comparison with the Parentis Basin. Tectonophysics, 636, 338-350.

FERRILL, D. A. & MORRIS, A. P. 2008. Fault zone deformation controlled by carbonate mechanical stratigraphy, Balcones fault system, Texas. AAPG bulletin, 92, 359-380.

FERRILL, D. A., MORRIS, A. P. & MCGINNIS, R. N. 2012. Extensional fault-propagation folding in mechanically layered rocks: The case against the frictional drag mechanism. Tectonophysics, 576-577, 78-85.

FERRILL, D. A., MORRIS, A. P. & SMART, K. J. 2007. Stratigraphic control on extensional fault propagation folding: Big Brushy Canyon monocline, Sierra Del Carmen, Texas. Geological Society, London, Special Publications, 292, 203-217.

FORD, M., LE CARLIER DE VESLUD, C. & BOURGEOIS, O. 2007. Kinematic and geometric analysis of fault-related folds in a rift setting: The Dannemarie basin, Upper Rhine Graben, France. Journal of Structural Geology, 29, 1811-1830.

GABRIELSEN, R. H., ODINSEN, T. & GRUNNALEITE, I. 1999. Structuring of the Northern Viking Graben and the Møre Basin; the influence of basement structural grain, and the particular role of the Møre-Trøndelag Fault Complex. Marine and Petroleum Geology, 16, 443-465.

GABRIELSEN, R. H., SOKOUTIS, D., WILLINGSHOFER, E. & FALEIDE, J. I. 2016. Fault linkage across weak layers during extension: an experimental approach with reference to the Hoop Fault Complex of the SW Barents Sea. Petroleum Geoscience.

GARETSKII, R., AISBERG, R. & STARCHIK, T. 2004. Pripyat Trough: Tectonics, geodynamics, and evolution. Russian Journal of Earth Sciences, 6, 217-250.

GE, Z., GAWTHORPE, R. L., ROTEVATN, A. & THOMAS, M. B. 2016. Impact of normal faulting and pre-rift salt tectonics on the structural style of salt-influenced rifts: The Late Jurassic Norwegian Central Graben, North Sea. Basin Research, n/a-n/a.

GEIL, K. 1991. The development of salt structures in Denmark and adjacent areas: the role of basin floor dip and differential pressure. First Break, 9, 467-483.

GROSS, M. R., BECKER, A. & GUTIÉRREZ-ALONSO, G. 1997. Transfer of displacement from multiple slip zones to a major detachment in an extensional regime: Example from the Dead Sea rift, Israel. Geological Society of America Bulletin, 109, 1021-1035.

GRUNNALEITE, I. & GABRIELSEN, R. H. 1995. Structure of the Møre basin, mid-Norway continental margin. Tectonophysics, 252, 221-251.

GUDLAUGSSON, S. T., FALEIDE, J. I., JOHANSEN, S. E. & BREIVIK, A. J. 1998. Late Palaeozoic structural development of the South-western Barents Sea. Marine and Petroleum Geology, 15, 73-102.

HAFID, M. 2000. Triassic–early Liassic extensional systems and their Tertiary inversion, Essaouira Basin (Morocco). Marine and Petroleum Geology, 17, 409-429.

HANAFI, B. R. 2013. The influence of basin architecture and synrift salt on structural evolution during and after rifting. MSc Thesis. Rutgers University. doi:10.7282/T37943C2.

HARRISON, J. C. & JACKSON, M. P. A. 2014. Exposed evaporite diapirs and minibasins above a canopy in central Sverdrup Basin, Axel Heiberg Island, Arctic Canada. Basin Research, 26, 567-596.

HARVEY, M.J. and STEWART, S.A., 1998. Influence of salt on the structural evolution of the Channel Basin. Geological Society, London, Special Publications, 133, 241-266.

HOSSACK, J. 1995. Geometric rules of section balancing for salt structures. In: JACKSON, M. P. A., ROBERTS, D. G., SNELSEN, S. Salt Tectonics: A Global Perspective. AAPG Memoir, 65, 1-28.

HOWARD, K. A. & JOHN, B. E. 1997. Fault-related folding during extension: Plunging basement-cored folds in the Basin and Range. Geology, 25, 223-226.

JACKSON, C. A. L. & LEWIS, M. M. 2016. Structural style and evolution of a salt-influenced rift basin margin; the impact of variations in salt composition and the role of polyphase extension. Basin Research, 28, 81-102.

JACKSON, D. I. & MULHOLLAND, P. 1993. Tectonic and stratigraphic aspects of the East Irish Sea Basin and adjacent areas: contrasts in their post-Carboniferous structural styles. Geological Society, London, Petroleum Geology Conference series, 4, 791-808.

KANE, K. E., JACKSON, C. A. L. & LARSEN, E. 2010. Normal fault growth and fault-related folding in a salt-influenced rift basin: South Viking Graben, offshore Norway. Journal of Structural Geology, 32, 490-506.

KELLER, J.V.A. and LYNCH, G., 1999. Displacement transfer and forced folding in the Maritimes basin of Nova Scotia, eastern Canada. Geological Society, London, Special Publications, 169, 87-101.

KOYI, H. & PETERSEN, K. 1993. Influence of basement faults on the development of salt structures in the Danish Basin. Marine and Petroleum Geology, 10, 82-94.

KOYI, H., TALBOT, C. J. & TORUDBAKKEN, B. 1995. Analogue models of salt diapirs and seismic interpretation in the Nordkapp Basin, Norway. Petroleum geoscience, 1, 185-192.

KOYI, H., TALBOT, C. J. & TØRUDBAKKEN, B. O. 1993. Salt diapirs of the southwest Nordkapp Basin: analogue modelling. Tectonophysics, 228, 167-187.

KRZYWIEC, P. 2010. Triassic evolution of the Kłodawa salt structure: basement-controlled salt tectonics within the Mid-Polish Trough (Central Poland). 2010, 48, 12.

LAMARCHE, J. & SCHECK-WENDEROTH, M. 2005. 3D structural model of the Polish Basin. Tectonophysics, 397, 73-91.

LĂPĂDAT, A., IMBER, J., YIELDING, G., IACOPINI, D., MCCAFFREY, K. J. W., LONG, J. J. & JONES, R. R. 2016. Occurrence and development of folding related to normal faulting within a mechanically heterogeneous sedimentary sequence: a case study from Inner Moray Firth, UK. Geological Society, London, Special Publications, 439.

LEWIS, H. & COUPLES, G. D. 1999. Carboniferous basin evolution of central Ireland — simulation of structural controls on mineralization. Geological Society, London, Special Publications, 155, 277-302.

LEWIS, M. M., JACKSON, C. A. L. & GAWTHORPE, R. L. 2013. Salt-influenced normal fault growth and forced folding: The Stavanger Fault System, North Sea. Journal of Structural Geology, 54, 156-173.

LISENBEE, A. L. 1978. Laramide structure of the Black Hills uplift, South Dakota-Wyoming-Montana. In: MATTHEWS, V. III (ed.) Laramide Folding Associated with Basement Block Faulting in the Western United States. Geological Society of America.

LYNCH, G., KELLER, J.V. and GILES, P.S., 1998. Influence of the Ainslie Detachment on the stratigraphy of the Maritimes Basin and mineralization in the Windsor Group of northern Nova Scotia, Canada. Economic Geology, 93, 703-718.

MATTHEWS III, V. & WORK, D. F. 1978. Laramide folding associated with basement block faulting along the northeastern flank of the Front Range, Colorado. Laramide folding associated with basement block faulting in the western United States: Geological Society of America Memoir, 151, 101-124.

MAURIN, J. C. & NIVIERE, B. 1999. Extensional forced folding and decollement of the pre-rift series along the Rhine graben and their influence on the geometry of the syn-rift sequences. Geological Society, London, Special Publications, 169, 73-86.

MEJÍA-HERRERA, P., ROYER, J.-J., CAUMON, G. & CHEILLETZ, A. 2015. Curvature Attribute from Surface-Restoration as Predictor Variable in Kupferschiefer Copper Potentials. Natural Resources Research, 24, 275-290.

MILNER, D., COLE, J. & WOOD, C. 2002. Asymmetric, multiple-block collapse at Rotorua Caldera, Taupo Volcanic Zone, New Zealand. Bulletin of Volcanology, 64, 134-149.

MORLEY, C. K. 2002. Evolution of large normal faults: Evidence from seismic reflection data. AAPG bulletin, 86, 961-978.

NILSEN, K. T., VENDEVILLE, B. C. & JOHANSEN, J.-T. 1995. Influence of regional tectonics on halokinesis in the Nordkapp Basin, Barents Sea.

OUDMAYER, B. C. & DE JAGER, J. 1993. Fault reactivation and oblique-slip in the Southern North Sea. Geological Society, London, Petroleum Geology Conference series, 4, 1281-1290.

PALMQUIST, J. C. 1978. Laramide structures and basement block faulting: Two examples from the Big Horn Mountains, Wyoming. In: MATTHEWS, V. III (ed.) Laramide Folding Associated with Basement Block Faulting in the Western United States. Geological Society of America.

PASCOE, R., HOOPER, R., STORHAUG, K. & HARPER, H. 1999. Evolution of extensional styles at the southern termination of the Nordland Ridge, Mid-Norway: a response to variations in coupling above Triassic salt. Petroleum Geology Conference Series, 5, 83-90.

PENGE, J., MUNNS, J. W., TAYLOR, B. & WINDLE, T. M. F. 1999. Rift–raft tectonics: examples of gravitational tectonics from the Zechstein basins of northwest Europe. Geological Society, London, Petroleum Geology Conference series, 5, 201-213.

PEROTTI, C., CHIARIOTTI, L., BRESCIANI, I., CATTANEO, L. and TOSCANI, G., 2016. Evolution and timing of salt diapirism in the Iranian sector of the Persian Gulf. Tectonophysics, 679, 180-198.

PETERSEN, K., CLAUSEN, O. & KORSTGÅRD, J. 1992. Evolution of a salt-related listric growth fault near the D-1 well, block 5605, Danish North Sea: displacement history and salt kinematics. Journal of Structural Geology, 14, 565-577.

PHILLIPS, T. B., JACKSON, C. A., BELL, R. E. & DUFFY, O. B. 2018. Oblique reactivation of lithosphere-scale lineaments controls rift physiography–the upper-crustal expression of the Sorgenfrei–Tornquist Zone, offshore southern Norway. Solid Earth, 9, 403.

PLACE, J., DIRAISON, M., NAVILLE, C., GÉRAUD, Y., SCHAMING, M. & DEZAYES, C. 2010. Decoupling of deformation in the Upper Rhine Graben sediments. Seismic reflection and diffraction on 3-component Vertical Seismic Profiling (Soultz-sous-Forêts area). Comptes Rendus Geoscience, 342, 575-586.

QUINTANA, L., ALONSO, J. L., PULGAR, J. A. & RODRÍGUEZ-FERNÁNDEZ, L. R. 2006. Transpressional inversion in an extensional transfer zone (the Saltacaballos fault, northern Spain). Journal of Structural Geology, 28, 2038-2048.

RAJCHL, M. & ULIČNÝ, D. 2001. Response of a Fluvial Depositional System to Unequal Com-paction of Underlying Peat (Neogene, Most Basin, Czech Re-public). GeoLines, 13, 105.

RAJCHL, M., ULIČNÝ, D., GRYGAR, R. & MACH, K. 2009. Evolution of basin architecture in an incipient continental rift: the Cenozoic Most Basin, Eger Graben (Central Europe). Basin Research, 21, 269-294.

RAJCHL, M., ULIČNÝ, D. & MACH, K. 2008. Interplay between tectonics and compaction in a rift-margin, lacustrine delta system: Miocene of the Eger Graben, Czech Republic. Sedimentology, 55, 1419-1447.

REICHE, S., HÜBSCHER, C. & BEITZ, M. 2014. Fault-controlled evaporite deformation in the Levant Basin, Eastern Mediterranean. Marine Geology, 354, 53-68.

REMMELTS, G. 1995. Fault-related salt tectonics in the southern North Sea, the Netherlands.

RODRÍGUEZ-LÓPEZ, J. P., LIESA, C. L., MELÉNDEZ, N. & SORIA, A. R. 2007. Normal fault development in a sedimentary succession with multiple detachment levels: the Lower Cretaceous Oliete sub-basin, Eastern Spain. Basin Research, 19, 409-435.

RUBINAT, M., ROCA, E., ESCALAS, M., QUERALT, P., FERRER, O. & LEDO, J. 2013. The influence of basement structure on the evolution of the Bicorb-Quesa Diapir (eastern Betics, Iberian Peninsula): contractive thin-skinned deformation above a pre-existing extensional basement fault. International Journal of Earth Sciences, 102, 25-41.

SACRISON, W. 1978. Seismic interpretation of basement block. Laramide folding associated with basement block faulting in the western United States, 151, 39.

SALAS, R. & CASAS, A. 1993. Mesozoic extensional tectonics, stratigraphy and crustal evolution during the Alpine cycle of the eastern Iberian basin. Tectonophysics, 228, 33-55.

SATYANA, A. H. & SILITONGA, P. D. 1994. Tectonic reversal in East Barito Basin, South Kalimantan: consideration of the types of inversion structures and petroleum system significance. Proceedings of the Indonesian Petroleum Association, 23rd Annual Convention, 57-74.

SINCLAIR, I. K. 1995. Transpressional inversion due to episodic rotation of extensional stresses in Jeanne d'Arc Basin, offshore Newfoundland. Geological Society, London, Special Publications, 88, 249-271.

SMIT, J., BRUN, J. P., FORT, X., CLOETINGH, S. & BEN-AVRAHAM, Z. 2008. Salt tectonics in pull-apart basins with application to the Dead Sea Basin. Tectonophysics, 449, 1-16.

SMITH, S. A. F., HOLDSWORTH, R. E., COLLETTINI, C. & IMBER, J. 2007. Using footwall structures to constrain the evolution of low-angle normal faults. Journal of the Geological Society, 164, 1187-1191.

STEARNS, D. W. 1978. Faulting and forced folding in the Rocky Mountains foreland. Geological Society of America Memoirs, 151, 1-38.

STEWART, I.J., 1993. Structural controls on the Late Jurassic age shelf system, Ula trend, Norwegian North Sea. Geological Society, London, Petroleum Geology Conference series, 4, 469-483.

STEWART, S. A. 2014. Detachment-controlled triangle zones in extension and inversion tectonics. Interpretation, 2, SM29-SM38.

STEWART, S. A. 2016. Structural geology of the Rub' Al-Khali Basin, Saudi Arabia. Tectonics, 35, 2417-2438.

STEWART, S. A. & CLARK, J. A. 1999. Impact of salt on the structure of the Central North Sea hydrocarbon fairways. Geological Society, London, Petroleum Geology Conference Series, 5, 179-200.

STEWART, S. A. & COWARD, M. P. 1995. Synthesis of salt tectonics in the southern North Sea, UK. Marine and Petroleum Geology, 12, 457-475.

STEWART, S. A., HARVEY, M. J., OTTO, S. C. & WESTON, P. J. 1996. Influence of salt on fault geometry: examples from the UK salt basins. Geological Society, London, Special Publications, 100, 175-202.

STEWART, S. A., RUFFELL, A. H. & HARVEY, M. J. 1997. Relationship between basement-linked and gravity-driven fault systems in the UKCS salt basins. Marine and Petroleum Geology, 14, 581-604.

STOVBA, S. M. & STEPHENSON, R. A. 2002. Style and timing of salt tectonics in the Dniepr-Donets Basin (Ukraine): implications for triggering and driving mechanisms of salt movement in sedimentary basins. Marine and Petroleum Geology, 19, 1169-1189.

SERANO-SUAREZ, B. E. 2013. Evolution of the Jeanne d’Arc basin, offshore Newfoundland, Canada. MSc Thesis. Rutgers University. doi:10.7282/T3V123DK.

TARI, G. & JABOUR, H. 2013. Salt tectonics along the Atlantic margin of Morocco. Geological Society, London, Special Publications, 369, 337-353.

TARI, G., MOLNAR, J., ASHTON, P. & HEDLEY, R. 2000. Salt tectonics in the Atlantic margin of Morocco. The Leading Edge, 19, 1074-1078.

TAVANI, S., BALSAMO, F. & GRANADO, P. 2018. Petroleum system in supra-salt strata of extensional forced-folds: A case-study from the Basque-Cantabrian basin (Spain). Marine and Petroleum Geology, 96, 315–330.

TAVANI, S., CAROLA, E., GRANADO, P., QUINTÀ, A. & MUÑOZ, J. A. 2013. Transpressive inversion of a Mesozoic extensional forced fold system with an intermediate décollement level in the Basque-Cantabrian Basin (Spain). Tectonics, 32, 146-158.

TAVANI, S. & GRANADO, P. 2014. Along-strike evolution of folding, stretching and breaching of supra-salt strata in the Plataforma Burgalesa extensional forced fold system (northern Spain). Basin Research, 1-13.

TAVANI, S., QUINTÀ, A. & GRANADO, P. 2011. Cenozoic right-lateral wrench tectonics in the Western Pyrenees (Spain): The Ubierna Fault System. Tectonophysics, 509, 238-253.

TOMASSO, M. & SINCLAIR, H. D. 2004. Deep-water sedimentation on an evolving fault-block: the Braux and St Benoit outcrops of the Gres d'Annot. Geological Society, London, Special Publications, 221, 267-283.

VENDEVILLE, B. C., GE, H. & JACKSON, M. P. A. 1995. Scale models of salt tectonics during basement-involved extension. Petroleum Geoscience, 1, 179-183.

WARSITZKA, M., KLEY, J., JÄHNE-KLINGBERG, F. & KUKOWSKI, N. 2017. Dynamics of prolonged salt movement in the Glückstadt Graben (NW Germany) driven by tectonic and sedimentary processes. International Journal of Earth Sciences, 106, 131-155.

WESTON, P. J., DAVISON, I. & INSLEY, M. W. 1993. Physical modelling of North Sea salt diapirism. In: PARKER, J. R. (ed.) Petroleum Geology of Northwest Europe: Proceedings of the 4th Conference. The Geology Society, London, 559-567.

WEINBERG, D. M. 1979. Experimental folding of rocks under confining pressure: Part VII. Partially scaled models of drape folds. Tectonophysics, 54, 1-24.

WILSON, P., ELLIOTT, G. M., GAWTHORPE, R. L., JACKSON, C. A.-L., MICHELSEN, L. & SHARP, I. R. 2013. Geometry and segmentation of an evaporite-detached normal fault array: 3D seismic analysis of the southern Bremstein Fault Complex, offshore mid-Norway. Journal of Structural Geology, 51, 74-91.

WILSON, P., ELLIOTT, G. M., GAWTHORPE, R. L., JACKSON, C. A., MICHELSEN, L. & SHARP, I. R. 2015. Lateral variation in structural style along an evaporite-influenced rift fault system in the Halten Terrace, Norway: Influence of basement structure and evaporite facies. Journal of Structural Geology, 79, 110-123.

WITHJACK, M. O. & CALLAWAY, S. 2000. Active normal faulting beneath a salt layer: an experimental study of deformation patterns in the cover sequence. AAPG bulletin, 84, 627-651.

ZULFITRIADI, Z. 2011. The Mesozoic Orpheus rift basin, offshore Nova Scotia and Newfoundland, Canada. MSc Thesis. Rutgers University. doi:10.7282/T3WD404M.

Appendix D – Fault-propagation fold database

Fault-propagation fold database may be downloaded here:
https://figshare.com/s/c6663901f6ca8c6f6fe4

Appendix E – Forced fold database

Forced fold database may be downloaded here:
https://figshare.com/s/c6663901f6ca8c6f6fe4

Appendix F – Uncertainties

This study measures growth fold parameters (Fig. 2) from a series of published examples in nature, physical, mechanical and kinematic models. Here, we illustrate using a series of examples how growth fold parameters were measured and their associated errors. As all of the errors are relatively minimal and the data points would still plot in similar locations (for example, on Figs. 11 – 12; 21), the general relationships/trends would remain largely the same. Changes in the measured values would inevitably shift the best-fit regressions and alter the derived parametric equations, but the trends would remain the same. References for each example are also shown.

Parameter	Values
Amplitude	10 - 13 mm
Width	96 - 100 mm
Prekinematic	40 - 41 mm
Fault throw	10 - 11 mm
Fault dip	45°
FSF	7 - 10

Parameter	Values
Amplitude	9 - 11 mm
Width	117 - 133 mm
Prekinematic	38 - 40 mm
Fault throw	9 - 11 mm
Fault dip	45°
FSF	11 - 15
Detachment	9 - 12 mm
C:D	3 - 4

Parameter	Values
Amplitude	0.6 - 0.65 km
Width	7.6 - 7.8 km
Prekinematic	5.4 - 5.5 km
Fault throw	0.6 - 0.65 km
Fault dip	50°
FSF	11.6 - 13

Mechanical model of a fault-propagation fold from Finch et al., 2004.

Parameter	Values
Amplitude	0.55 - 0.6 km
Width	1.4 - 1.55 km
Prekinematic	1.49 - 1.5 km
Fault throw	0.55 - 0.6 km
Fault dip	60°
FSF	2.3 - 2.8

Trishear fault-propagation fold from Hardy and McClay, 1999

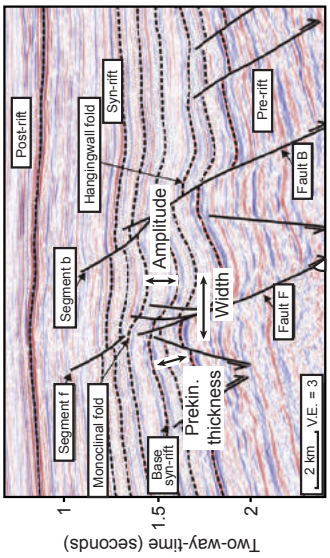

Parameter	Values
Amplitude	0.3 - 0.4 km
Width	2 - 2.1 km
Prekinematic	0.4 - mm
Fault throw	0.4 - 0.6 km
Fault dip	42 - 45°
FSF	5 - 7

FPF above Fault F from Lapadat et al., 2016

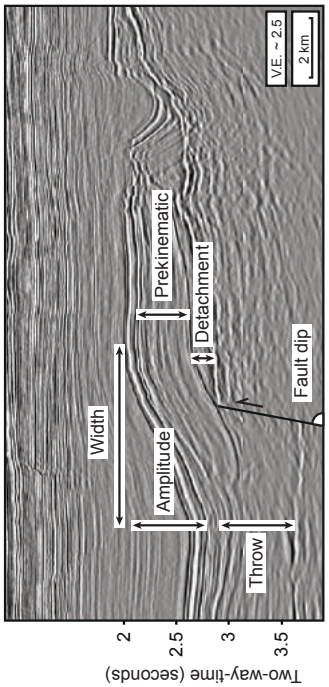

Parameter	Values
Amplitude	0.9 - 1 km
Width	5.5 - 5.6 km
Prekinematic	0.5 - 0.7 km
Fault throw	1.2 - 1.25 km
Fault dip	66 - 68°
FSF	5.5 - 6.2
Detachment	0.3 - 0.36 km
C:D	1.4 - 2.3

Forced fold from Lewis et al., 2013 using velocity of 2.8 km/s from Jackson and Lewis, 2012

Appendix G - Principal Component Analysis (PCA) Explanation

To demonstrate how PCA works we first consider the following scenario: envision a multi-variate dataset consisting of three measured variables (or 'dimensions'), x, y and z. If the x- and y- variables are plotted, we can see that they are highly correlated (Fig. G.1A). PCA allows us to represent these data along a best-fit, single axis (PC1 - the black line on Fig. G.1A), termed a 'principal component' (PC). This principal axis explains the largest data variation and permits the simplification of two-dimensional data i.e., the x- and y- variables, in this case, to one dimension. By reducing the data to fewer dimensions, the relationship between the x- and y-variables can no longer be explicitly calculated (as in linear regression) but the relationships between the variables are maintained. In other words, when we plot the original data against the principal component, the data is spread along the length of the axis (Fig. G.1B). This suggests that the x- and y- variables are highly correlated, and the principal component explains a large proportion of the data variation, as shown in Fig. G.1A.

Given that we also have a third variable, z, we cannot explain all of the data variance with a single principal component, additional principal components may be calculated to explain further data variance (PC2 - grey line on Fig. G.1A). Each successive principal component introduced into the analysis explains a successively smaller portion of the data (data variance is larger on Fig. G.1B than Fig. G.1C) and is geometrically orthogonal to the others (e.g. Wold et al., 1987; Jolliffe, 1993; Ringner, 2008; Abdi and Williams, 2010; Lever et al., 2017), but together, these principal components cumulatively explain the data variance. The number of principal components can be as large as the number of samples or the number of components. As PC1 and PC2 explain the majority of the data variance, we may project the original data (consisting of the x-, y- and z- values) and their trends onto new axes, comprised of the principle components (black arrows on Fig. G.1D). If particular variables are correlated, they will plot close to one-another. It should be noted that the sign of any principal component, i.e. the direction of the arrows on Fig. G.1D, is completely arbitrary (e.g. Jolliffe, 1987). In our example case, the x- and y- variables plot very close to one-another and the PC1 axis, so are strongly correlated. The z-variable in contrast, is correlated with the PC2 axis, but is also relatively close to the y-variable. We can therefore interpret that the x- and z-variables are both correlated to y variable (Fig. G.1C), and there may be a reason for their correlation, such as the x- and z-variables control the y-variable. Furthermore, principal components identify major trends in highly-dimensional data and the correlated variables. If a data point only has missing values for

particular variables i.e. the data point has an x-, and y- value but not a z-value, the position of the principal components that explains the most data variation may slightly change. Furthermore, the original data may be projected slightly differently.

The PCA method described above can also be applied to our growth fold dataset. However, instead of three variables (e.g. x, y and z), we have more variables or dimensions (e.g. fault dip, fault throw, fold amplitude, fold width etc.). Following the same method, we can thus, determine which parameters are correlated and speculate a geological reasoning for the relationship. Where missing values for particular parameters are missing (i.e. data gaps), then a best-fit, iterative value is used to fill in the record (as discussed in Appendix H). A full description of the PCA method is described in Josse and Husson (2016).

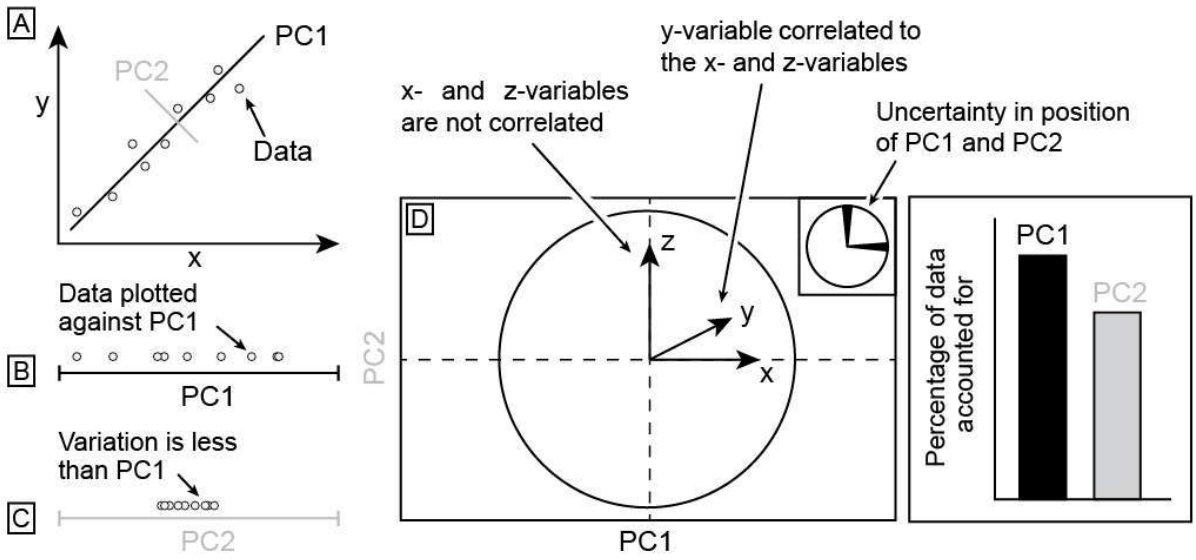

Figure G.1. – Summary of principal component analysis (PCA) method using example data with x-,y- and z-variables. The x-variable is plotted against the y-variable for the example data (A). The most and second-most data variation is described by PC1 and PC2, respectively. By projecting the data onto two new axes, PC1 (B) and PC2 (C), the data can be analysed for clustering and hidden trends. The x-, y- and z-variables are then plotted to see which variables are likely related (D). Where values are missing in the dataset, uncertainty is introduced in the analysis hence the trend and position of PC1 and PC2 (on panel A) may shift. PC1 and PC2 each account a certain amount of the data as shown in the bar chart.

References for Appendix G

ABDI, H. and WILLIAMS, L. J. 2010. Principal component analysis. Wiley interdisciplinary reviews: computational statistics, 2, 433-459.

JOLLIFFE, I. T. 1990. PRINCIPAL COMPONENT ANALYSIS: A BEGINNER'S GUIDE — I. Introduction and application. Weather, 45, 375-382.

JOLLIFFE, I. T. 1993. Principal component analysis: A beginner's guide — II. Pitfalls, myths and extensions. Weather, 48, 246-253.

JOLLIFFE, I. T. 2002. Principal component analysis, New York, Springer.

LEVER, J., KRZYWINSKI, M. and ALTMAN, N. 2017. Points of significance: Principal component analysis. Nature Publishing Group.

RINGNÉR, M. 2008. What is principal component analysis? Nature Biotechnology, 26, 303.

WOLD, S., ESBENSEN, K. and GELADI, P. 1987. Principal component analysis. Chemometrics and Intelligent Laboratory Systems, 2, 37-52.

Appendix H - Principal component analysis sensitivity

Principal component analysis (PCA) simplifies the complexity of high-dimensional multi-variate data, such as our growth fold dataset (Appendices D – E), while retaining trends and patterns (e.g. Jolliffe, 1993; Jolliffe, 2002; Lever et al., 2002). This allows us to identify possible relationships between parameters which are non-linear or very complex.
In an ideal scenario, all structural and stratigraphic parameters (cf. Fig. 2 in the main text) may be measured but this may not be possible in all cases. Therefore, the best-fit position of each principal component (PC) may vary, and an uncertainty is introduced. We explore this uncertainty using two examples: (i) a numerical model, and (ii) a real example from our growth fold database.

Example 1 – Numerical trishear forward model

To quantitatively investigate the effect of missing parameters within individual examples, we used FaultFold (Allmendinger, 1998) to generate a series of 2D trishear forward models for fault-propagation folds with different structural and stratigraphic parameter variations. As the initial parameters are known, and the fold geometry can be measured, none of the forward models are missing any values and there is no uncertainty in the PCA analysis – '*Dataset 1*', 491 records, each with 5 parameters. We then randomly removed 20% of the values (any parameter from any record) to reflect a dataset with missing values – '*Dataset 2*'. We then undertook PCA on *Dataset 2* with the missing values to see how uncertainty affected the strength, and thus, the interpretation of the PCA using three methods (Fig. H.1; cf. Josse and Husson, 2012; Josse et al., 2012; Audiger et al., 2016; Josse and Husson, 2016):

1) Ignore incomplete records (and reduce the sample size);
2) Replace missing values in individual records with the mean value for an appropriate parameter (sample size remains the same);
3) Replace missing values in individual records using a regularised iterative value for the appropriate parameter (sample size remains the same).

We can see that regardless of the PCA method used on *Dataset 2*, the correlations (the directions of the arrows and the relative positions of arrows) are very similar. In this example, we see a correlation between the prekinematic thickness, the total slip, the fold amplitude and to a lesser

extent, the fold width. In addition, we see a correlation between the fold-shape-factor (FSF) and the fault dip, and to a lesser extent, the fold width. The PCA for *Dataset 2* (with missing values) is almost identical to *Dataset 1* (without missing values), suggesting PCA may be used even on incomplete datasets, at least with caution.

It is important to mention that these examples are similar sized, thus, replacing a data gap with a mean value has a negligible effect on the correlation. If the sample contained lots of different sized folds, the replaced variable may be unrealistic and a magnitude larger or smaller. Similarly, removing the record completely (and all of the other parameters, even if only one value is missing), may significantly reduce the sample size, making the dataset susceptible to extremes. An iterative approach tackles both of these issues, giving a parameter that is not out of character with the rest of the record values, and does not remove the record from the sample. This is our preferred method for PCA, but we include the uncertainty associated with the missing value so that correlations can be qualitatively checked in all cases.

Example 2 – Natural examples of fault-propagation folds

Now applying the same sensitivity test to the dataset of natural examples of fault-propagation folds (cf. Appendix D) that already contains missing values. We may compare the results of PCA using the same three methods (Fig. H.2; cf. Josse and Husson, 2012; Josse et al., 2012; Audiger et al., 2016; Josse and Husson, 2016):

1) Ignore incomplete records (and reduce the sample size);
2) Replace missing values in individual records with the mean value for an appropriate parameter (sample size remains the same);
3) Replace missing values in individual records using a regularised iterative value for the appropriate parameter (sample size remains the same).

Similar to Example 1, the PCA results for Example 2 are largely similar irrespective of the method. Our results show there is a correlation between the amplitude and width of the fold, the fault throw and the thickness of the prekinematic cover. The fold-shape-factor is seemingly uncorrelated to the other variables. However, we do see slight changes in the direction of the arrows. In order to not drastically reduce the number of sample records in our analysis, missing values have been replaced using iteration (method 3).

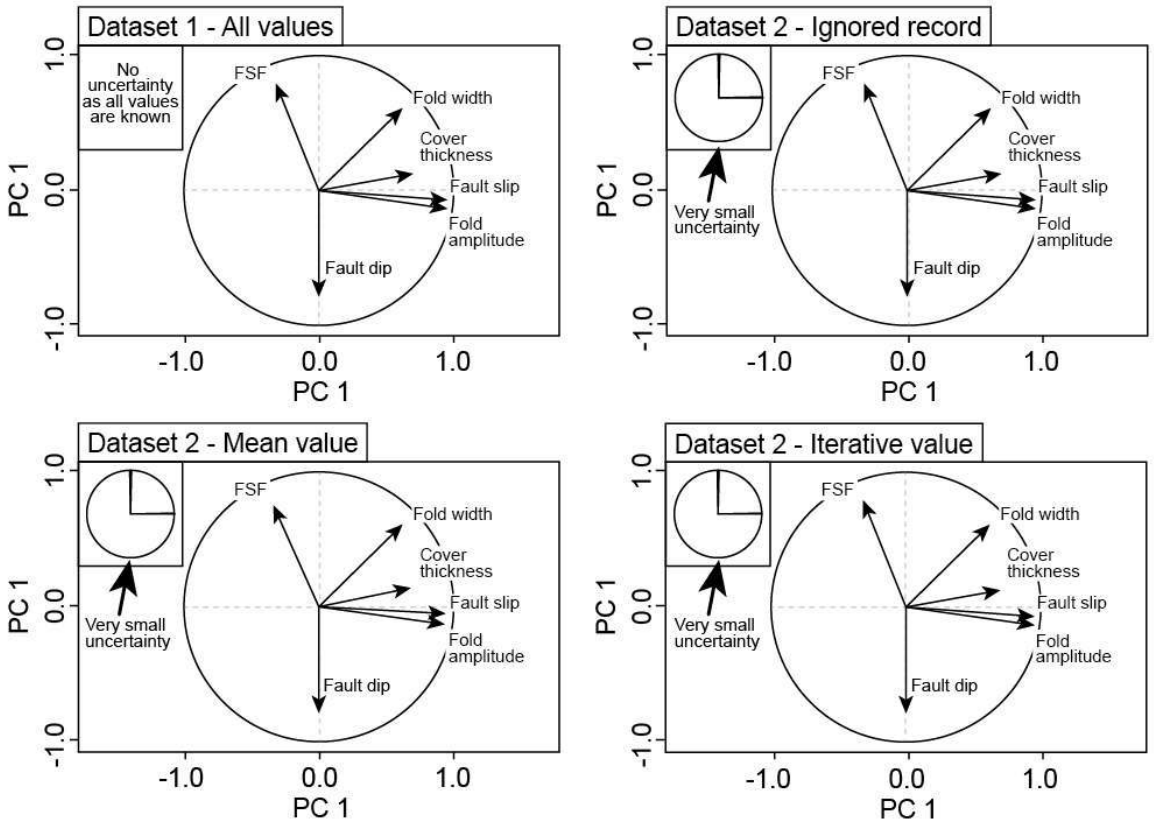

Figure H.1. – Summary of principal component analysis (PCA) sensitivity for the trishear forward model dataset. Top left – Dataset 1 (without missing values). Top right – Dataset 2 (with missing values), where records with missing values are ignored. Bottom left - Dataset 2 (with missing values), where records with missing values for a particular variable are replaced with the mean value for that variable of the entire data. Bottom right - Dataset 2 (with missing values), where records with missing values for a particular variable are replaced with a regularized iterative value for that variable in that record.

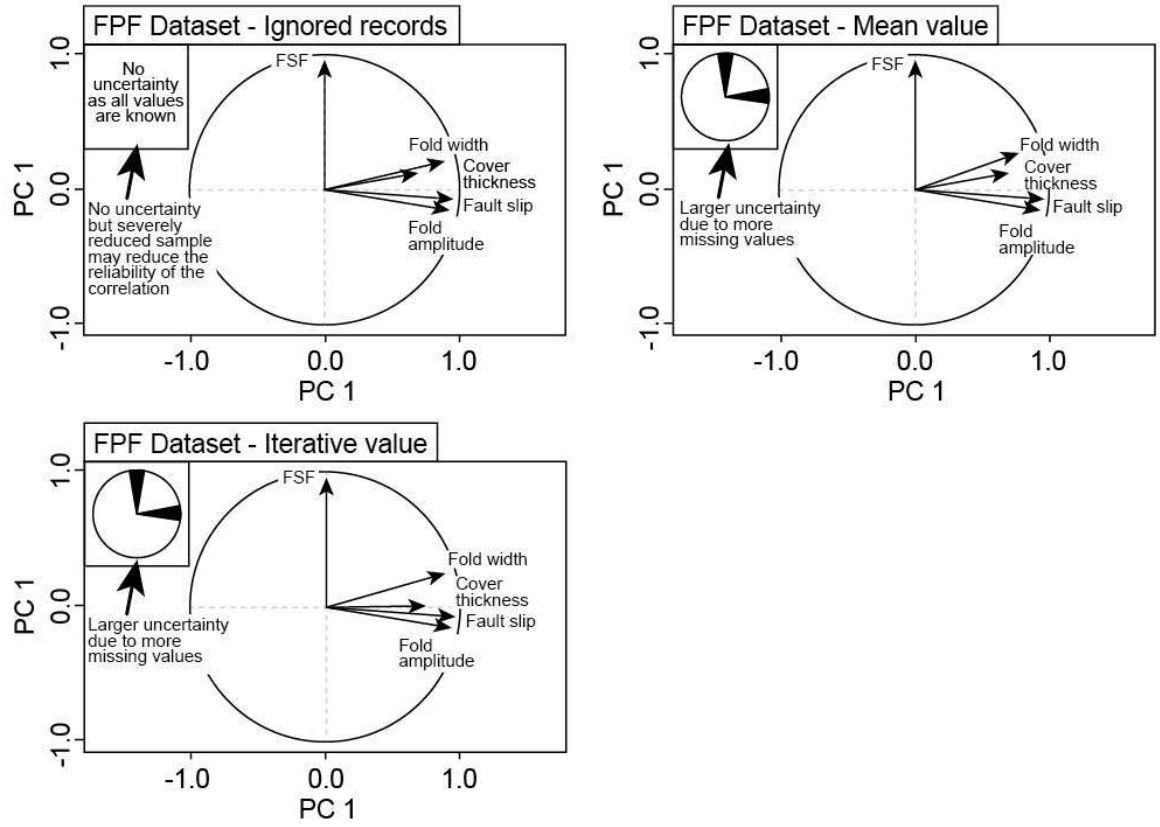

Figure H.2. – Summary of principal component analysis (PCA) sensitivity for the fault-propagation fold dataset of natural examples. Top left – Original dataset of real examples (with missing values). Top right – Dataset 2, where missing values are replaced by the mean value for that particular parameter. Bottom left - Dataset 2 where missing values replaced with a regularized iterative value for that variable in that record.

References for Appendix H

ALLMENDINGER, R. W. 1998. Inverse and forward numerical modeling of trishear fault-propagation folds. Tectonics, 17, 640-656.

AUDIGIER, V., HUSSON, F. and JOSSE, J. 2016. A principal component method to impute missing values for mixed data. Advances in Data Analysis and Classification, 10, 5-26.

JOLLIFFE, I. T. 1993. Principal component analysis: A beginner's guide — II. Pitfalls, myths and extensions. Weather, 48, 246-253.

JOLLIFFE, I. T. 2002. Principal component analysis, New York, Springer.

JOSSE, J., CHAVENT, M., LIQUET, B. and HUSSON, F. 2012. Handling missing values with regularized iterative multiple correspondence analysis. Journal of classification, 29, 91-116.

JOSSE, J. and HUSSON, F. 2012. Selecting the number of components in principal component analysis using cross-validation approximations. Computational Statistics and Data Analysis, 56, 1869-1879.

JOSSE, J. and HUSSON, F. 2016. missMDA: a package for handling missing values in multivariate data analysis. Journal of Statistical Software, 70, 1-31.

LEVER, J., KRZYWINSKI, M. and ALTMAN, N. 2017. Points of significance: Principal component analysis. Nature Methods, 14, 641-642.